Carpathian Journal of Electrical Engineering

Volume 13, Number 1, 2019

Carpathian Journal of Electrical Engineering

Carpathian Journal of Electrical Engineering

CONTENTS

AWARENESS OF DEMAND-SIDE MANAGEMENT PRACTICES AMONG STAFF OF AN EDUCATIONAL INSTITUTION

Emmanuel Asuming **FRIMPONG**, Elvis **TWUMASI**

Department of Electrical and Electronic Engineering, Kwame Nkrumah University of Science and Technology, Kumasi, Ghana
eafrimpong.soe@knust.edu.gh, elvistwumasi@gmail.com

Abstract*:* Awareness of demand-side management practices among staff of educational institutions is critical for energy savings. This paper presents the results of a survey to determine the extent to which staff of the Kwame Nkrumah University of Science and Technology are aware of measures for energy efficiency and also assess their preparedness to support efforts towards reducing energy wastage. Questionnaires were administered to Senior members, Senior staff and Junior staff of the institution. The questionnaires were designed to collect data on their level of energy efficiency awareness in the use of refrigerators, airconditioners, light bulbs and electronic devices. The extent to which staff are engaged in energy saving activities and their preparedness to get involved in energy saving activities were also determined. The analysis of the collected data was done using the Statistical Package for Social Sciences (SPSS) software. Analysis of responses received show that more than seventy-seven percent of staff are ignorant of the fact that keeping refrigerators close to walls resulted in energy wastage. About fifty-seven percent of them are aware of the fact that when airconditioners are not cleaned regularly, much energy is wasted. Almost eighty-five percent of staff indicated awareness of the fact that keeping electronic devices on standby for long periods could be a source of significant energy wastage. Over eighty-three percent of staff indicated that they had been switching light bulbs off when there is adequate illumination from the sun so as to conserve energy. About thirty-six percent of staff are already engaged in at least one form of energy conservation. Lastly, over 94% of them expressed willingness to take part in energy saving activities.

1. INTRODUCTION

Development of national economies and improvements of people's quality of life have resulted in high electrical energy consumption. The rapid growth in world energy demand has

raised concerns over supply difficulties, exhaustion of resources, and impact on environment [1]. To address challenges associated with the rise in energy demand, a number of strategies have been put in place. One of such strategies is Demand-side management (DSM). DSM is a leading strategy employed to reduce energy demands. It refers to technologies, actions and programmes on the demand-side of electric meters that seek to manage or decrease electricity consumption. The benefits of DSM include reduction in electricity consumption, overall electricity system expenditures and carbon emissions [2]. Activities under DSM include (a) promotion of high efficiency building practices, (b) use of energy-efficient products, (c) shifting of non-critical usage of electricity form peak periods to off-peak periods, (d) institution of programmes that provide limited utility control of customer equipment such as airconditioners, and (e) promotion of energy efficiency awareness [1], [3], [4].

A key target for education on energy efficiency, with the view of cutting down energy wastage, is educational institutions. Educational institutions; particularly universities, are high energy consumption sectors across the globe [5], [6]. Also, their products take up responsibilities in other sectors where energy efficient practices are required. Gains in energy conservation in educational institutions cannot be achieved without the active involvement of staff and students. The extent to which staff and students are aware of energy efficient practices and their preparedness to support efforts towards reduction in energy wastage are critical.

Studies conducted in [7]-[9] show that the inefficient use of electricity in educational institutions is largely due to the lack of energy efficiency awareness among staff and students. Behavioural changes to reduce energy consumption, while technological and policy considerations are taken into account, significantly contribute to reduction in energy wastage [10], [11]. Providing energy awareness and conservation measures to staff will equip them with useful and relevant information to modify the way they use energy and build their capacity to educate students to do same. This will go a long way to promote energy conservation in institutions [12]-[15].

Efforts toward educating staff on energy conservation, for onward transfer to students may yield minimal success if the education does not consider their current levels of awareness of energy conservation issues. Knowledge of their level of awareness will determine the issues to stress on as well as the overall approach to use. Additionally, the preparedness of staff to support energy conservation activities will affect the success of energy savings efforts, and this must be determined. Thus, there is the need for research into the electric energy conservation perspective of staff [16], [17]. This need has not been adequately addressed in literature.

This paper presents the results of a survey which sought to determine the level of energy conservation awareness among staff of the Kwame Nkrumah University of Science and Technology. The study determined their levels of knowledge in the efficient use of various consumer appliances found in offices. Also, the extent to which they are already engaged in energy conservation activities was determined. Furthermore, their preparedness to support efforts by the University to conserve energy was assessed. The study was carried out through

the administration of questionnaires. The results of the study provide useful input for any policy aimed at conserving energy in educational institutions.

2. METHODOLOGY

The survey was conducted by distributing questionnaires to teaching and non-teaching staff of the Kwame Nkrumah University of Science and Technology. The survey questions were chosen carefully with simple and understandable terms. The research questions partly focused on awareness of energy conservation measures related to the use of various electrical appliances found in offices. The loads considered were: electronic devices, refrigerators, air-conditioners and light bulbs. With regards to the preparedness of staff to engage in energy saving activities, questions were asked to determine if they were already performing any energy saving activity and whether they were willing to participate in energy saving activities. In both cases, a list of energy saving activities was presented for them to select from. Additionally, staff were asked about their willingness to participate in energy awareness campaigns and whether their involvement in such campaigns will hinge on the provision of incentives.

The sample size for the survey was determined using the population of staff of the University. The population of staff was obtained as 3435 from the Quality Assurance and Planning Unit (QAPU) of the University. Using equation (1) [18], the sample size was obtained as 346. However, 350 questionnaires were printed and distributed. The z-score, estimated proportion of attribute, and margin of error values used in the computation of the sample size using equation (1) were 1.96, 0.5, and 0.005 respectively.

The analysis of the collected data was done using the Statistical Package for Social Sciences (SPSS) software. The descriptive statistics model in SPSS was employed to summarize the data into figures, tables and charts.

$$n_0 = \frac{\left(\dfrac{Z^2 pq}{e^2} \right)}{1 + \left(\dfrac{\dfrac{Z^2 pq}{e^2} - 1}{N} \right)} \tag{1}$$

where n is the sample size, z is the z-score, p is the estimated proportion of an attribute that is present in the population, $q = 1 - p$, e is the margin of error or confidence interval and N is the population.

3. RESULTS AND ANALYSIS

Out of the 350 questionnaires distributed to both academic and non-academic staff, 318 were completed and returned. The response rate of the survey is thus 90.86%, which is high for a survey of this kind [19]. In the sub-sections that follow, the results of the study and analysis done are presented.

3.1. Energy efficiency awareness in the use of refrigerators

The respondents were asked whether they knew that leaving fridge and freezer doors ajar, keeping refrigerators close to walls, not defrosting freezing compartments, and putting hot foods in refrigerators, lead to energy wastage. Three hundred and eighteen staff gave responses to all the questions. *Figure 1* shows details of the results obtained. Close to twenty-three percent (22.64%) of them indicated knowledge of the fact that keeping refrigerators close to walls results in energy wastage. The remaining staff, constituting more than seventy-seven percent (77.36%), were ignorant of this. With regards to energy wastage due to not defrosting freezer compartments, about thirty-one percent (31.13%) of respondents knew about this while the rest, constituting almost sixty-nine percent (68.87) were unaware of this. Also, 79.87% of staff knew that leaving refrigerator doors ajar lead to them consuming more energy than required. Finally, close to sixty-seven percent of staff indicated knowledge of the fact that putting hot foods in refrigerators cause them to draw more energy than required.
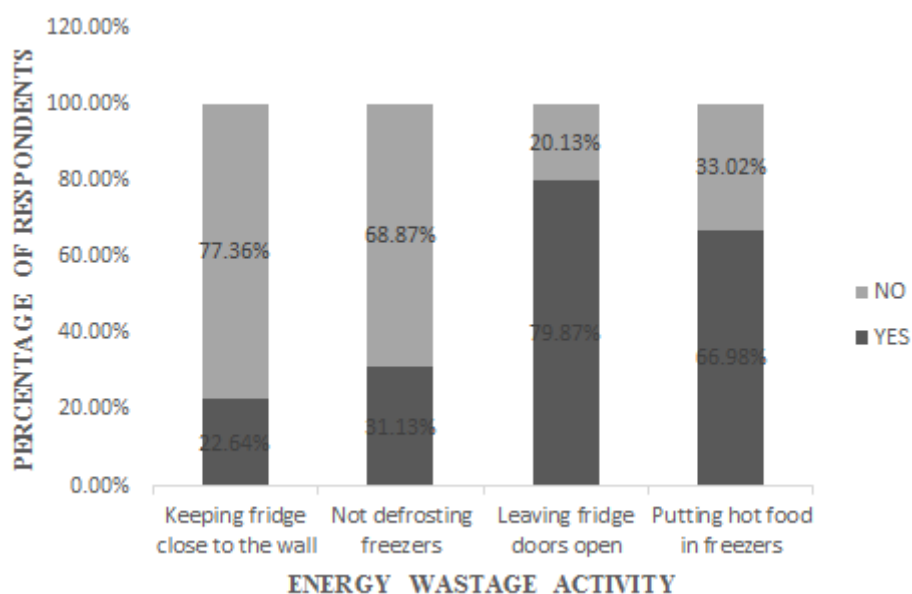
Fig. 1. Energy efficiency awareness in the use of refrigerators

3.2. Energy efficiency awareness in the use of airconditioners

Airconditioners contribute largely to the energy bills of educational institutions. Not closing doors and windows properly when airconditioners are switched on amount to energy wastage. Also, not cleaning airconditioners regularly make them consume more energy than required. The respondents were asked about their knowledge of these facts. *Figure 2* shows results obtained. About fifty-seven percent (56.60%) of them were aware of the fact that when airconditioners are not cleaned regularly, much energy is wasted. The rest did not know that. With regards to knowledge of the fact that leaving doors and windows not properly closed result in energy wastage, a little over eight-two percent (82.40%) of the respondents indicated knowledge of this fact. Thus, majority of staff are aware of energy wastage issues relating to the use of airconditioners.
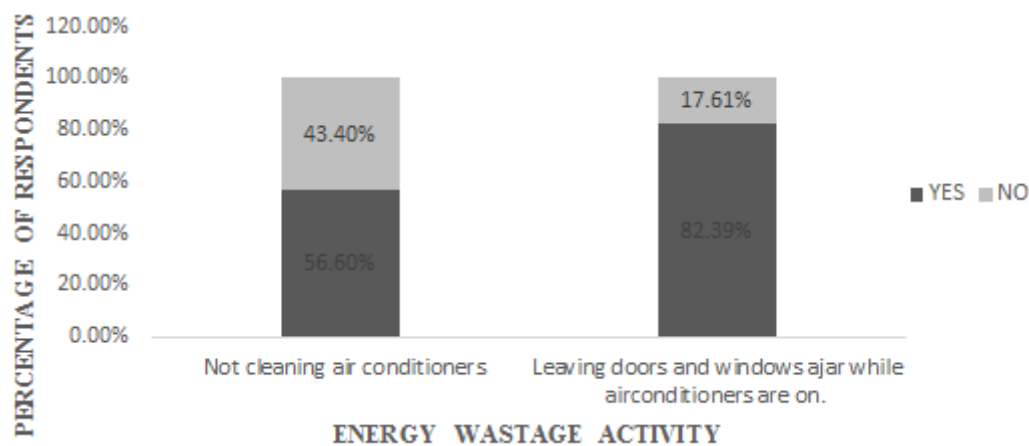
Fig. 2. Energy efficiency awareness in the use of airconditioners

3.3. Energy efficiency awareness in lighting

Lighting is critical in educational institutions and contributes significantly to energy bills. Keeping bulbs on when there is adequate illumination from sunlight amounts to energy wastage. It is common to find electric bulbs in corridors and other areas switched on even when they are not needed. In the absence of automatic lighting control devices, the involvement of staff in switching such bulbs off will bring about significant energy savings. The staff were asked if they had been switching light bulbs off when there is adequate illumination from the sun. *Figure 3* shows the results obtained. Two hundred and sixty-five staff representing over 83% of respondents indicated that they had been doing that. The rest constituting less than 17% of respondents indicated they were not doing that. The high number of staff already involved in putting light bulbs off when not required is encouraging.
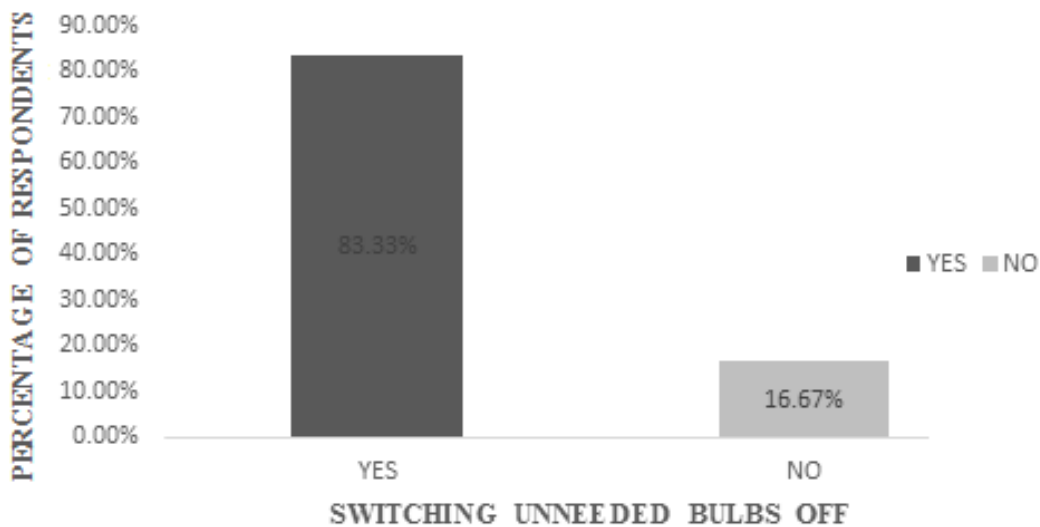
Fig. 3. Energy efficiency awareness in the use of light bulbs

3.4. Energy efficiency awareness in the use of electronic devices

Electronic devices on standby consume a small amount of energy. However, keeping several of them on standby for long periods could be a source of significant energy wastage. Knowledge of this fact could bring about significant energy savings. Staff were asked whether they knew about this fact. The result obtained is shown in *Figure 4*. Almost 85% of the staff indicated knowledge of this fact. Less than 15% were ignorant of this.
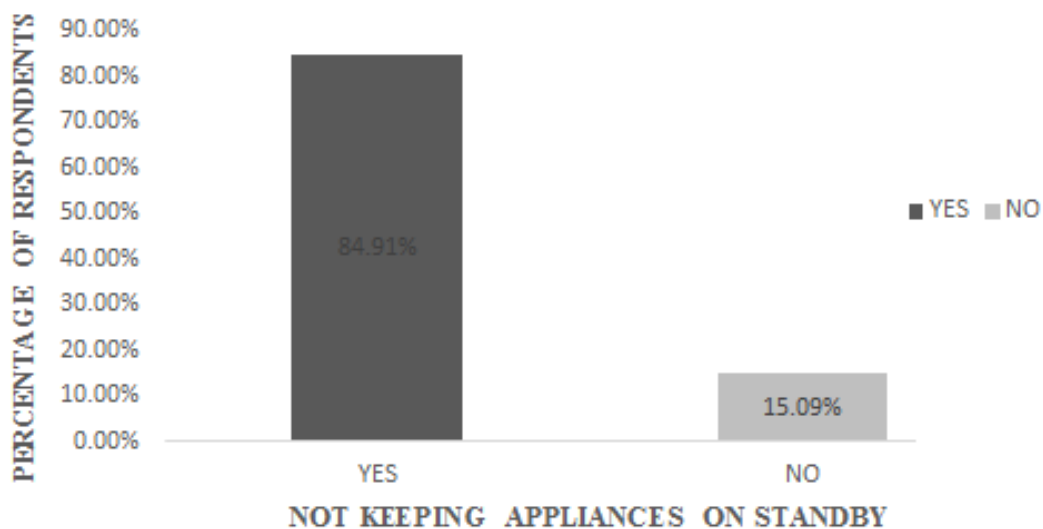
Fig. 4. Energy efficiency awareness in the use of electronic devices

3.5. Engagement in energy saving activities

Involvement of staff in energy saving activities is critical if significant gains are to be made in energy conservation. Respondents were asked whether they were already engaged in

energy saving activities. Those who indicated involvement in energy saving activities were asked to select from a list of energy saving activities, the specific activities they were engaged in. Two hundred and eighty-eight staff representing over 88% of respondents indicated that they were already involved in energy saving activities. *Table 1* shows details of the number of staff engaged in specific energy saving activities. It is noted from *Table 1* that majority of staff close doors and windows when airconditioners are on. However, less than 37% percent of staff switch off their airconditioners when leaving the office for more than 10 minutes. It is also noted that most staff prefer to use airconditioners instead of allowing natural ventilation. Thus there is the need to install devices to automatically turn off airconditioners during periods when staff are not in their offices, to cut down on energy wastage.

Table 1. Energy saving activities currently engaged in by 288 staff

No.	Activity	No. of staff engaged in activity	Percentage (%)
1	Turning off printers, photocopiers and computers after use.	240	84.81
2	Putting off airconditioners and fans when leaving the office for more than 10 minutes.	106	36.81
3	Turning off unnecessary light bulbs during and after work.	223	77.43
4	Turning off fridges after close of work on Fridays.	168	58.33
5	Not leaving chargers on and not keeping electronic devices on standby.	226	78.47
6	As much as possible, using natural ventilation and fans instead of airconditioners.	115	39.93
7	Keeping doors and windows closed when airconditioners are on.	181	62.85

A question was also asked to know whether staff were prepared to continue to engage in or now begin to take part in energy saving activities. Out of the 318 respondents, 299 staff representing a little over 94% expressed willingness to take part in energy saving activities. Details of the specific activities that the 299 staff are prepared to engage in are presented in *Table 2*.

Table 2. Energy saving activities to be engaged in by 299 staff

No.	Activity	No. of staff engaged in activity	Percentage (%)
1	Turning off printers, photocopiers and computers after use.	280	93.65

No.	Activity	No. of staff engaged in activity	Percentage (%)
2	Putting off airconditioners and fans when leaving the office for more than 10 minutes.	176	58.86
3	Turning off unnecessary light bulbs during and after work.	271	90.64
4	Turning off fridges after close of work on Fridays.	247	82.61
5	Not leaving chargers on and not keeping electronic devices on standby.	265	88.63
6	As much as possible, using natural ventilation and fans instead of airconditioners.	280	93.65
7	Keeping doors and windows closed when airconditioners are on.	259	86.62

Again, staff were asked whether it was necessary for incentives to be provided to encourage them to continue or start energy saving activities. *Figure 5* shows the results obtained. Nearly 67% of staff were of the view that the provision of incentives was necessary. Thus, it is important for educational institutions to provide some form of incentives to staff to whip up the interest of many to get involved in energy saving activities.
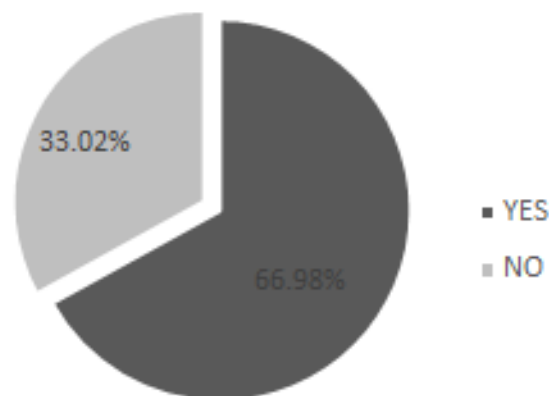
Fig. 5. Responses to the provision of incentives for energy savings

3.6. Willingness to join energy efficiency awareness campaigns

Education on energy efficiency brings about significant gains in energy savings. Here, staff were asked about their willingness to take part in educational campaigns on energy efficiency. *Figure 6* shows the responses obtained. Over 77% of respondents indicated willingness to join such educational campaigns. This is very encouraging, considering the fact that staff of educational institutions can contribute significantly to behavioural change in students.
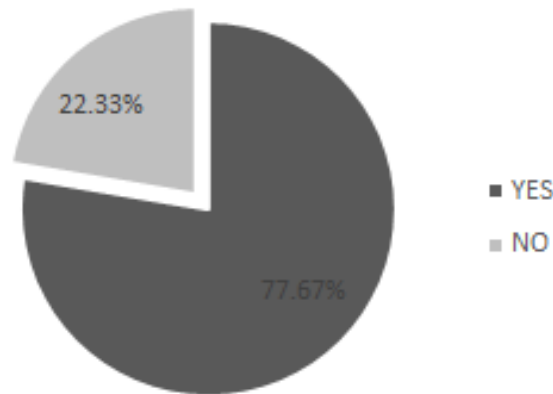
Fig. 6. Willingness to join educational campaigns on energy efficiency

4. CONCLUSION

This paper has presented and discussed the results of a study conducted to determine the level of energy efficiency awareness among staff of the Kwame Nkrumah University of Science and Technology, and also assess their preparedness to engage in, as well as promote energy saving activities. It was realised that at least fifty-seven percent of staff have significant knowledge about measures employed to conserve energy. Not less than Eighty-eight percent of staff are already engaged in at least one form of energy saving activity. Over ninety-four percent of staff expressed willingness to take part in energy conservation activities. Also, more than seventy-seven percent expressed interest in participating in educational campaigns that focus on energy conservation. However, nearly sixty-seven percent of staff wanted the institution to provide incentives to encourage them to conserve energy. The results of this study will be a useful input in formulating energy conservation policies in educational institutions.

ACKNOWLEDGMENT

REFERENCES

[1]   D. S. Choi, M. E. Lee, K. H. Cho, H. C. Jeon & J. H. An, *An Analysis of Energy Consumption and Greenhouse Gas Emissions in University Buildings,* Proceedings of Advanced Science and Technology Letters, vol. 69, pp. 17-20, 2014.

[2]   P. Warren, *Electricity demand-side management: best practice programmes for the UK,* Energy and Sustainability IV, vol. 176, pp. 69, 2013.

[3]   Parcificorp, *Demand-side management* , May 2017. Retrieved from http://www.pacificorp.com/es/dsm.html.

[4]   C. W. Gellings, *The concept of demand-side management for electric utilities*, Proceedings of the IEEE, vol. 73, no.10, pp.1468-1470, 1985.

[5]   I. Ward, A. Ogbonna, & H. Altan, *Sector review of UK higher education energy consumption*, Energy Policy, vol. 36, no. 8, pp. 2939-2949, 2008.

[6]   Higher education, *An overview of energy use and energy efficiency opportunities*, 2017, Retrieved from https://www.energystar.gov/sites/default/files/buildings/ tools/SPP%20Sales%20Flyer%20for%20Higher%20Education_0.pdf.

[7]   G. Kok, S. H. Lo, G. J. Y. Peters & R. A. Ruiter, *Changing energy-related behavior: An Intervention Mapping approach*, Energy Policy, vol. 39, no. 9, pp. 5280-5286, 2011.

[8]   A. Emeakaroha, C. S. Ang & Y. Yan, *Challenges in improving energy efficiency in a university campus through the application of persuasive technology and smart sensors*, Challenges, vol. 3, no. 2, pp. 290-318, 2012.

[9]   N. Maistry, *Energy efficiency at a South African higher education institution: a case study of the Auckland Park Kingsway campus*, University of Johannesburg, 2014.

[10] S. C. Staddon, C. Cycil, M. Goulden, C. Leygue & A. Spence, *Intervening to change behaviour and save energy in the workplace: A systematic review of available evidence*, Energy Research & Social Science, vol. 17, pp. 30-51, 2016.

[11] S. Kelly, *Energy Consumption in Creighton University Residence Halls: Comparing Attitudes and Behaviors*, Quest: A Journal of Undergraduate Research, vol. 5, pp. 51-80, 2016.

[12] K. Crosby, A. B. Metzger, *Powering Down, A toolkit for Behavior-based Energy Conservation in K-12 Schools*, Proceedings of Behaviour, Energy and Climate Change Conference, Washington DC, December 8, 2014.

[13] Eskom Energy Management Information Pack: Brochure 4, *Creating an energy awareness programme: behavioural change at work*. Retrieved from *http://www.eskom.co.za/sites/idm/Documents/AdvisoryServiceCreatingAnEnergyAwarenessCampBrochure.pdf.*

[14] Office of Energy Efficiency, *ecoENERGY Efficiency for Buildings, Implementing an energy efficiency awareness program*, 2012. Retrieved from https://www.nrcan.gc.ca/sites/www.nrcan.gc.ca/files/oee/files/pdf/publications/commercial/Awareness_Program_e.pdf.

[15] N. A. Siweya, Innovative Energy Efficiency Communication and Awareness Campaign, *Proceedings of the 8th Conference on the Industrial and Commercial Use of Energy*, pp. 181-183, 2011.

[16] *Creating an Energy Awareness Program: A Handbook for Federal Energy Managers*, Step 2, Retrieved from https://www1.eere.energy.gov/femp/pdfs/step2_hndbk.pdf.

[17] E. A. Frimpong and E. Twumasi, *Electricity conservation and safety awareness among senior high school students,* Carpathian Journal of Electrical Engineering, vol. 12, no. 1: 69-86, 2018.

[18] J. S. Kim & R. J. Dailey, *Confidence intervals and sample size*, Biostatistics for Oral Healthcare, pp.113, 2008.

[19] *Response rates,* May 2017, Retrieved from, https://facultyinnovate.utexas.edu/sites/default/files/response_rates.pdf

OPTIMIZED SPACE-VECTOR-MODULATED QUASI Z-SOURCE NPC INVERTER FOR SOLAR PV APPLICATION

Francis Boafo **EFFAH**[1], Philip **OKYERE**[1], Patrick **WHEELER**[2],
Alan **WATSON**[2], Jon **CLARE**[2]

[1] *Kwame Nkrumah University of Scince and Technology, Kumasi, Ghana.*
[2] *University of Nottingham, Nottingham, UK.*
fbeffah.coe@knust.edu.gh

Abstract*: An optimized space vector modulation technique for controlling a quasi Z-source NPC inverter for solar photovoltaic application is presented in this paper. The presented algorithm optimizes the number of switching transitions over a switching cycle by modifying the placement of the shoot-through states in some of the sub-triangles of the space vector diagram of a conventional neutral point clamped inverter. This approach leads to a reduction in the total losses of the quasi Z-source inverter by reducing the switching losses. The presented concepts are expected to be cheaper than existing methods because a reduction in losses will lead to the use of smaller and cheaper heat sinks in practical implementation. In this paper, the effectiveness of the proposed optimized space vector modulation technique has been demonstrated through simulations in SABER®.*

1. INTRODUCTION

Conventional power generation based on fossil fuel resources is considered to be unsustainable in the long term. This has been the main driver for an extensive deployment of renewable energy resources such as wind power, solar photovoltaic (PV), hydropower, biomass power, among others, into the power grid in the last several years [1, 2]. Among the major renewables, solar PV has continued to be expanded at a rapid rate over the years, and it already plays a substantial role in electricity generation in some countries [3].

Power electronic converters have been acknowledged to be an enabling technology for more renewable energy integration into the grid, including solar PV systems [4]. These

converters are to provide stable output voltage in spite of unstable input variables at the highest efficiency, lowest cost and minimum size. This has led to the development of many new interface power electronic converters. Most of the converter topologies employed in PV systems are characterized as two-stage converters. Two-stage converters employ a cascade of dc-dc converter and voltage source inverter (VSI) for processing the dc power available from the PV panels into ac power suitable for grid integration [5]. To improve the spectral performance of the output voltage fed into the grid, multilevel inverters are usually employed. One of such topologies is the neutral-point-clamped (NPC) inverter. Some of the advantages of the NPC inverter over the two-level counterpart include lower voltage stress across semiconductor devices, lower switching losses and better harmonic performance [6, 7]. However, the ac output voltage of the NPC inverter is limited and cannot exceed the available input voltage. Also, dead time is needed to prevent shoot-through problem caused by electromagnetic interference, which causes waveform distortion.

At present, the Z-source concept improves the structure of traditional inverters by bringing onboard voltage buck-boost capability in a single-stage structure [8]. A single-stage structure is an attractive approach because of its compactness, low cost and reliability. The Z-source NPC (ZNPC) inverter combines the properties of Z-source network with those of NPC inverter [9, 10]. However, the ZNPC inverter draws discontinuous input current which is not suitable for PV application. To overcome this drawback, the quasi Z-source NPC (qZNPC) inverter was proposed [11]. The qZNPC inverter draws continuous current from the PV array and is capable of handling a wide input voltage range [12]. Other advantages of the qZNPC inverter include employment of lower rated components, reduction in switching ripples to the PV panels, and lower EMI problems.

Space vector modulation (SVM) technique for controlling ZNPC/qZNPC has been reported in the literature [13-15]. A study of the switching patterns adopted in [13-15] reveals that there are some regions where the number of switching transitions can be optimized. This paper seeks to bridge that research gap by optimizing the number of switching transitions in these regions in the implementation of SVM strategy for optimal performance of the qZNPC inverter in PV application. The rest of the paper is organized as follows. In section 2, the operating principles as well as steady state analysis of the qZNPC inverter is presented. Section 3 describes the optimized space vector modulation strategy for controlling the qZNPC inverter to perform voltage buck-boost functionality. Simulation results are presented in section 4 to verify the proposed optimized algorithm.

2. TOPOLOGY AND OPERATING PRINCIPLES

Figure 1 illustrates the topology of the qZNPC inverter. The PV string is coupled to the inverter by the quasi Z-source network. Four switches with antiparallel diodes and

associated clamping diodes form a phase leg of the inverter. The switching states of the qZNPC inverter are categorized into non-shoot-through (NST) and shoot-through (ST) states. The NST states are P, O and N. The P state means two upper switches in a phase leg are switched on, O means two middle switches conduct and N signifies turning on of two bottom switches. The shoot-through states are classified as full-shoot-through (FST), lower-shoot-through (LST) and upper-shoot-through (UST) states. FST refers to the simultaneous turn on of all four switches in a phase leg, UST means the three upper swtches are turned on while LST signifies the turning on of three bottom switches in a phase leg. The behaviour of qZNPC inverter is usually represented by equivalent circuits showing NST, UST and LST states for the partial shoot-through operation mode as shown in *fig. 2*.
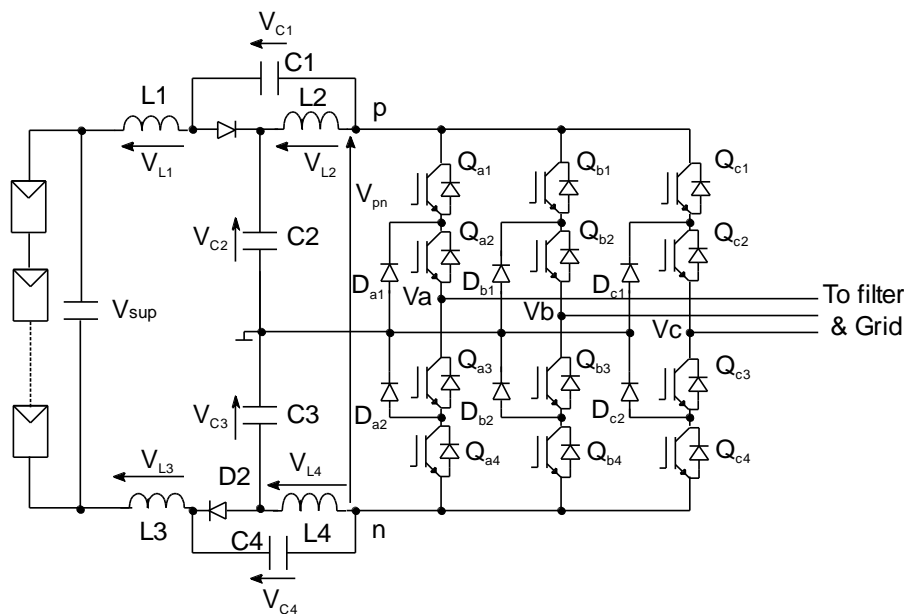
Fig. 1. Quasi Z-source NPC inverter
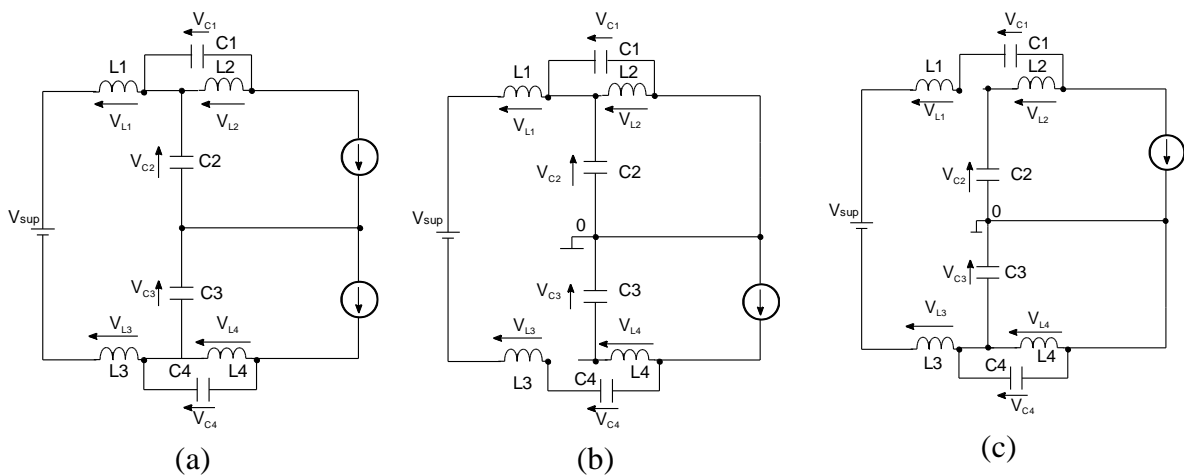
Fig.2. Simplified representation of qZNPC inverter in (a) NST, (b) UST, and (c) LST states.

Assuming symmetric quasi Z-source network and operation in the continuous conduction mode, the operation of the qZNPC inverter can be written as:

$$D_N + D_U + D_L = 1 \qquad (1)$$

where D_N, D_U and D_L represent the duty cycles of the NST, UST and LST states, respectively. To ensure symmetric operation, D_U and D_L are set to be equal and represented by D_0. The peak of the dc-link voltage is given by the sum of the capacitor voltages, as

$$V_{C1} + V_{C2} + V_{C3} + V_{C4} = \widehat{V}_{pn}. \qquad (2)$$

Performing inductor voltage balance over a switching period yields:

$$V_{C1} = V_{C4} = \frac{D_0 \cdot V_{\text{sup}}}{2 - 4D_0}, \qquad (3)$$

$$V_{C2} = V_{C3} = \frac{(1 - D_0) \cdot V_{\text{sup}}}{2 - 4D_0}. \qquad (4)$$

The peak dc-link voltage and the peak output line-to-line voltage are then found to be given by (5) and (6) respectively.

$$\widehat{V}_{pn} = \frac{V_{\text{sup}}}{1 - 2D_0}. \qquad (5)$$

$$\widehat{V}_{out} = M \cdot \left(\frac{1}{1 - 2D_0} \right) \cdot V_{\text{sup}} = B_F \cdot \left(M \cdot V_{\text{sup}} \right), \qquad (6)$$

In (6), $D_0 < 0.5$ is the shoot-through ratio, B_F is the boost factor while M is the modulation index, respectively.

3. OPTIMISED SVM TECHNIQUE FOR QUASI Z-SOURCE NPC INVERTER

Space vector modulation uses the concept of space vectors to compute duty cycles of the switches. The operation of each phase leg of a traditional NPC inverter can be represented

by switching states P, O, and N. *Figure 3* shows the space vector diagram (SVD) of a conventional NPC inverter.
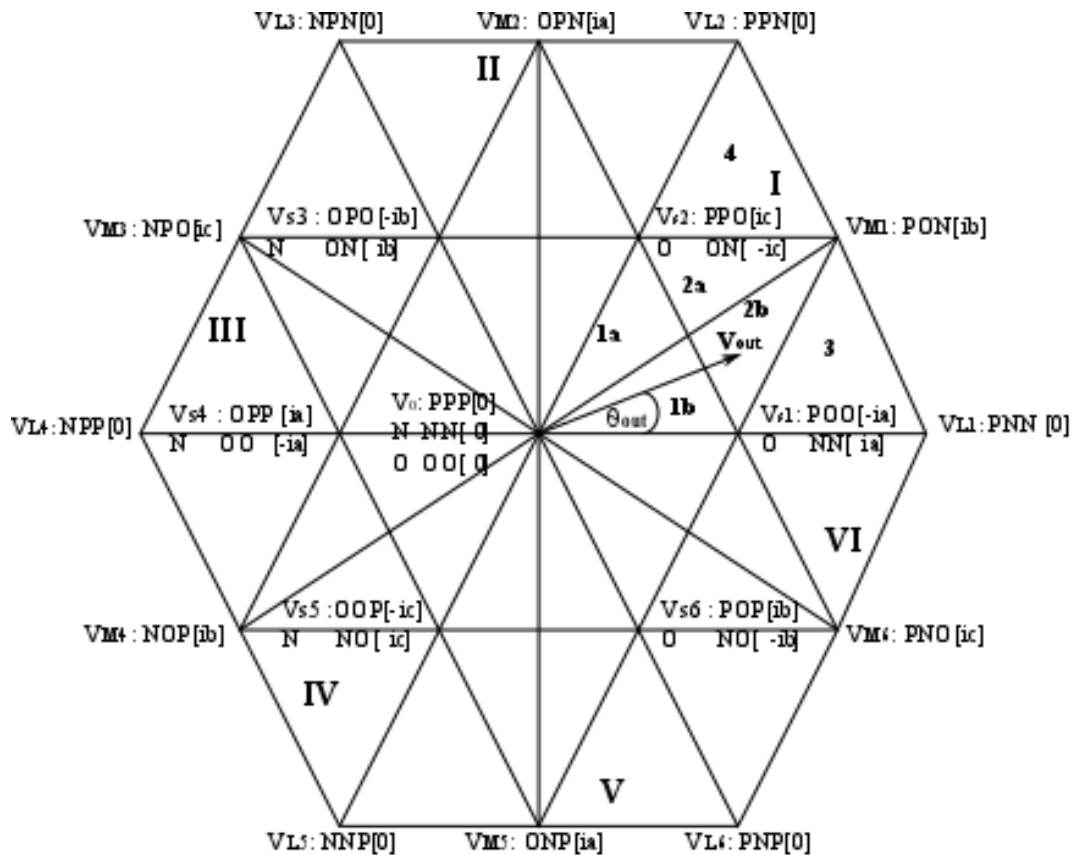
Fig. 3. Space vector diagram of conventional NPC inverter

The SVD is divided into six sectors (I to VI) and contain 27 switching states classified as zero (V_0), small (V_{S1} to V_{S6}), medium (V_{M1} to V_{M6}) and large (V_{L1} to V_{L6}) vectors. Each sector contains four smaller triangles labelled 1 (1a and 1b), 2 (2a and 2b), 3 and 4, respectively. The rotating reference vector V_{out} represents the desired three-phase output voltage which is synthesized with the nearest three vectors in each switching cycle. For three-level operation of the conventional NPC inverter, the modulation index M should be between 0.57 and 1. Under such conditions, the reference vector traverses triangles 2, 3 and 4 in each sector. If the reference vector is located in triangle 3 of sector I, for instance, then it has to be synthesized with the vectors V_{S1}, V_{M1} and V_{L1}.

The space vector modulation process is completed by applying the selected voltage vectors to the output according to a switching sequence. A sequence that results in minimum number of transitions is the preferred choice because that leads to high quality output voltage waveform and lower switching losses. To achieve minimum number of switching transitions, a 7-segment switching sequence is usually adopted. It is often convenient to perform "origin shifting" and subsequently perform a three-level modulation using two-level principles [16].
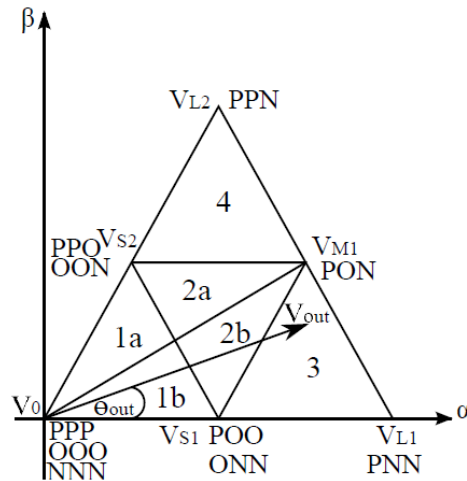
Fig. 4. Space vector diagram for sector I of the conventional NPC inverter

Consider *fig. 4* which depicts the vectors in sector I of the SVD shown in *fig.3*. If the origin is shifted from [PPO/OOO/NNN] to [POO/ONN], the the equivalent null (E-null) state is transferred to [POO/ONN] while the equivalent active (E-active) states are transferred to [PPP/OOO/NNN], [PPO/OON], PON and PNN, respectively. The sequence over time of the application of the selected converter switching states has to be decided for every switching cycle. For instance in triangle 3 the voltage vectors V_{S1} [PPO/ONN], V_{M1} [PON], and V_{L1} [PNN] are selected to synthesize the reference vector V_{out} so the switching sequence used is ONN → PNN → PON → POO → PON → PNN → ONN. The number of switching transitions here is twelve (12).

To enable boost capability, shoot through states have to be inserted in appropriate phase legs. In case of two-level quasi Z-source inverter, shoot-through states are applied using the duration of the null vectors only. The two null vectors in two-level SVM both produce zero line-to-line voltage. Both null vectors and shoot-through states produce zero line-to-line voltage so they can replace each other for voltage boosting. The shoot-through states in the two-level quasi Z-source inverter applies a full short circuit across the dc link.

For the case of qZNPC inverter, the small vectors serve the same purpose as the null vectors of the two-level quasi Z-source inverter. However, there is a difference in that none of the small vectors produces zero line-to-line volage. Thus, if nearest three vector switching is desired then full shoot through cannot be applied. This is the main reason behind the choice of alternate UST and LST in modulating qZNPC inverters. While doing this, we have to ensure that the number of switching transitions is minimized.

We now consider the insertion of shoot-through states when the reference voltage vector is located in triangles 2, 3 and 4. Triangle 1 is not considered because when the reference vector is located in that triangle, the output voltage degenerates into two levels which defeats the purpose of multilevel output voltage. Tables 1 to 4 show the switching sequences and number of switching transistions when the reference voltage vector is located in triangle 2a, 2b, 3 and 4, respectively.

Table 1. Switching transitions in triangle 2a with conventional SVM for qZNPC inverter

	STATES	Qa 1,2,3,4	Qb 1,2,3,4	Qc 1,2,3,4	Switchings
	PPO	1100	1100	0110	
LST	PPL	1100	1100	0111	1
	POO	1100	0110	0110	3
	PON	1100	0110	0011	2
UST	UON	1110	0110	0011	1
	OON	0110	0110	0011	1
UST	UON	1110	0110	0011	1
	PON	1100	0110	0011	1
	POO	1100	0110	0110	2
LST	PPL	1100	1100	0111	3
	PPO	1100	1100	0110	1
Total					16

Table 2. Switching transitions in triangle 2b with conventional SVM for qZNPC inverter

	STATES	Qa 1,2,3,4	Qb 1,2,3,4	Qc 1,2,3,4	Switchings
	ONN	0110	0011	0011	
UST	UNN	1110	0011	0011	1
	OON	0110	0110	0011	3
	PON	1100	0110	0011	2
LST	POL	1100	0110	0111	1
	POO	1100	0110	0110	1
LST	POL	1100	0110	0111	1
	PON	1100	0110	0011	1
	OON	0110	0110	0011	2
UST	UNN	1110	0011	0011	3
	ONN	0110	0011	0011	1
Total					16

Table 3. Switching transitions in triangle 3 with conventional SVM for qZNPC inverter

	STATES	Qa 1,2,3,4	Qb 1,2,3,4	Qc 1,2,3,4	Switchings
	POO	1100	0110	0110	
LST	POL	1100	0110	0111	1
	PON	1100	0110	0011	1
	PNN	1100	0011	0011	2
UST	UNN	1110	0011	0011	1
	ONN	0110	0011	0011	1

	STATES	Qa 1,2,3,4	Qb 1,2,3,4	Qc 1,2,3,4	Switchings
UST	UNN	1110	0011	0011	1
	PNN	1100	0011	0011	1
	PON	1100	0110	0011	2
LST	POL	1100	0110	0111	1
	POO	1100	0110	0110	1
Total					12

A critical study of the switching transitions in Tables 1 to 4 reveals that the switching transitions for triangles 3 and 4 are same as those encountered for the conventional NPC inverter. However, in triangle 2, the number of switching transitions is 16 per switching cycle instead of 12. For an ideal case the number of switching transitions per switching cycle should be 12. However, when shoot-through states are inserted into small vectors, there are regions on the SVD where 12 switching transitions per switching cycle is not possible in three-level SVM for Z-source converters. This is because as the reference vector traverses, there are two types of triangular regions (triangle 2 and triangles 3, 4) that come into the picture over a fundamental cycle. Triangles 3 and 4 offer 12 switching transitions while triangle 2 offers 16 switching transitions per switching cycle. This is the approach employed in [12-14].

Table 4. Switching transitions in triangle 4 with conventional SVM for qZNPC inverter

	STATES	Qa 1,2,3,4	Qb 1,2,3,4	Qc 1,2,3,4	Switchings
	OON	0110	0110	0011	
UST	UON	1110	0110	0011	1
	PON	1100	0110	0011	1
	PPN	1100	1100	0011	2
LST	PPL	1100	1100	0111	1
	PPO	1100	1100	0110	1
LST	PPL	1100	1100	0111	1
	PPN	1100	1100	0011	1
	PON	1100	0110	0011	2
UST	UON	1110	0110	0011	1
	OON	0110	0110	0011	1
Total					12

In triangle 2a, if the positions of PPL and PPO are interchanged the number of switching transitions can be reduced to 14. Similarly, in triangle 2b if the positions of UNN and ONN are interchanged, the number of switching transitions is reduced to 14. Since it is not possible to get 12 switching transitions in triangle 2 over a switching period, the minimum

number of switching transitions after 12 is considered to be the optimal value. Therefore, 14 switching transitions in triangle 2 is considered as an optimal solution. The optimized switching patterns are shown in Tables 5 and 6 respectively.

The proposed optimized SVM approach leads to a reduction in the average switching frequency of the qZNPC inverter compared to the SVM methods found in previous works. This is the main contribution of this paper. With the number of switching transitions in a switching cycle optimized using the proposed approach, the position of UST/LST states in triangle 2 becomes different to those of triangles 3 and 4.

Table 5. Switching transitions in triangle 2a with proposed SVM for qZNPC inverter

	STATES	Qa 1,2,3,4	Qb 1,2,3,4	Qc 1,2,3,4	Switchings
LST	PPL	1100	1100	0111	
	PPO	1100	1100	0110	1
	POO	1100	0110	0110	2
	PON	1100	0110	0011	2
UST	UON	1110	0110	0011	1
	OON	0110	0110	0011	1
UST	UON	1110	0110	0011	1
	PON	1100	0110	0011	1
	POO	1100	0110	0110	2
	PPO	1100	1100	0110	2
LST	PPL	1100	1100	0111	1
Total					14

Table 6. Switching transitions in triangle 2b with proposed SVM for qZNPC inverter

	STATES	Qa 1,2,3,4	Qb 1,2,3,4	Qc 1,2,3,4	Switchings
UST	UNN	1110	0011	0011	
	ONN	0110	0011	0011	1
	OON	0110	0110	0011	2
	PON	1100	0110	0011	2
LST	POL	1100	0110	0111	1
	POO	1100	0110	0110	1
LST	POL	1100	0110	0111	1
	PON	1100	0110	0011	1
	OON	0110	0110	0011	2
	ONN	0110	0011	0011	2
UST	UNN	1110	0011	0011	1
Total					14

4. RESULTS AND DISCUSSION

A simulation exercise in SABER® was undertaken to verify the proposed optimized SVM technique for controlling the qZNPC inverter to perform voltage buck-boost function. The parameters presented in Table 7 were used for the simulation exercise.

Table 7. Parameters used for simulation studies

PV panel output voltage	500 – 600 V
Output voltage to grid	380 - 415 V, line-to-line rms
Grid frequency	50 Hz
Switching frequency	5 kHz
L_1, L_2, L_3, L_4	1 mH
C_1, C_2, C_3, C_4	470 µF

The main contribution of this paper is the optimization of the number of switching transitions during the control of qZNPC inverter to be as close as possible to that of a conventional NPC inverter. When a three-level nearest three vector SVM is implemented in a conventional NPC inverter, the number of switching transitions recorded when the reference vector traverses triangles 2, 3 and 4 is 36. When a similar exercise is done for a qZNPC inverter, the number of switching transitions recorded is 40. Applying the optimized SVM approach to the qZNPC inverter reduces the number of switching transistions from 40 to 38, which is the optimized number obtainable.

Simulation results for the case where the output of the PV array is assumed to be at a maximum of 600 V are shown in *fig. 5*. Under this condition, the qZNPC inverter works in the VSI mode. The required output voltage to the grid is synthesized with a modulation index of 0.915 with the shoot-through duty cycle set to 0. This operation results in a peak output line-to-line voltage of 547.2 V (387 V rms) as expected. This is clearly seen in *fig. 5a*. An output line-to-line voltage waveform with nearest three vector switching is shown in *fig. 5b; fig. 5c* – displays balanced output currents fed to the grid; *fig. 5d* – shows the current drawn from the PV array which is without ripples because shoot-through states have not been activated; *fig. 5e* – shows the capacitor voltages on C_1, C_4 and C_2, C_3 which are 0 V and 300 V, respectively.

To demonstrate the effectiveness of the optimized SVM algorithm described above for controlling the qZNPC inverter to perform voltage-boost operation, we assume the PV array's output voltage drops to the minimum of 500 V as a result of poor weather conditions. To synthesize the required grid voltages, the output of the PV array needs to be boosted. This

is achieved by setting the modulation index and shoot-through ratio to 0.9 and 0.1, respectively. *Figure 6* depicts the main waveforms obtained when shoot-through states are used.
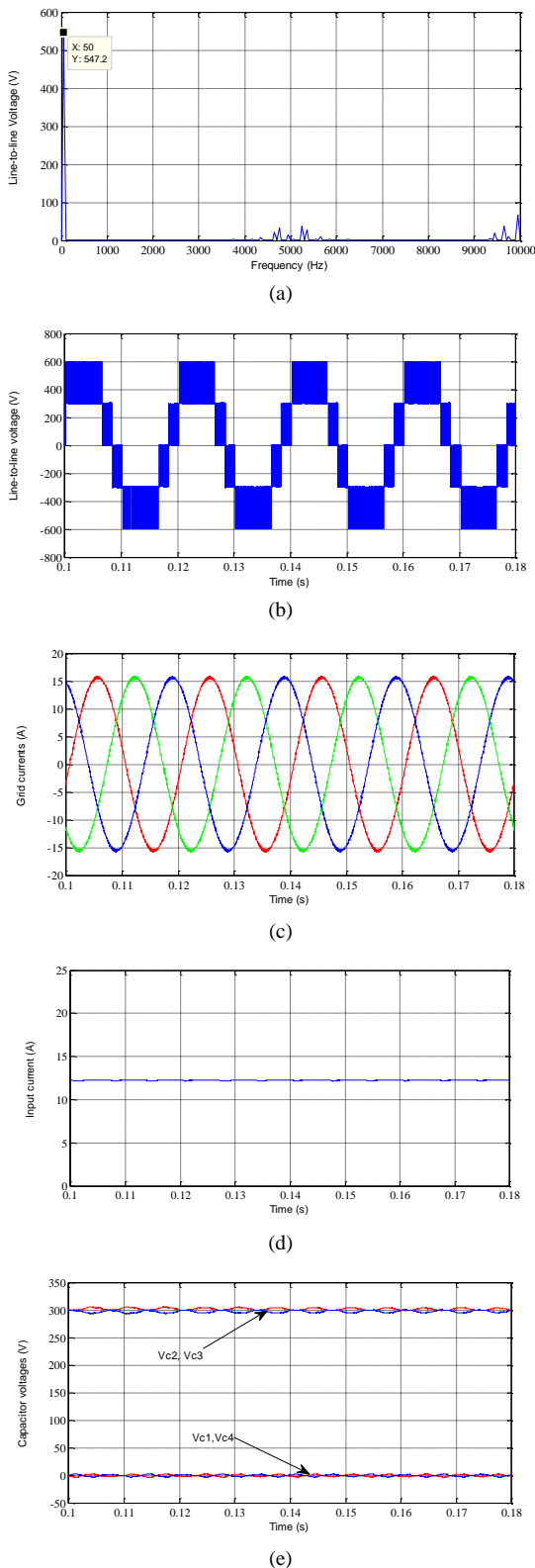
Fig.5 Buck-mode simulation results
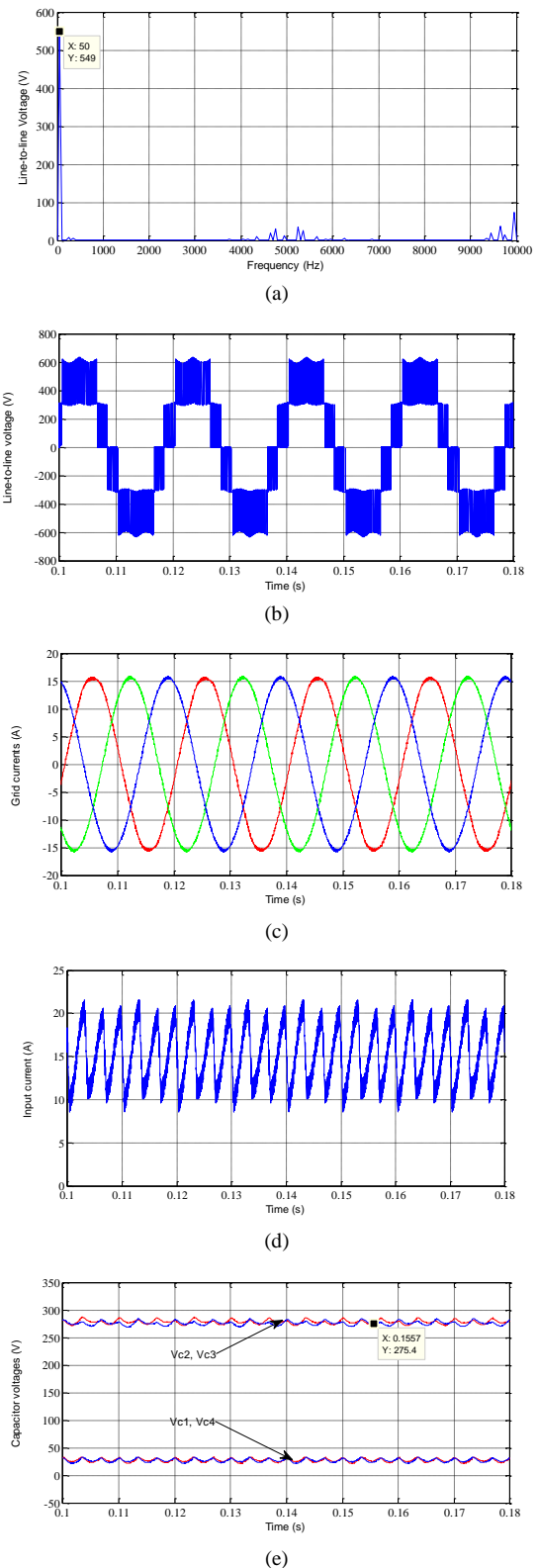
Fig. 6 Boost-mode simulation results

The spectrum of the output line-to-line voltage is shown in *fig. 6a*. This figure clearly shows a fundamental peak line-to-line voltage of 549 V as expected. The waveform for the output line-to-line voltage with nearest three vector switching is clearly shown in *fig. 6b*. *Figure 6c* shows the output currents of the qZNPV inverter which are still balanced and sinusoidal even when shoot-through states are inserted.

The current drawn from the PV array during this operating mode is shown in *fig. 6d*. This current is continuous with ripples resulting from the exchange of energy between the qZ-source inductors and capacitors during the insertion and removal of shoot-through states. The continuous input current drawn by the qZNPC inverter is very beneficial to the PV array. The voltages on the qZ-souce capacitors are also shown in *fig. 6e*.

The simulation results clearly agree well with the presented concepts thereby verifying the optimized SVM algorithm presented earlier. Compared with conventional SVM methods applied to the qZNPC inverter, the approach presented in this paper is cheaper since a reduction in the number of switching transitions will lead to decreased switching losses and therefore decreased total losses which will lead to the use of smaller (and cheaper) heat sinks in the practical implementation.

5. CONCLUSIONS

An optimized SVM technique for controlling a qZNPC inverter has been presented in this paper. Inserting UST and LST states into the conventional NPC inverter's state sequence, voltage buck-boost functionality is achieved in a single-stage structure. The placement of the UST and LST states has been optimized in this paper leading to a reduction in the number of switching transitions per switching cycle compared to existing methods. Using the proposed optimized SVM algorithm leads to reduction in switching losses of the qZNPC inverter. The presented concepts have been verified using simulation results. It is expected that the presented solution will be cheaper than existing methods because of reduction in switching losses which will mostly result in lower overall losses and therefore smaller and cheaper heat sinks will be required in a practical implementation.

REFERENCES

[1]   O. Ellabban, H. Abu-Rub, and F. Blaabjerg, *Renewable energy resources: Current status, future prospects and their enbling technology*, Renew. Sust. Energy Rev., 39, 748-764, November 2014.

[2]   L. Hassaine, E. OLias, J. Quintero, and V. Salas, *Overview of power inverter topologies and control structures for grid connected photovoltaic systems*, Renew. Sust. Energy Rev., 30, 796-

807, February 2014.

[3]   REN21, *Renewables 2015 global status report, 2015*. Available: http://www.ren21.net. Retrieved on November 13, 2018.

[4]   F. Blaabjerg, K. Ma, and Y. Yang, *Power Electronics-The key technology for renewable energy systems*, in proceeding of EVER, pp. 1-11, Monte –Carlo, Monaco, March 2014.

[5]   E. Romero-Cadaval, G. Spagnuolo, I. Garcia Franquelo, C. A. Ramos-Paja, T. Suntio, and W. M. Xiao, *Grid-connected photovoltaic generation plants: Components and operation*, IEEE Ind. Electron. Mag., 7(3), 6-20, September 2013.

[6]   T. B. Soeiro and J. W. Kolar, *The new high-efficiency hybrid neutral-point-clamped converter*, IEEE Trans. Ind. Electron.,vol. 60, no.5, pp. 1919-1935, 2013.

[7]   M. Schhweizer, T. Friedli, and J. Kolar, *Comparative Evaluation of Advanced 3-phase 3-level Inverter/Converter Topologies against 2-level Systems*, IEEE Trans. Ind. Electron, vol. 60, no. 12, pp. 5515-5527, 2013.

[8]   F. Z. Peng, *Z-source inverter*, IEEE Trans. Ind. Appl., 2003, 39, (2), pp. 504-510.

[9]   P. C. Loh, S. W. Lim, and F. Gao, *Three-level Z-source inverters using a single LC impedance network*, IEEE Trans. Power Electron., vol. 22, no. 2, pp. 706-711, 2007.

[10]   P. C. Loh, F. Blaabjerg and C. P. Wong, *Comparative evaluation of pulsewidth modulation strategies for Z-source neutral-point-clamped inverter*, IEEE Trans. Power Electron., vol. 22, no. 3, pp. 1005-1013, 2007.

[11]   J. Anderson and F. Z. Peng, *A class of Quasi Z-source Inverters*, 2008 IEEE Industry Applications Society Annual Meeting, Edmonton, Alta., 2008, pp. 1-7.

[12]   O. Husev, C. Roncero-Clemente, E. Romero-Cadaval, D. Vinnikov, T. Jalakas, *Three-level three-phase quasi-Z-source neutral-point-clamped inverter with novel modulation technique for photovoltaic application*, Electric Power Systems Research, vol. 130, no. 1, pp. 10-21, 2016.

[13]   F.B. Effah, P. Wheeler, J. Clare and A. Watson, *Space-Vector-Modulated Three-Level Inverters With a Single Z-Source Network*, IEEE Trans. Power Electron., vol. 28, no. 6, pp. 2806-2815, June 2013.

[14]   X. Xing, C. Zhang, A. Chen, J. He, W. Wang and C. Du, *Space-Vector-Modulated Method for Boosting and Neutral Voltage Balancing in Z-Source Three-Level T-Type Inverter*, IEEE Trans. Ind. Appl., vol. 52, no. 2, pp. 1621-1631, Mar/Apr. 2016.

[15]   F. B. Effah, P. W. Wheeler, A. J. Watson and J. C. Clare, *Quasi Z-source NPC Inverter for PV Application*, in Proceedings of IEEE PES-IAS Power Africa Conference.

[16]   J. H. Seo, C. H. choi, and D. S. Hyun, *A new simplified space-vector PWM method for three-level inverters*, IEEE Trans. Power Electron., vol. 16, no. 4, pp. 545-550, Jul. 2001.

DIAGNOSIS OF BEARING DEFECTS BY ANFIS IN THE INDUCTION MOTOR

Nabil **TALBI**[1], Abderrezak **METATLA**[1], Toufik **SEBBAGH**[1], Nadir **BOUTASSETA**[2], Mohamed **HASSANI**[2]

[1] *Department of Mechanical Engineering, Faculty of Technology, Université 20 août 1955 Skikda BP 26 Road of El hadaiek,Skikda, Algeria.*

[2] *Research Center in Industrial Technologies CRTI, P.O.Box 64, Cheraga, Algeria.*

n.talbi@ univ-skikda.dz, a.metatla@ univ-skikda.dz, t.sebbagh@ univ-skikda.dz,
boutasseta@gmail.com, moha82.hassani@hotmail.fr

Abstract*: In this paper, we developed a robust technique for fault classification in the induction motor, which was used by the Adaptive Network Reference Information System (ANFIS). A robustness and precision test of the proposed method was performed on a small database. To speed up the response and minimize the calculation time, the most sensitive indicators have been used to ensure the learning of the classifier. The database used was carried out at the University of Case Western, this database has two modes of healthy operation and with rolling defects located side coupling. The objective of the technique used in this paper is to extract the indicators and to test them to select the most sensitive to the apparition of defects. The obtained results show the effectiveness and sensitivity of the proposed approach to identify the nature of the defect even at the birth stage.*

1. INTRODUCTION

The asynchronous motor sometimes called induction motor is the most used motor in the industrial world because of its robustness. In addition, its cost is low as well as the cost of the maintenance and its simplicity [1]. During its operation the induction motor subjected to constraints generates defects which negatively affect the profitability of the drive systems and consequently the productivity of the installations. To ensure the proper functioning of the drive systems therefore the continuity of productivity, it is necessary to ensure a policy of

maintenance to detect and identify the occurrence of defects at the birth stage and to avoid the unexpected shutdown of the installations that causes significant economic losses.

Several categories of methods are proposed for the diagnosis of defects in the literature, surveyed recently in [2], from data processing perspective. We can divide those methods in to three types of methods, namely model-based, signal-based and knowledge-based methods.

The first family of methods that uses a mathematical model describing the normal operating state of the induction motor, model-based methods of fault diagnosis algorithms are developed to monitor the consistency between the measured results of practical systems and model predictions, such as state observing methods, parametric estimation, and parity space utilization. The advantage of this type of method is that the fault diagnosis is very simple since one carries out a direct mapping with the physical coefficients [3].

The methods based on prior knowledge that can be divided into two groups: qualitative methods based on symbolic intelligence and quantitative methods using artificial intelligence. Qualitative methods include failure trees, logging and expert systems, while quantitative methods such as unsupervised learning systems like K-means, C-means, and principal component analysis (PCA) and supervised learning systems including Fuzzy logic, support vector machines (SVM), shallow and deep neural networks, also some hybrid systems like PCA and autoencoder [4], [5], [6].

A study was carried out by Bonnettet. al [7], in the context of diagnosis of various rolling defects in the induction motor. Diallo et.al [8], presented an analysis by shape recognition, were defects created on the rotor and on the stator of the induction motor. Decision procedures based on the k-nearest neighbor rule and direct limit calculation, were used to detect defects. Another work was developed by [9], the authors proposed a technique for detecting and identifying the defects of the induction motor based on the analysis of structured residues of the stator currents. The simulation results obtained by this technique are satisfactory since it is able to detect and identify the defects of breaking bars, ring portions and eccentricity with a good estimate of their tripping time. In [10], the author has developed a method for pattern recognition based on a Multi-Layer Perception Artificial Neural Network (MLPANN) in order to detect and identify eccentricity defects and demagnetization of the synchronous machine. In the study presented in [11], where the author used an approach which based on the classical spectral analysis and a method of classification, inspired by the supervised learning theory of supported vector machines (SVM), enable the detection and identification of the ball bearing defect in the induction motor. In [12], the author proposed a technique of diagnosis of rotor electrical defects in the induction motor based on the analysis of acoustic signals; three motor states have been analyzed.

In addition, the work proposed by [13] presents a fault diagnosis technique in the single-phase induction motor based on acoustic signals. The authors use three classifiers namely the closest neighbor, the closest average and the Gaussian mixing models. Despite the low

operating cost of the proposed technique, the last remains non-invasive since it is sensitive to interference from environmental noise while the classification rate is relatively low.

Reference [14] has proposed an appropriate approach to diagnose rotor imbalance defect in rotating machinery. It's used as a technique of the two classifiers k-nearest neighbor (KNN) and (SVM). Features were taken from the FFT amplitude of the vibratory signals. The classification results obtained by this approach show that the SVM rate of 95.87% is significantly higher than the KNN rate of 77.51%. SVM has been the subject of many applications, this technique has already been exploited by [15] to ensure an automatic classification of bar break defects in induction motors. This technique was also used by [16] and [17] to detect and diagnose the real-time rolling defect and it was very successful. Good bibliographic research was presented by [18] from 2001 to 2014, the purpose of SVM in various data mining tasks such as classification, clustering and forecasting, etc. Despite the effectiveness and good quality of the results obtained by this method, some problems related to this method were mentioned. In the same sense [19] is developed diagnostic technique based on Artificial Neural Networks (ANN) to classify roller bearing defects. The results obtained by this technique give a fault classification accuracy of 93%. In the works of [20] and [21] a fairly efficient technique called adaptive network-based fuzzy inference system (ANFIS) was used to identify the bearing fault in the induction motor. Through this study, we develop a new approach for detecting and classifying induction motor defects using ANFIS.

It allows the identification of the majority of faults from birth precisely and in real time. In order to allow early classification of defects using limited samples, which facilitates online diagnosis, the approach has been optimized.

Our goal is to synthesize a new diagnostic approach and establish criteria of choice for their use in order to make a very advanced practical contribution to the diagnosis of induction motor defects. Our contribution is structured as follows:

• In the literature, many works use vibration signal processing with different approaches to signal processing. In our study, instead of using the vibration signal, we propose an approach based on an ANFIS algorithm to classify induction motor defects.

• In a second step, a fault diagnosis approach based on an efficient classifier formed on a small dataset was proposed.

This work is organized as follows. In section 2 we present a statistical study of defects that affect the induction motor. A detailed description of the test bench used in this work is presented in Section 3. The fourth section was devoted to the architecture of the developed approach. First, we presented the vibratory signals, this step will be followed by a pre-processing step which consists of extracting the characteristics related to the evolution of defects in order to give a reduced representation of the vibratory signals before performing the identification and classification of defects. The fifth section was devoted to the presentation of the ANFIS classifier used for the classification of defects. In the last section contains an

experimentation phase and discussion of obtained results. The study was terminated by conclusion and perspective.

2. DEFECTS IN INDUCTION MOTOR

Any extraordinary stress that penalizes and causes total or partial paralysis and disrupts the good functioning of the engine is considered as a defect. The induction motor fault is original: electrical, mechanical and magnetic. It can occur on one of the organs that constituted them namely: the bearing, the stator, the rotor and the shaft. According to the recent statistical study presented in [22], the default rate for each component of the motor is shown in the figure below:
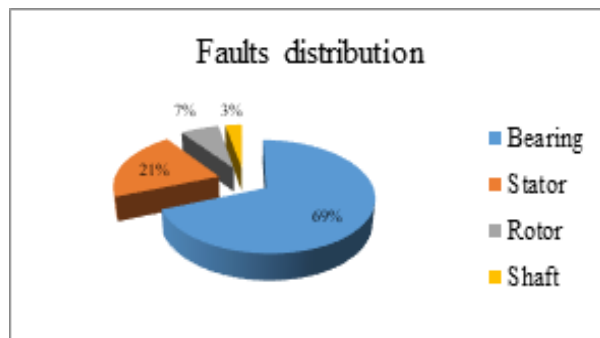
Fig. 1. Statistical study of induction motor defects [23]

In this study, the bearing failure rate has a large range compared to other defects, for this reason, it is recommended to guide our study into bearing defaults and this to show its influence on the dynamic behavior of the induction motor.

The causes and consequences of rolling fault are presented in the following table:

Table 1. Faults description in the induction motor.

Defects	Illustration	Causes	Effects
Rolling fault		The rolling fault is generally related to the wear of the bearingand more specifically a degradation of the balls, or the tread, caused by: ➢ Wear due to aging, ➢ High operating temperature, ➢ Loss of lubrication, ➢ Contaminated oil.	Oscillation of the load torque, ➢ Appearance of additional losses, ➢ Vibration by the displacement of the rotor around the longitudinal axis, ➢ Generates additional harmonicson the signature of power supplies.

3. DATABASE DESCRIPTION

The effectiveness of the proposed method cannot be definitively validated until the real conformity of the obtained data that is why one refers to the data acquired on the test bench available which are posted on the website of University Case Western Reserve [23]. This test bench illustrated in *figure 2* is a very simple design, it allows the assembly and disassembly of the two bearings tested, it consists essentially of a 2-horse induction motor and a dynamometer that allows applying different loads (in this case the applied loads are of the order 0, 1, 2 and 3 Hp). The latter is connected to the motor by an elastic coupling. In order to measure the vibrations of the motor, two accelerometers were placed at the level of the bearing on one side drive and the other side fan. There is also a speed sensor to measure the actual speed of rotation of the motor.
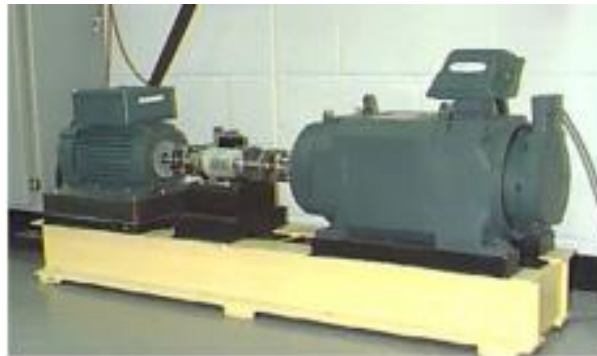
Fig.2. Test bench [24].

Defects are inserted separately on the three elements of the bearing as follows: the outer ring, inner ring and rolling elements. The defects studied on the turnover of the coupling end (drive side) are characterized by the following parameters:

- Number of holes = 1
- Diameter of the defect = 0.07, 0.14 and 0.21 inches.
- Depth of defect = 0.0118 inches.

The defect realized is well explained in the *figure 3*:
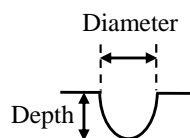
Fig. 3 Point defect on a bearing

4. ARCHITECTURE OF THE DEVELOPED APPROACH

The principle of the approach developed in this work is based on the use of a rather robust technique for classifying rolling defects from the vibratory signals that characterize each mode of operation.

The proposed approach has been divided into three stages. In a first step, we have represented the vibration signals for each mode of operation. In the next step, a data preprocessing operation was performed; firstly, the calculation of the fifteen statistical indicators was performed on the dataset. Among which, the most sensitive to defects have been taken into consideration. Finally, the ANFIS classifier was used with different operating scenarios of the induction motor. The different stages of the approach developed were presented in *figure 4*.
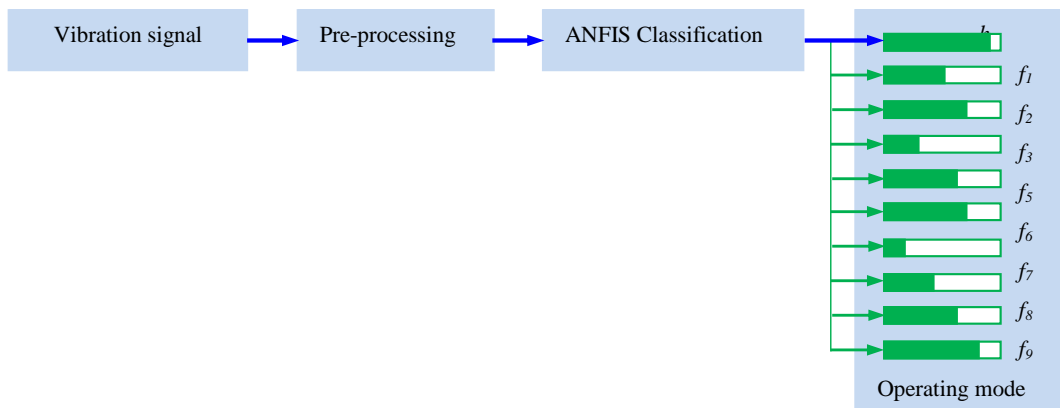
Fig.4. Breakdown Different stages of the approach.

5. VIBRATION SIGNAL

In this study, only ten (10) operating states were used for classification because of the availability of information needed for these cases. *Figure 5 (a - j)* shows the vibratory signals measured at the level of the rolling bearing on the coupling side in a normal state, then in a failed state. The fault state is divided into three types of defects occurring on the inner ring, the outer ring and the balls, each of which is expressed by three drill sizes of the order of 0.07, 0.14 and 0.21 inches. Knowing that the sampling frequency is 12000Hz.

It is found that at each state of operation of the bearing presented by a signal which is characterized by a very large number of points (N = 24000) which is difficult to exploit. For this purpose, it is necessary to minimize this number by means of the statistical indicators which make it possible to characterize each signal.
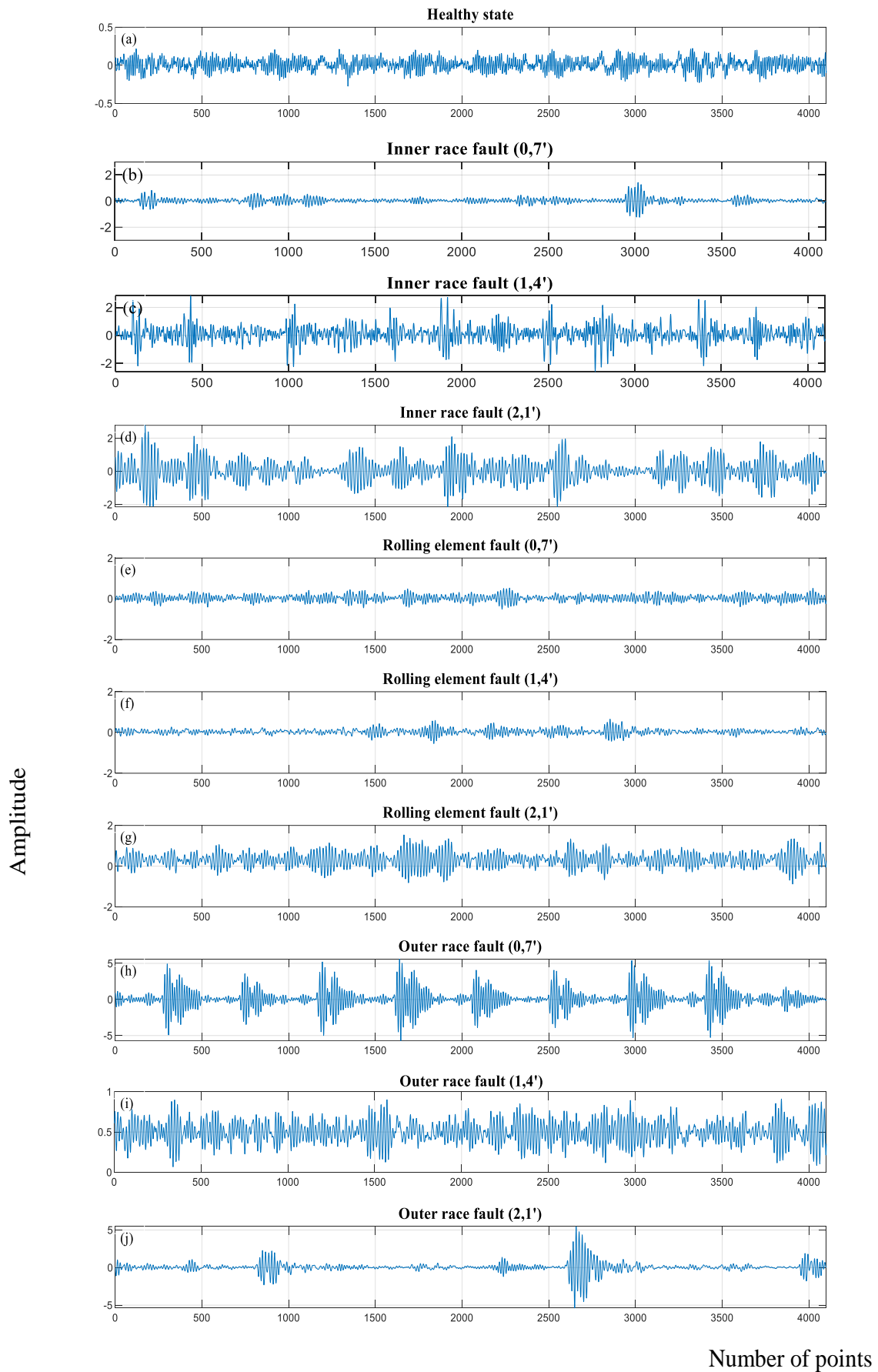
Fig.5. Vibratory signals of different rolling states.

6. PRETREATMENT (PRE-PROCESSING)

This step involves the extraction of the indicators that characterize the vibratory signals. First, the calculation of the statistical indicators on the dataset was done. Second, among these indicators those most sensitive to defects were selected.

Several statistical indicators exist in literatures, more or less efficient and adequate to characterize a given signal. The most used indicators are described in Table 2.

Table 2. Statistical indicators

Statistical parameters	Equation
Average	$X_{\text{var}} = \sum\limits_{k=1}^{N} x(n)/N$
Standard deviation	$\sigma' = \sqrt{\sum\limits_{n=1}^{N} (x(n) - x_m)^2 / N}$
Variance	$X_{\text{var}} = \sum\limits_{k=1}^{N} (x(n) - x_m)^2 / N$
RMS value	$X_{\text{eff}} = \sqrt{(1/N)\sum\limits_{n=1}^{N} x((n))^2}$
Maximum amplitude	$X_{\max} = \max \vec{x}|x(n)|$
Minimum amplitude	$X_{\min} = \min|x(n)|$
Skewness (biais)	$X_{ske} = \sum\limits_{n=1}^{N} (x(n) - x_m)^3 /(N-1)\sigma^3$
Kurtosis	$x_{kur} = \sum\limits_{n=1}^{N} (x(n) - x_m)^4 /(N-1)\sigma^4$
Crest factor CF	$\text{CF} = x_{\max}/x_{eff}$
Clearance factor CLF	$CLF = x_{\max} / \left(\dfrac{1}{N} \sum\limits_{n=1}^{N} \sqrt{|x(n)|} \right)^2$
Shape factor SF	$SF = x_{eff} / \dfrac{1}{N} \sum\limits_{n=1}^{N} |x(n)|$
Impulse factor IF	$IF = x_{\max} / \dfrac{1}{N} \sum\limits_{n=1}^{N} |x(n)|$
Mean absolute deviation MAD	$MAD = \sum\limits_{n=1}^{N} \left(\left| \sum\limits_{n=1}^{N} (x(n) - x_m) \right| / N \right)$
Central Moment CM	$CM = \sum\limits_{n=1}^{N} \left(\sum\limits_{n=1}^{N} (x(n) - x_m)^p / N \right)$
Range	$x_{range} = |x_{\max} - x_{\min}|$

For extracting the most effective indicators, we tested their sensitivity to the detection of defect. The choice was made on the most sensitive among the samples. We found that RMS, standard deviation, minimum, maximum and Skewness are the most sensitive; their evolution is influenced by the presence and size of the defect.

Figures. 6 and *7* respectively illustrate the shape of the time signals and the variation of the indicators for N samples, in a healthy state of rolling afterwards in a state where it turns out that the fault comes from the outer ring with three drilling sizes different (i.e. with a drilled diameter of 0.7, 0.14 and 0.21).
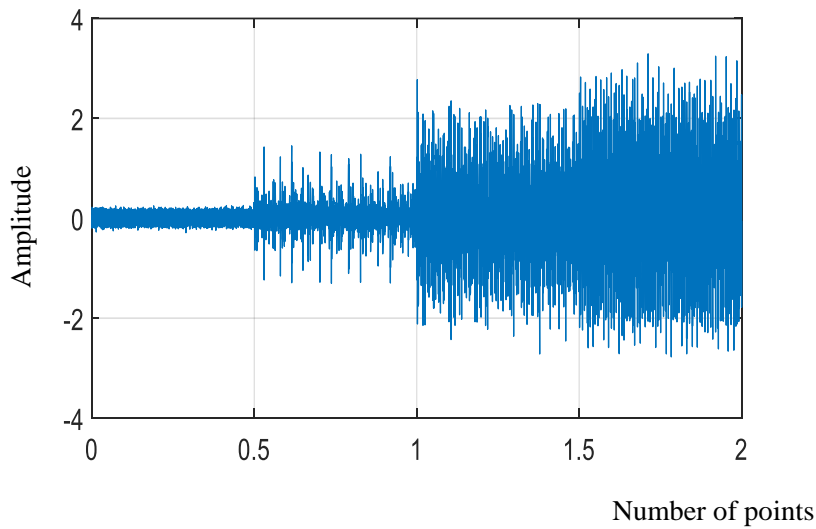
Fig.6. Succession of vibratory signals.
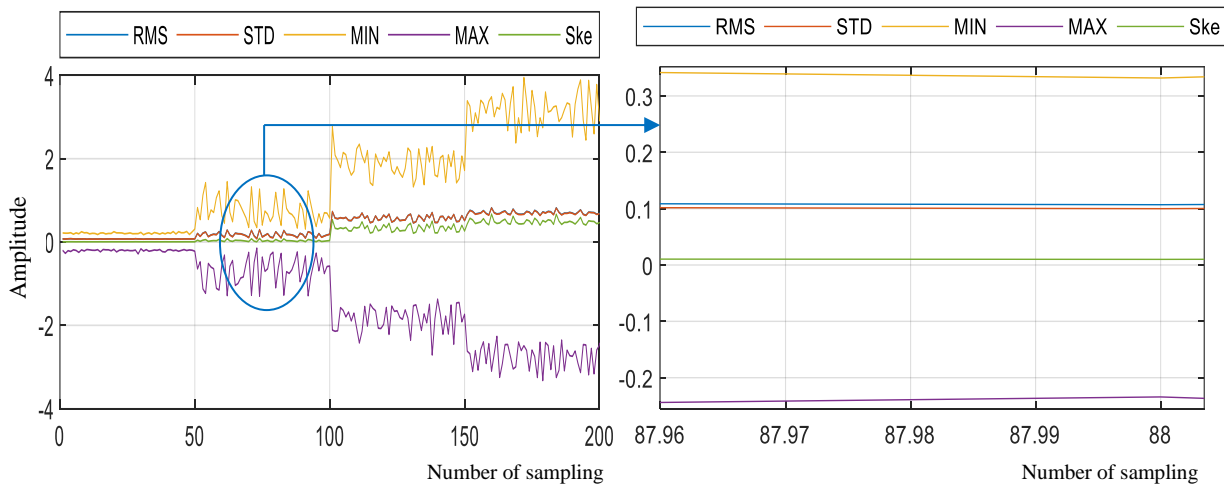
Fig.7.Evolution of the most sensitive indicators.

After selecting the most significant indicators, the classification step is followed to identify the nature and size of defects generated.

7. GENERAL INFORMATION ABOUT ANFIS

An adaptive network-based fuzzy inference system (ANFIS) is an improved type of artificial neural network based on the fuzzy inference system. The method was developed by Jang in 1993 [24]. ANFIS is the result of the fusion of the two combined methods. It simultaneously integrates hybridization of the neural network and fuzzy logic. Its inference system corresponds to a set of fuzzy (if - then) rules with the ability to learn nonlinear functions.

In this article, the classification of defects has been modeled by a new concept, it exploits the set of results obtained from the computation of the relevant temporal indicators (f_1, f_2 ...) on vibratory signals. *Figure 8* is the architecture of the adaptive fuzzy inference system, where: A_1, A_2, B_1, B_2 are fuzzy sets and the terminology of the three nodes are: *M*: multiplication, *N*: normalization, *S*: summation.

The output function *F* is expressed as follows:

$$F = \frac{w_1}{w_1 + w_2}\left(p_1.f_1 + q_1.f_2 + r_1\right) + \frac{w_2}{w_1 + w_2}\left(p_2.f_1 + q_2.f_2 + r_2\right) \quad (1)$$

where w_1, w_2 are the synaptic weights.

If we ask that: $W_1 = \dfrac{w_1}{w_1 + w_2}$ and $W_2 = \dfrac{w_2}{w_1 + w_2}$ these last two are called the standardized versions.

The linear combination of the design parameters p_1, q_1, p_2, q_2 obtained during the learning process makes us rewrite the output function as follows:

$$F = W_1\left(p_1.f_1 + q_1.f_2 + r_1\right) + W_2\left(p_2.f_1 + q_2.f_2 + r_2\right) \quad (2)$$
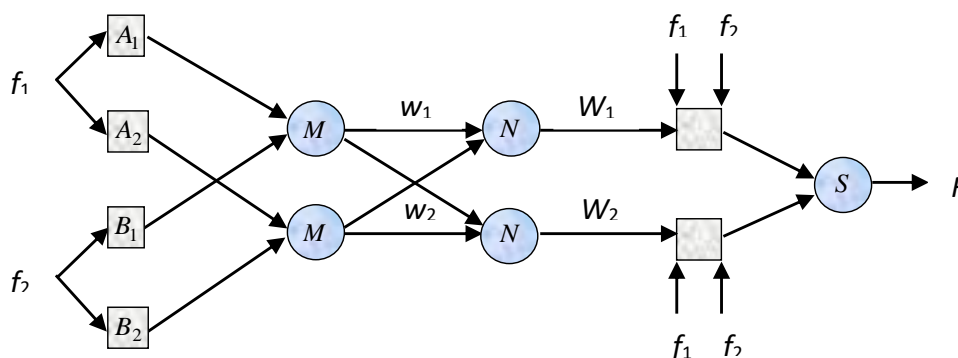
Fig.8.Architecture of ANFIS

To validate the proposed technique, we have taken ten rolling operation scenarios in different states (normal functional, defected for three size cases) that are presented in *figure 3*. This study therefore becomes a classification problem. where the number of classes is equal to the number of cases. Each signal is fragmented into several sections of the same size (N = 4100 samples). On each section the five selected indicators are calculated. The total of all data is equal to 590 samples, which are divided into two groups of data, one for the training that contains 490 samples and the other for the test that contains 200 samples that will be inserted into the sample ANFIS classifier. The data sets as well as the different states of the bearing are illustrated in detail in Table 3.

Table 3. Description of the database

Rolling condition	Diameter of the defect (in inches)	Charge (Ch)	Number of samples for learning	Number of samples for the test	Class
Healthy (h)		0, 1, 2, 3	49	10	1
Outer race (f_1)	0.07	0, 1, 2, 3	49	10	2
Outer race (f_2)	0.14	0, 1, 2, 3	49	10	3
Outer race (f_3)	0.21	0, 1, 2, 3	49	10	4
Inner race (f_4)	0.07	0, 1, 2, 3	49	10	5
Inner race (f_5)	0.14	0, 1, 2, 3	49	10	6
Inner race (f_6)	0.21	0, 1, 2, 3	49	10	7
Rolling element (f_7)	0.07	0, 1, 2, 3	49	10	8
Rolling element (f_8)	0.14	0, 1, 2, 3	49	10	9
Rolling element (f_9)	0.21	0, 1, 2, 3	49	10	10
Total			590		

8. EXPERIMENTS

To be able to quickly diagnose faults, it is necessary to make a compromise between learning speed, memory utilization, accuracy and interoperability. This is why we chose to use an ANFIS classifier in this work, with the extraction of the indicators directly from the data signals already made during the pre-processing phase.

Our algorithm is essentially written in MATLAB. We used Image Processing Toolbox TM as well as Statistics and Machine Learning Toolbox TM. The application is run on a Core i5 processor with a clock of 2.70 GHz and 8 GB of RAM.

Once the learning process is functional in a suitable manner, the test step validates the effectiveness of the proposed method, and this through the illustrated confusion matrix as follows:

$$C = \begin{bmatrix} 10 & 0 & 0 & 0 & 0 & 0 & 0 & 0 & 0 & 0 \\ 0 & 10 & 0 & 0 & 0 & 0 & 0 & 0 & 0 & 0 \\ 0 & 0 & 10 & 0 & 0 & 0 & 0 & 0 & 0 & 0 \\ 0 & 0 & 0 & 10 & 0 & 0 & 0 & 0 & 0 & 0 \\ 0 & 0 & 0 & 0 & 10 & 0 & 0 & 0 & 0 & 0 \\ 0 & 0 & 0 & 0 & 0 & 10 & 0 & 0 & 0 & 0 \\ 0 & 0 & 0 & 0 & 0 & 0 & 10 & 0 & 0 & 0 \\ 0 & 0 & 0 & 0 & 0 & 0 & 0 & 10 & 0 & 0 \\ 0 & 0 & 0 & 0 & 0 & 0 & 0 & 0 & 10 & 0 \\ 0 & 0 & 0 & 0 & 0 & 0 & 0 & 0 & 0 & 10 \end{bmatrix}$$

Fig.9.Confusion matrix obtained by the classifier ANFIS

The confusion matrix, in the terminology of supervised learning, is a tool for measuring the quality of a classification system. Each column of the matrix represents the number of occurrences of an estimated class, while each row represents the number of occurrences of an actual (or reference) class. The data used for each of these groups must be different. One of the interests of the confusion matrix is that it quickly shows whether the system is able to classify correctly or not.

We consider a classification system whose purpose is to classify e-mail into two classes: normal e-mails and spam. We will want to know how many normal emails will be falsely estimated as spam (false alarms) and how many spam will not be estimated as such (no detections).

All the classification results obtained by the ANFIS are summarized in the table.

Table 4: Score with execution time

Type of classifier	Classification score %	Execution time (s)
ANFIS	100%	24,364

From the results displayed by the confusion matrix, we find that among the set of classes tested, it turns out that all the states are well assigned to their classes. Especially since this approach is able to classify large and small size defects.

A perfect classification rate is only the sum of the diagonal elements.

We clearly notice that the three low gravity defects were perfectly assigned to their appropriate classes, and this reinforces our belief that this system is viable. In the continuation of our work and for the good decision of the reliability of the proposed method, one uses a large database.

9. ACCURACY OF DEFECT CLASSIFICATION

To ensure the safety of people and equipment in the world of industry, a system is needed to know the occurrence of a failure in real time. This type of system is affected by two main factors:

1- The time needed to make a good prediction,
2- The time needed to make a good decision.

We test our method by reducing the number of samples needed to create a discriminant descriptor in order to obtain a good classification (minimization of execution time or fast response speed).

To evaluate the minimum number of samples needed to obtain a good classification of defects. *Figure 10* illustrates the number of samples necessary to give a good decision with the classifier used.

From the appearance of the variation of the error as a function of the number of iterations, we find that at the 6th iteration the error decreases to the value zero.
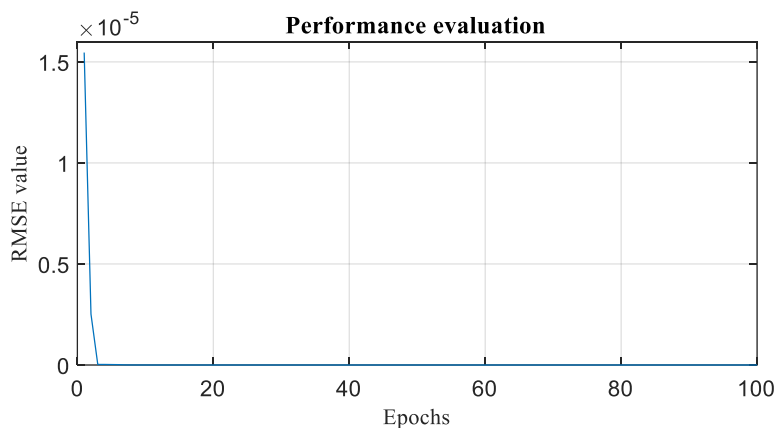
Fig.10.Performance of the ANFIS

10. CONCLUSION

In this paper, a new approach based on the use of ANFIS as a modern technique is developed. It makes possible to diagnose the nature of defect as well as, its gravity; the learning of this technique is also based on the indicators most sensitive to defects. The test results clearly show that there are five most sensitive indicators that are RMS, standard deviation, minimum, maximum and Skewness.

To obtain the classification rate of rolling defects the ANFIS classifier previously formed by the most defect-sensitive indicators is used. The results obtained show that the

proposed technique has made it possible to classify the nature of the defect as well as its size with great precision.

REFERENCES

[1]   N. Bessous, S.E.Zouzou, W.Bentrah, S.Sbaa, and M. Sahraoui, *Diagnosis of bearing defects in induction motors using discrete wavelet transform*, International Journal of System Assurance Engineering and Management, vol. 15, no. 4, pp. 1-9, Jul. 2015.

[2]   Y. Merizalde, L. Hernandez,-Callejo and O. Duque-Perez, *State of the art and trend in the monitoring detection and diagnosis of failures in electric induction motors*, Energies, Vol, 10, 1056, 2017.

[3]   X. Dai and Z. Gao, *From Model, Signal to Knowledge: A Data- Driven Perspective of Fault Detection and Diagnosis*, IEEE Transactions on Industrial Informatics, vol. 9, no. 4, pp. 2226–2238, 2013.

[4].   Y. Qi, S. Changquing, D. Wang, J.Shi, X. Jiang and Z. Zhu, *Stacked space auto encoder based deep network for fault diagnosis of rotating machinery*, IEEE Access, doi, 10, 1109/Access, 2728010,volume 5,pp: 1506-15079, 2017.

[5]   G.E. Hinton, *Learning multiple layers of representation*, Trends in cognitive sciences, vol. 11, no. 10, pp, 428-434, 2007.

[6]   Y. Kim, *Convolutional neural networks for sentence classification*, arXiv preprint arXiv : 1408.5882, 2014.

[7]   A. H. Bonnett, *Cause and analysis of anti-friction bearing failures in A.C induction motors*, IEEE Transactions on Industry Application., pp. 14-23, Sept/Oct, 1993.

[8]   D. Diallo, M. E.Benbouzid, D.Hamad, and X. Pierre, *Fault detection and diagnosis an induction machine Drive: A pattern recognition approach based on Concordia stator mean current vector*, IEEE Transactions on energy conversion, Institute of electrical and Electronics engineering, vol. 20, no. 3, pp. 512-519. 2005.

[9]   A. Metatla, S.Benzahioul, and S. Haddad, *Induction Motor Failure Identification by Analyzing Structured Residues*, Proceeding of the 9th International Conference on Ecological Vehicles and Renewable Energies (EVER). 2014.

[10]   K. Guota,and A.Kaut,*A review on fault diagnosis on induction motor using artificial neural networks, International journal of science and research*, vol. 3. 2014.

[11]   F. Ta_nine, F.Mokrani, K. Antoni, J.Kabla, and Z. Asradj, *Introduction des SVM en MCSA*, 4th International conference, Sciences of electronic, technologies of information and telecommunications. March 25-29, Tunisia 2007.

[12]   A. Glowacz, *Recognition of acoustic signals on induction motors with the use of MSAF10 and byes classier*, Arc. Metall. Mater., vol. 60, no. 1, pp. 153-158. 2016.

[13]   A. Glowacz, W.Glowacz, Z.Glowacz, and J.Kozik, *Early fault diagnosis of bearing and stator faults of thesingle-phase induction motor using acoustic signals*, Measurement. vol. 113, pp. 1-9. 2018.

[14] M. Moosavian, H.Ahmadi, B.Sakhaei, R.Labbafi, *Support vector machine and K-nearest neighbour for unbalanced fault detection*, J. Q. Maint. Eng, vol. 20, pp.65–75. 2014.

[15] N. Hamdad, and K. Hammouche, *Hilbert Huang Transform and Pattern Recognition to detect defects in induction motor*, 4th International Conference on Electrical Engineering (ICEE). 13-15 Dec. 2015.

[16] J. S. L. Senanayaka, S. T. Kandukuri, Huynh Van Khang, and K. G. Robbersmyr, *Early detection and classification of bearing faults using support vector machine algorithm*. IEEE Workshop on Electrical Machines Design, Control and Diagnosis (WEMDCD) (Nottingham: UK). pp. 250-255. 2017

[17] W. Jie, T. Tang, C. Ming, and H. Tianhao, *Self-Adaptive Spectrum Analysis Based Bearing Fault Diagnosis*, Sensors, vol.18, 2018

[18] J. Nayak, B. Naik, and H. S. Behera,*A comprehensive survey on support vector machine in data mining tasks: Applications and challenges*. International Journal of Database Theory and Application, Vol.8, no. 1, pp.169-186.2015.

[19] J. B. Ali, N. Fnaiech, L. Saidi, B. Chebel-Morello,F. and Fnaiech, *Application of empirical mode decomposition and artificial neural network for automatic bearing fault diagnosis based on vibration signals*, Applied Acoustics, vol. 89, pp. 16–27, 2015.

[20] I. Attoui, N. Fergani, N. Boutasseta, B. Oudjani, and A. Deliou, *A new time–frequency method for identification and classification of ball bearing faults*, J. Sound Vibrat., vol. 397, pp. 241–265, Jun. 2017.

[21] I. Attoui, N. Boutasseta, N. Fergani, B. Oudjani, A. Deliou, *Vibration-based bearing fault diagnosis by an integrated DWT-FFT approach and an adaptive neuro-fuzzy inference system*, 3rd International Conference on Control, Engineering & Information Technology, IEEE, pp. 1–6. 2015.

[22] MA. Khan, Y. Kim, J. Choo, *Intelligent fault detection via dilated convolutional neural networks,* IEEE International Conference on Big Data and Smart Computing (Big Comp), pp 729–731. 2018.

[23] Case Western Reserve University Bearing Data Center Website (http://csegroups.case.edu/bearingdatacenter/home).

[24] J.-S.R.Jang,*ANFIS: adaptive-network-based fuzzy inference system*, IEEE Transactions on Systems, Man, and Cybernetics, Vol. 23, no. 3 , pp. 665 – 685, 1993.

OPTIMIZATION AND CONTROL STRATEGY OF MULTI-SOURCE SYSTEM USING GENETIC ALGORITHM

Amina **GABOUR**, Samia **BENZAHIOUL**, Abbderrezak **METATLA**, Toufik **SEBBAGH**

LGMM Laboratory, Université 20 Aout 1955 - Skikda, Algeria

a.gabour@univ-skikda.dz, sbenzahioul@univ-skikda.dz, a.metatla@univ-skikda.dz, t.sebbagh@univ-skikda.dz

Abstract*: The aim of this paper is to design the sizing and optimization of multi-source system PV/Diesel/Battery, whereat the power management algorithm is applied to feed load in Algeria where the GA method is used to find the best configuration of the system and for sizing purpose of the components, based on the minimum total cost of the system (STC) subject to renewable energy fraction (FR).Thus, the results show the impact of RF on the STC in addition to the choice of the best configuration and the most adequate one.*

1. INTRODUCTION

Renewable energy systems gained an outstanding significant interest. They are considered as a solution to face the reduction of fossil fuel resources which cause the CO emissions.

Besides, Algeria initiates a dynamics of green energy by launching an ambitious program for development purpose of Renewable energy and energy efficiency, for which purpose, the Government aims to developing solar energy. Likewise, Algeria is located in the centre of North Africa between the 358 and 388 of latitude north and 88 and 128 longitude east, whose surface is assessed to 2,381,741 km^2 whereat the Sahara occupies 80% of the total area [1], it is characterized by high solar radiation intensity. Subsequent to which, the photovoltaic systems have recently been used for various applications in Algeria, in respect such as: Electrification, pumping water, telecommunication, public lighting etc.

At the current time, solar systems are considered as one of the most popular sources, namely in research level. Further, there exist a lot of studies in the literature related to hybrid PV system size optimization, cost analysis, among which [2-9].

In the paper [2], genetic algorithms are applied for sizing remote PV systems and a comparison with two classical methods, worst month method and loss of power supply probability (LPSP) method are made. A year of synthetic hourly meteorological data of Adrar, Algeria, generated by PVSYST software, has been used in the simulation. The methods have been applied to a PV lighting systems with orientation due south and inclination angles between 0° and 90° to define the lowest cost of the system. Genetic algorithms and worst month methods give results close to each other between 0° and 60° but the system is largely oversized by the worst month method when the tilted angle is over 60°. Yahiaoui et al. [3], worked on optimization of PV/DG systems in Algeria using particle swarm optimization (PSO) algorithm. The constraint method has applied to minimize three objectives' functions, the total cost of the system, loss of load probability (LLP) and CO_2 emission of the hybrid power generation system. Results demonstrated that the combination of the two power sources (PV-Diesel) is required to be able to cover the energy deficit. Also in [4], PSO and the ε-constraint method have been applied to minimize optimal sizing of an autonomous hybrid PV/diesel system in a rural village of Ilamane, province of Tamanrasset, Algeria. Three objective functions are considered the total cost of the system (ACS), the loss of load probability (LPP) and the total CO_2 emissions produced by diesel generators. In the study, the ε-constraint method is used to handle constraints and multiple objectives of the system with simplicity and computational efficiency. In another study [5], PSO is used for an Optimal Sizing for PV systems in isolated island in East Nusa Tenggara, Indonesia. The objective function of the system is considered the Annual cost of system (ACS). The optimal sizing consists of 75,300 × 165W PV panels, 3×5MWh of battery banks (Batt) and 12MW of Diesel Generator (DG) units. A modeling and Cost Analysis of three different power generating configurations DG, PV/Batt and PV/DG/Batt in Tunisia, Jordan and Kingdom of Saudi Arabia (KSA), are presented in [6]. Further, two criteria are considered in this approach: initial investment and operational costs in addition to pollutant emission. Also, numerical simulations are applied to model these systems then characterize their performance. The best solution in Saudi Arabia was using diesel engine. However, using diesel engines leads to rise in pollutant emissions. Likewise, it was found that the best power supplying configuration in Tunisia and Jordan is the PV/DG/Batt. In [7] a developed simulation program using iterative approach is used to optimize the sizes of PV/Batt system, for electrification of small community in Palestine. Economic analysis is done based on life cycle cost to define the lowest Cost Of Energy (COE). The results showed that the lowest COE is found 0.326 $/kWh and happens at 100% PV contribution and 0.7 autonomy days (AD). Artificial Bee Colony Algorithm (ABC) applied in [8] for optimal sizing of stand-alone PV system in Helwan city, Egypt. Two objective functions are used. The first is the maximization of the PV module

output power, whilst the second represents the minimization the life cycle cost (LCC). Also, comparison between ABC algorithm and Genetic Algorithm (GA) optimal results is made. The results demonstrated that the ABC is more efficient than GA in obtaining the optimal cost of the PV system. In the paper from Bataineh [9], PV system design is presented to provide electricity for a single residential household in rural area in Jordan. A computer program is developed to finding the optimal combination of PV array and batteries for the design of stand-alone photovoltaic systems in terms of reliability and costs. Life cycle cost (LCC) and annualized unit electrical cost of system are calculated.

In addition, there exist several commercial software in literatures which were developed for optimization of standalone and hybrid PV systems, they can be found in [10] in full details.

Above and beyond, for evaluation purpose of the performances of PV-Battery-Diesel system to supply electricity to the remote site in Algeria, GA was used to find the best configuration considering different constraints.

This paper explores the importance of the renewable factor (RF) in minimizing the total investment cost (STC) of the multi-source system.

2. CONFIGURATION AND MODELING OF THE MULTI-SOURCE SYSTEM

The multi-source system proposed in this study is shown in *figure 1*. Thus, the power system consists of photovoltaic generator, Diesel generator and a battery bank.
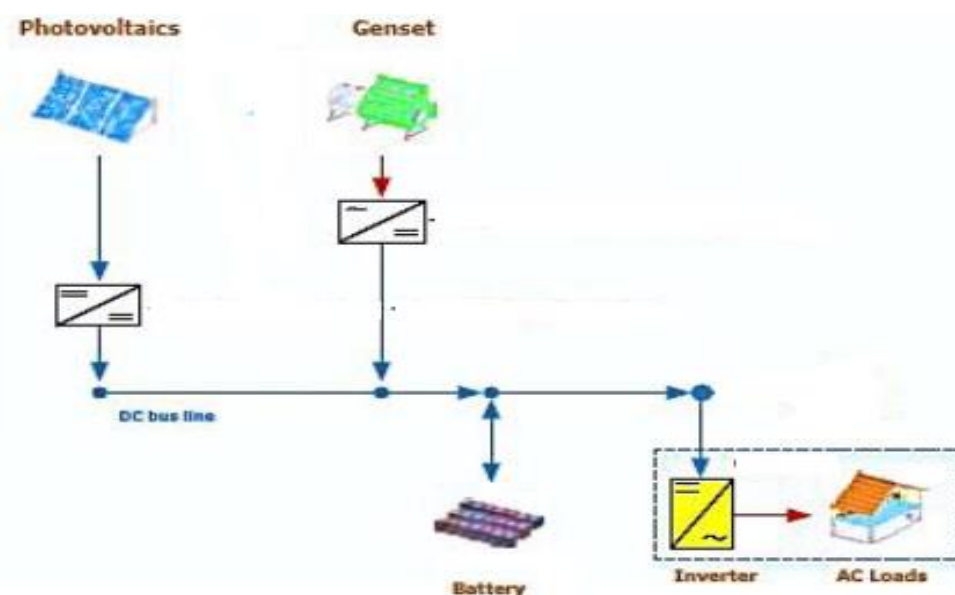
Fig.1. Configuration of a multi-source system

2.1. PV system

The hourly output power of a PV panel can be written as follows [11]:

$$P_{PV}(t) = V_{CO}(t).I_{sc}(t).FF \tag{1}$$

$$I_{sc}(t) = [I_{sct} + K_i.(T_c(t) - 25)].\frac{G(t)}{1000} \tag{2}$$

$$V_{CO}(t) = V_{cost} - K_v.T_c(t) \tag{3}$$

$$T_c(t) = T_a(t) + \frac{NOCT - 20}{800}.G(t) \tag{4}$$

where: I_{sct} (A) is the standard short circuit current, K_i (A /°C) is the short circuit current temperature coefficient, $G(t)$ (W/m²) is the global irradiance incident on the PV module, V_{cost} (V) is the standard open circuit voltage, K_v(V/°C) is the open circuit voltage temperature coefficient, T_c (°C) is the temperature which can be estimated from the ambient temperature, T_a (°C) and the solar radiation and FF is the fill factor.

The total hourly output power of the PV modules ($P_{PV}(t)$) can be calculated by:

$$P_{PV}(t) = N_{PV,p}.N_{PV,s}.P_{PV}(t) \tag{5}$$

where $N_{PV,p}$ is the number of panels connected in parallel, variable of optimisation, $N_{PV,s}$ is the number of panels connected in series, it is calculated as:

$$N_{PV,s} = \frac{V_{bus}}{V_{PV,nom}} \tag{6}$$

V_{bus} is the DC bus voltage, it is chosen to be equal to 48 V and $V_{PV,nom}$ is the nominal voltage of the PV module.

2.2. Battery bank

For charging process and discharging process of the battery bank, the storage battery capacity is subject to the following constraints [12]:

$$C_{batmin} \leq C_{bat}(t) \leq C_{batmax} \tag{7}$$

C_{batmin} and C_{batmax} are calculated as discussed in [13], they are the maximum and minimum allowable storage capacity.

C_{batmin}, is determined by:

$$C_{batmin} = (1 - DOD)C_{batmax} \qquad (8)$$

The total number of the batteries is defined by:

$$N_{BAT} = N_{BAT,p}.N_{BAT,s} \qquad (9)$$

where: $N_{BAT,p}$ is the number of panels connected in parallel, variable of optimization; $N_{BAT,s}$ is the number of batteries connected in series, is calculated as:

$$N_{BAT,s} = \frac{V_{bus}}{V_{BAT,nom}} \qquad (10)$$

The storage battery capacity is computed during the charging state as follows:

$$C_{bat}(t) = C_{bat}(t-1) + (P_{RE}(t) - (P_{load}(t)/\eta_{inv}))\eta_{cha}\Delta t \qquad (11)$$

And for the discharging state, the storage battery capacity is computed as follows:

$$C_{bat}(t) = C_{bat}(t-1) + (P_{RE}(t) - (P_{load}(t)/\eta_{inv})) / \eta_{dech})\Delta t \qquad (12)$$

η_{cha}, η_{dech} are the charging and discharging efficiency of the battery, η_{inv} is the inverter efficiency. (In this article, $\eta_{cha} = 90\%$, $\eta_{dech} = 85\%$ and $\eta_{inv} = 95\%$ [14]).

2.3. Diesel generator

The diesel fuel consumption $F(t)$ during a period of time t, and the fuel cost is calculated for a year, as per discussed in [15], as follows:

$$F(t) = 0.246 \, P_{DG}(t) + 0.08415 \, P_R \qquad (13)$$

$$C_f = P_f.\sum_{t=1}^{8760} F(t) \qquad (14)$$

where: $P_{DG}(t)$ is the DG generated power, kW, P_R is the DG rated power, kW, and P_f is the fuel cost per liter.

The operational of DG has to be in range between the rated capacity and specified minimum value:

$$P_{DGmin}(t) \leq P_{DG}(t) \leq P_{DGmax}(t) \qquad (15)$$

2.4. Control strategies

This strategy can be explained by the following steps:

$$\Delta P = P_{PV}(t) - P_L(t) \tag{16}$$

$$P_L(t) = \frac{P_{load}}{\eta_{inv}} \tag{17}$$

where: $P_{PV}(t)$: the renewable power of the system which is in our case the Photovoltaic's power, P_{load}: the demanded load power.

1. If $\Delta P = 0$, the battery banks is either charged or discharged and the $C_{bat}(t)$ of the battery banks depends on the previous value at the time t. The diesel generator is turned off.

2. If $\Delta P > 0$, the remaining power will be used to charge the battery bank. The diesel generator is turned off. When the $C_{bat}(t)$ of battery banks reaches its maximum value C_{batmax}, the excess power is dumped.

3. If $\Delta P < 0$, the deficient power will be supplied by the battery bank or by the diesel generator. If the demand load is less than the minimum power of diesel generator, these later run at their rated power P_R, the batteries will be charged with the remaining power.

A flowchart of the proposed operational strategy for the multi source system is shown in *figure 2*.

3. PROBLEM DESCRIPTION AND THE PROPOSED APPROACH

3.1. Cost analysis

The System Total Cost (STC) is one of the indicators in economic analysis, it can be determined from the following equation [16]:

$$F_c(x) = \sum N_{PV,P} \times N_{PV,S} \times (C_{A,PV} + 20 \times C_{M,PV} + C_{I,PV}) + \sum N_{BAT,P} \times N_{BAT,S} \times (C_{A,BAT} + C_{I,BAT} + (r_{BAT} \times (C_{A,BAT} + C_{I,BAT})) + (20 - r_{BAT} - 1) \times C_{M,BAT}) + C_{T,D} \tag{18}$$

where $C_{A,PV}$ is the acquisition cost of PV panel *(€)*, $C_{M,PV}$ is the maintenance cost per year of the PV panel *(€ /year)*, $C_{I,PVb}$ is the installation cost of the PV panel *(€)*, $C_{A,BAT}$ is the acquisition cost of battery *(€)*, $C_{M,BAT}$ is the maintenance cost per year of the battery *(€/year)*,

$C_{I,BAT}$ is the installation cost of the battery (€), r_{BAT} is the expected number of battery replacements during the lifetime of the system operation, $C_{T,D}$ is the operation cost of the diesel generator, is calculated as follows:

$$C_{T,D} = C_{I,D} + M_D + \frac{C_D}{Life_D} + C_f \tag{19}$$

where $C_{I,D}$ is the installation cost of the diesel generator (€), C_D is the diesel generator acquisition cost (€), M_D is the diesel generator's hourly maintenance cost (€/h) ,$Life_D$ is the diesel generator lifetime (h),C_f is the fuel cost (€).
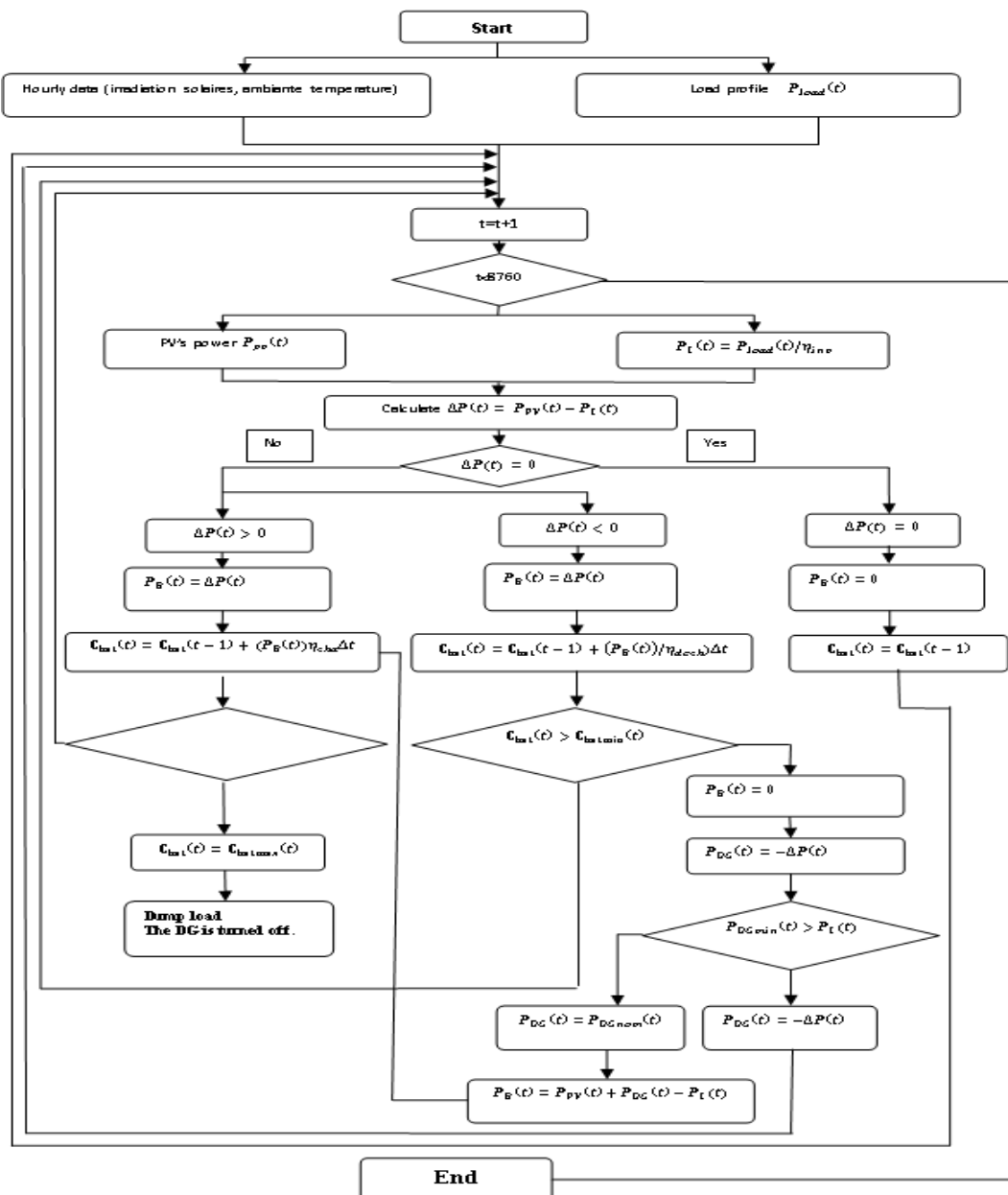
Fig. 2. Flow chart of the proposed operational strategy for the multi source ystem

The electrical energy supplied to the required load demand through the renewable energy sources is known as a renewable factor (RF) [17] or renewable energy fraction (FR) [18], FR is a number between 1 and 0, if FR equal to 1 means total generated power supply to the load from renewable energy source, in other side, if the value of FR is zero, the load is supplied by DG sources. The renewable fraction calculated is shown as [18]:

$$FR = \frac{E_{RE}}{E_{RE}+P_{DG}} \qquad (20)$$

where: E_{RE} represents the produced renewable energy which is consider the Photovoltaic's power (P_{PV}) in our case, P_{DG} represents the diesel generator power, $E_{RE} + P_{DG}$ represents the total energy production of the multi-source system.

3.2. Genetic algorithm

GA is a stochastic optimization proposed for the first time by Holland [19], GAs are adaptive heuristic search algorithms based on the evolutionary ideas of natural selection and genetics. GAs are utilized to solve NP-Hard optimization problems which cannot be solved with classical methods due various complexities such as non-linearity, non-convexity, multimodality, discontinuity, and mixed-types variables among others [20]. Design of energy systems is among such complex problems.

The most important three operators of GAs are: selection, crossover and mutation.

The first step of a GA is the random generation of the initial population. Then a GA follows an iterated procedure that consists of the following steps [21]:

1. Evaluation of objective(s) function(s).
2. Reproduction of population, which makes duplicates of good solutions and eliminates bad solutions.
3. Crossover, in which existing population members (parents) are mated in order to produce new population members (offspring).
4. Mutation, which randomly changes the values at a portion of population members.

In a single objective optimisation, there is one goal: the search for an optimum solution. However, in multi objective optimisation there are two goals or more than two.

3.3. Case study

3.3.1. Components characteristics

PV panels and batteries constitute the inputs of the optimal sizing procedure. The technical specification and the costs of each component are described below:

Table 1. Specification of PVpanels [22]

$V_{OC}(V)$	45.50
$I_{sc}(A)$	8.90
$K_v(\%/°c)$	- 0.335
$K_i(\%/°c)$	0.047
$NCOT$ (°C)	46.00
$C_{A,PV}$ (€)	228.65
$C_{I,BAT}$ (€)	33.50
$C_{M,BAT}$ (€/year)	6.85

Table 2. Specification of batteries [22]

C_B (Ah)	180.00
$C_{BAT,nom}$(Ah)	12.00
$V_{BAT,nom}$ (V)	80.00
DOD (%)	85.00
$C_{A,BAT}$ (€)	147.90
$C_{I,BAT}$ (€)	20.88
$C_{M,BAT}$ (€/year)	5.68

The life of the system is assumed equal to 20 years, the service life of the battery is 4 years.

One diesel generator of a rated power of 16 kW is used; its lifetime is 7000 h. The fuel price is 0.17 €/l according to [23]. The capital cost and the maintenance cost of the diesel generator are respectively 6830 € and 0.2 €/h [16].

3.3.2. Meteorological Data and Load Profile

The system is assumed to be installed in the site of Ghardaia, Algeria, latitude: 32°24'N, longitude: 3°48'E and altitude: 450 m above sea level and it is proposed in order to meet the power demand of remote consumers. A community consisted of around 100 individual residential buildings.

The hourly solar radiation and hourly temperature are presented in *figure 3* and the hourly load profile is presented in *figure 4*.

3.4. The Objective Function and the Constraints

In order to examine the relation between the cost and RF, the objective function is the *STC* and the constraint is the *RF*.

The objective function:

$$Min \ (STC) \tag{21}$$

is subject to:

$$RF_{désired} \leq RF \tag{22}$$

We consider two scenarios:
- ✓ **Senario 1:** $RF_{désired} = 0.5$
- ✓ **Senario 2:** $RF_{désired} = 0.8$
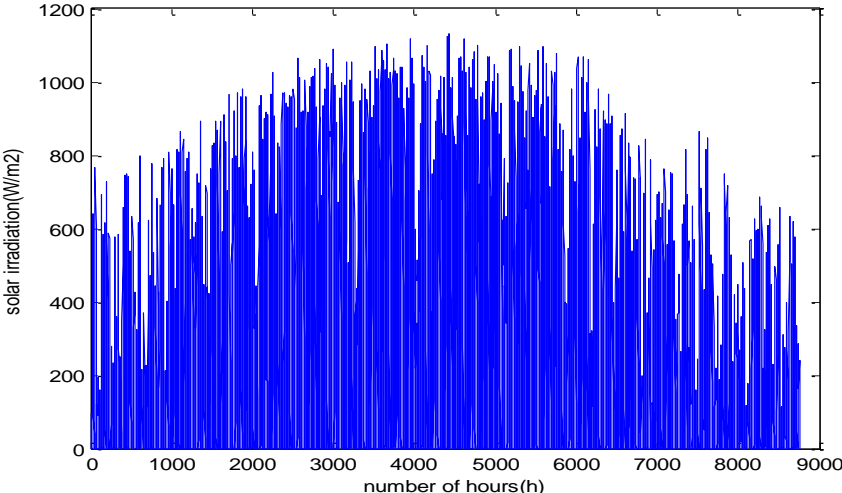
(a) Solar irradiation
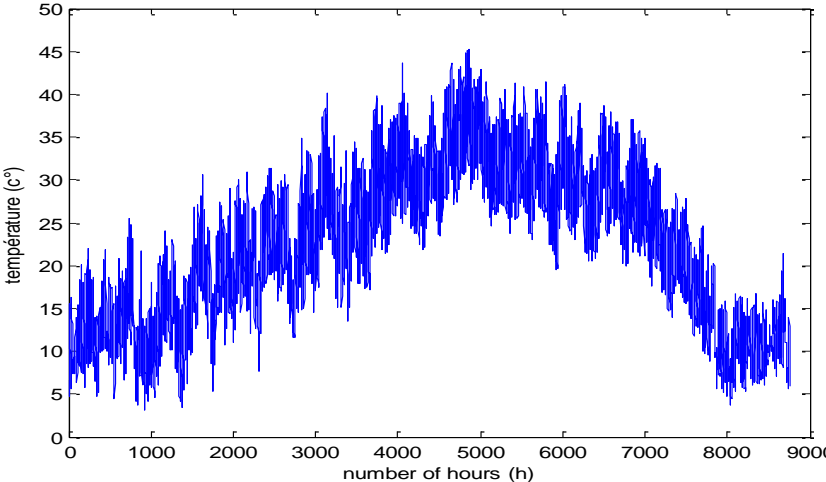
(b) Ambient temperature

Fig. 3. Hourly means values of meteorological conditions
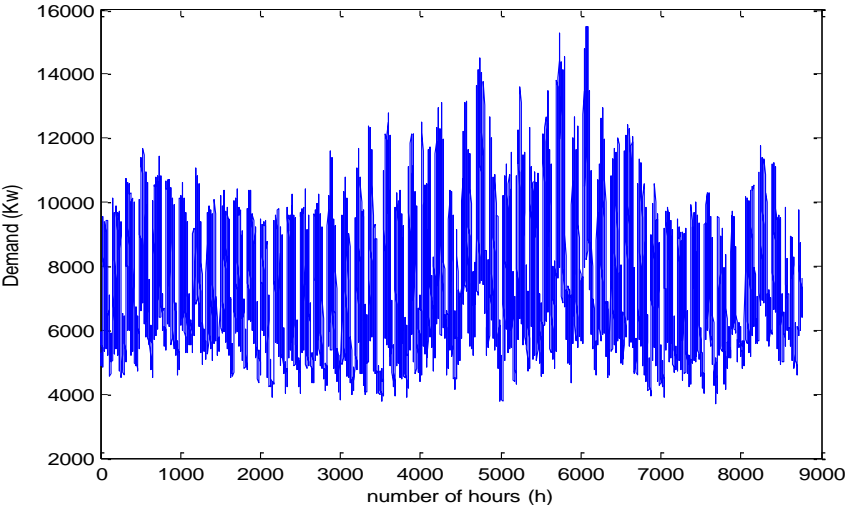
Fig. 4. Load profile during one year

The upper limit is defined by the constraint on number of components:

$$\begin{cases} 1 \leq N_{PV,p} \leq N_{PV,pmax} \\ 1 \leq N_{BAT,p} \leq N_{BAT,pmax} \end{cases} \tag{23}$$

and additional constraints:

$$C_{bat_{min}} \leq C_{bat}(t) \leq C_{bat_{max}} \tag{24}$$

$$P_{DGmin}(t) \leq P_{DG}(t) \leq P_{DGmax}(t) \tag{25}$$

A genetic algorithm implemented in Matlab as "ga" command [24], is used for optimization to find out the optimal sizing of the multi-source system consisting of PV, Diesel generator and Batteries as a storage system, to supply the studied area. In this simulation, GA parameters consist of:

✓ 40 populations size according to the following equation:

$$number\ of\ populations = max(min(10.\ number\ Of\ Vars, 100), 40) \tag{26}$$

Number Of Vars represents variables' number.

✓ 100 maximum generations.

For the other parameters, we used the default settings like stopping criterion:

✓ The average change in the fitness function value below the function tolerance, which is considered 10^{-6},

✓ The stall generation, which is considered 50.

Each chromosome consists of two genes (PV's number and battery's number). Optimization routine takes a long time to compute solution.

4. RESULTS AND DISCUSSSION

According to the control strategy adopted in this study, the demand is always satisfied. The application of the chosen approach leads to obtain the results presented in Table 3 and *figures 5, 6, 7* and *8*.

Table3. Optimal results

	$N_{PV,P}$	$N_{BAT,P}$	STC (€)	Operating hours of diesel (h/year)	Energy delivered by PV (Wh/year)	Energy delivered by diesel generators (Wh/year)
Senario 1	35	7	236294	4007	6.37×10^7	2.65×10^7
Senario 2	50	7	244073	3451	9.11×10^7	2.28×10^7
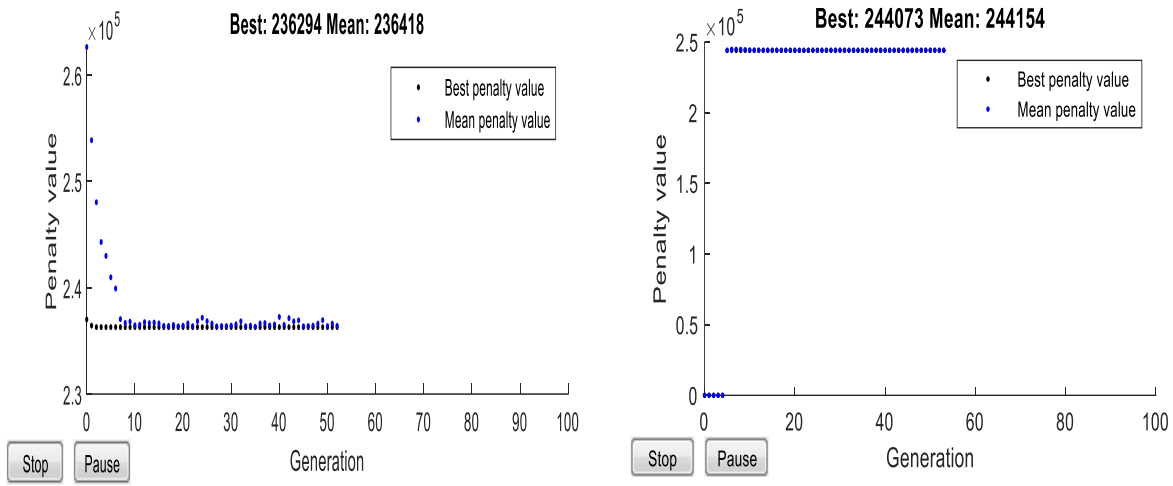
a)FR=0.5   b)FR=0.8

Fig. 5. Performance of genetic algorithm
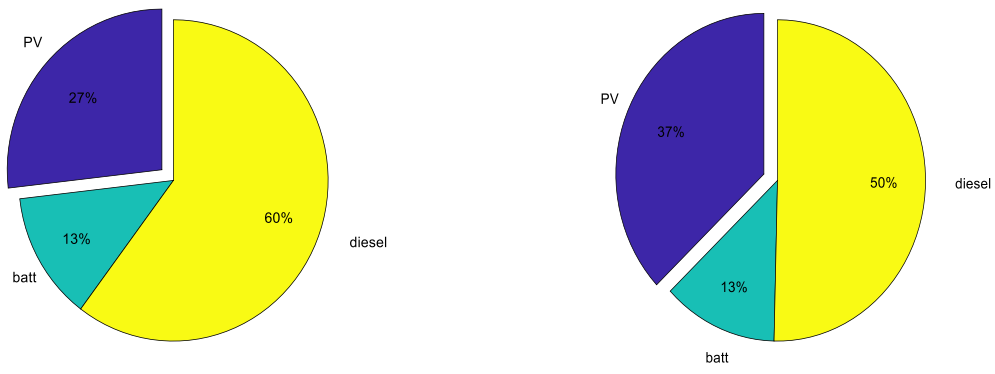
a)FR=0.5   b)FR=0.8

Fig. 6. Details of STC

According to the result analysis presented and shown in Table 3 and *figures 5-8*, respectively:

✓ It can be depicted from results that the *STC* is dependent on *RF*, the increase of the renewable factor *RF* results in theincrease of *STC*.

✓ It also shows the highest renewable penetration of 80% with the value of *STC* = 244073(€). The combination includes 50 PV Panels and 07 batteries. Here, the diesel generators are operated for 3451 h in a year, the utilization of PV system with high penetration can minimize the operational cost of Diesel generator as shown *figure 6,* and reduces the fuel consumption accordingly.

✓ The case study shows that the use of the system with a renewable factor $RF_{desired} =$ 0.5 is the most cost-effective system with a STC of 236294 €. The minimum value for the system's STC is obtained at the 52th iteration of the algorithm as shown in *figure* 5.

✓ The optimum PV selection is not affected only by the metrological condition (solar irradiation and temperature) or by the PV characteristics, but also by the desired RF.

A simulation of the produced powers by the optimal configuration over a period of one year is presented in *figure 7:*

✓ Regarding the state of charge of the batteries, we can verify that throughout the year, it can never exceed the permissible maximum value SOC_{max} (100% of SOC) and it can never be below the permissible minimum value, SOC_{min} (20% of SOC).

✓ It can be seen that the number of start / stop of the diesel generator depends on the state of charge of the battery.
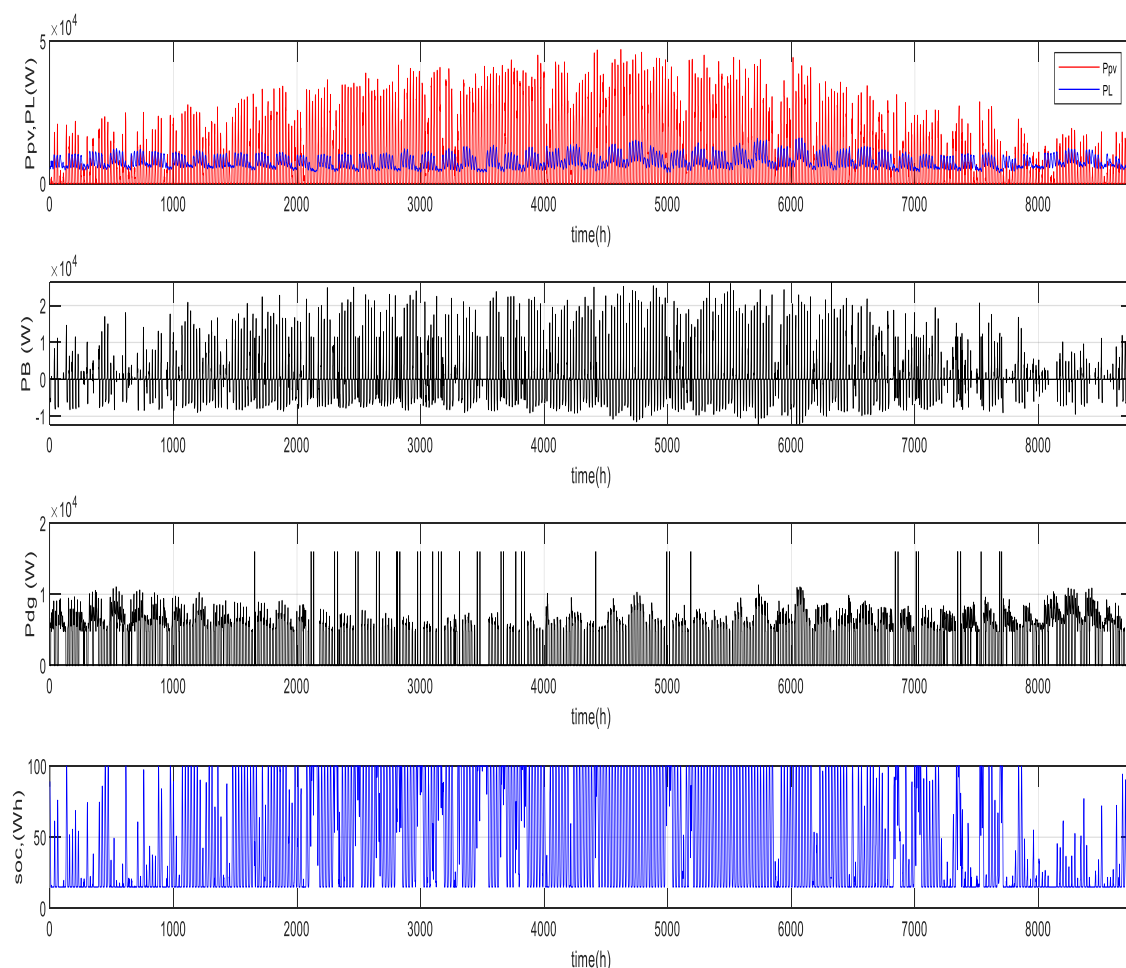
Fig. 7. Evolution of the powers $P_{PV}(t)$, $P_L(t)$, $P_B(t)$, $P_{DG}(t)$ and the state of charge of batteries in percent (SOC) during one year.

A simulation of the different powers produced by the optimal configuration of multi-source system over a period of 15 days is presented in *figure 8*.

According to the simulation results related to the case studied:

- ✓ The storage battery bank capacity never exceeds the allowable maximum value and can never be below the allowable minimum value, which respects the constraint fixed by us at the level of the management of the battery.
- ✓ When the power $P_{PV}(t)$ is greater than $P_L(t)$, the bank of batteries is charged $(P_B(t) > 0)$ and discharged $(P_B(t) < 0)$ in the opposite case,
- ✓ The diesel generator starts when the power $P_{PV}(t)$ is lower than $P_L(t)$ and the batteries are discharged, the diesel generator is used to cover the energy deficit,
- ✓ Moreover, the DG never operates below the allowable minimum value, 30% of its rated power.
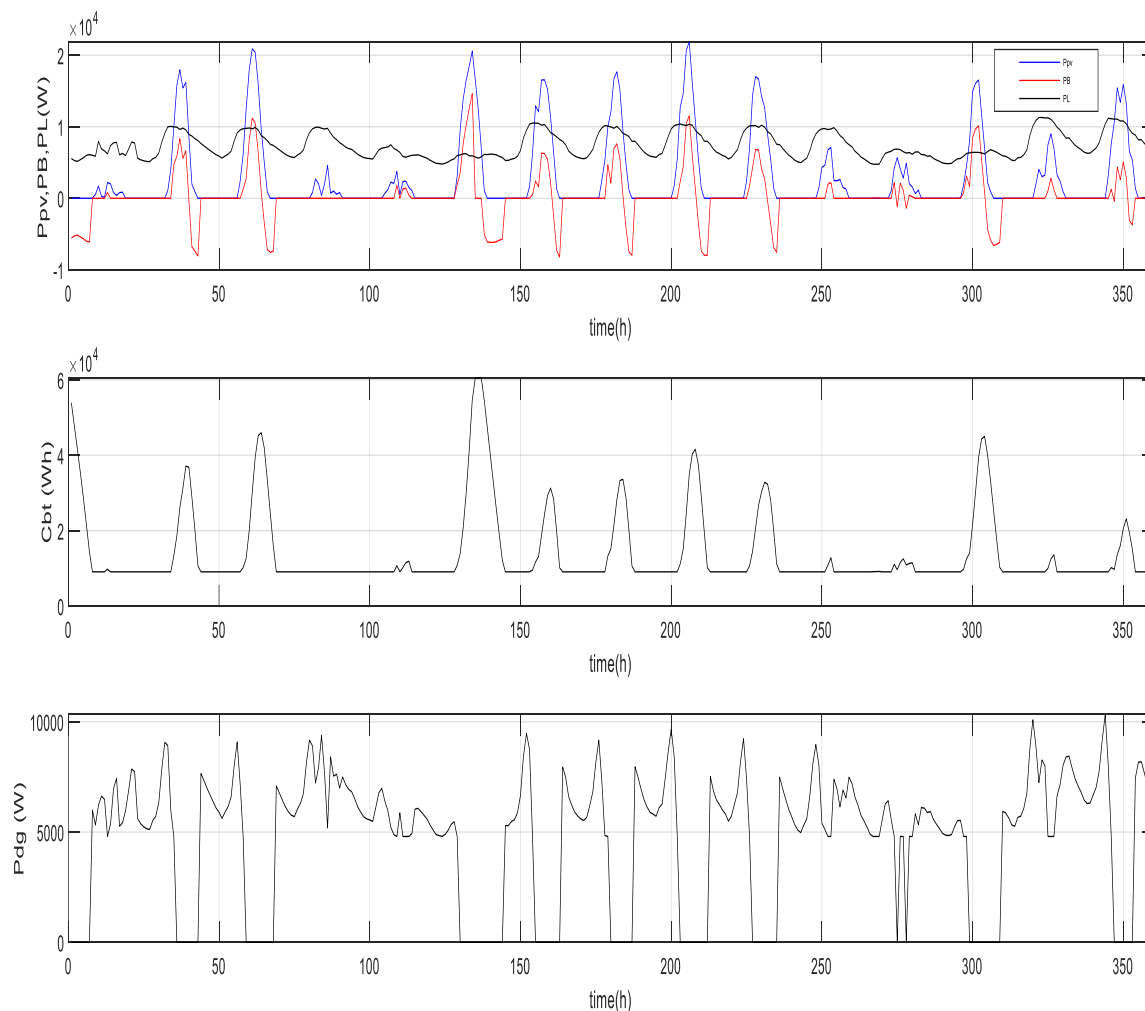
Fig. 8. Produced powers by the renewable resource $P_{PV}(t)$, demanded by the consumer $P_L(t)$, input / output of the bank of batteries $P_B(t)$, storage battery bank capacity $C_{bat}(t)$ and the power produced by the diesel generator $P_{DG}(t)$

5. CONCLUSION AND PERSPECTIVE

The performed work represents the sizing optimization of PV- diesel-battery system. Then, GA is used to find the optimal configuration of the number of PV panels and batteries. Also, the results obtained from the simulation show that the design and sizing optimization of the hybrid system can be achieved by using the proposed methods to find the best solution for the system.

The possibility of using this method is a great interest, it can be implemented in different cases for the optimal sizing and management of multi-source renewable energy system, for different load profile and meteorological conditions.

Further works will take into consideration other criteria like CO_2 emission, loss of probability of charge LPSP…etc and be focused on the study of the multi-objectives' optimization in order to examine the relation between the STC and RF or STC and other factors.

REFERENCES

[1]   Y. Himri, A. S. Malik, A. B. Stambouli, S. Himri, and B. Draoui, *Review and use of the Algerian renewable energy for sustainable development*, Renewable and Sustainable Energy Reviews , vol. 13, pp. 1584–1591, 2009.

[2]   S. Makhloufi, *Comparative study between classical methods and genetic algorithms for sizing remote PV systems*, International Journal of Energy and Environmental Engineering, vol. 6, no. 3, pp. 221–231, 2015.

[3]   A. Yahiaoui, K. Benmansour, and M. Tadjine, Control, *analysis and optimization of hybrid PV-Diesel-Battery systems for isolated rural city in Algeria*, Solar Energy, vol. 137, pp. 1–10, 2016.

[4]   F. Fodhil, A. Hamidat, and O. Nadjemi, *Optimal Sizing of Stand-Alone Hybrid PV- Diesel-Battery System Using PSO and the ε - Constraint Method*, *3rd Int. Conf. Green Energy Environ. Eng. (GEEE-2016), Hammamet, Tunis*, April, 2016.

[5]   H. Suryoatmojo, A. A. Elbaset, F. A. Pamuji, D. C. Riawan, and M. Abdillah, *Optimal Sizing and Control Strategy of Hybrid PV-Diesel-Battery Systems for Isolated Island*, ADCONP Hiroshima 2014.

[6]   A. Atieh, *Modeling and Cost Analysis for different PV / Battery / Diesel operating options Driving a Load in Tunisia , Jordan and KSA*, Sustainable Cities and Society, 2016.

[7]   M. S. Ismail, M. Moghavvemi, and T. M. I. Mahlia, *Design of a Pv / Diesel Stand Alone Hybrid System for a Remote Community in Palestine*, Journal of Asian Scientific Research journal, vol. 2, no. 11, pp. 599–606, 2012.

[8]   A. F. Mohamed, M. M. Elarini, and A. M. Othman, *A new technique based on Artificial Bee*

Colony Algorithm for optimal sizing of stand-alone photovoltaic system, Journal of Advanced Research, vol. 5, no. 3, pp. 397–408, 2014.

[9]　K. Bataineh, *Optimal Configuration for Design of Stand-Alone PV System*, Smart Grid Renewable Energy, vol. 3, no. 2, pp. 139–147, 2012.

[10]　M. Lalwani, D. Kothari, and M. Singh, *Investigation of solar photovoltaic simulation softwares,* International Journal of Applied Engineering Research, vol. 1, pp. 585–601, 2010.

[11]　B. O. Bilal, V. Sambou, P. A. Ndiaye, and C. M. F. Kébé, *Multi-objective Design of PV-Wind-Batteries Hybrid Systems by Minimizing the Annualized Cost System and the Loss of Power Supply Probability (LPSP)*, IEEE IntConfIndTechnol (ICIT), Cape Town, South Africa, pp. 861–868, 2013.

[12]　S. Diaf, G. Notton, M. Belhamel, M. Haddadi, and A. Louche, *Design and techno-economical optimization for hybrid PV/wind system under various meteorological conditions*, Applied Energy, vol. 85, no. 10, pp. 968–987, 2008.

[13]　A. Chauhan and R. P. Saini, *Discrete harmony search based size optimization of Integrated Renewable Energy System for remote rural areas of Uttarakhand state in India*, Renewable Energy, vol. 94, pp. 587–604, 2016.

[14]　A. M. Eltamaly, M. A. Mohamed, and A. I. Alolah, *A novel smart grid theory for optimal sizing of hybrid renewable energy systems*, Solar Energy, vol. 124, pp. 26–38, 2016.

[15]　H. Suryoatmojo, T. Hiyama, A. a Elbaset, and M. Ashari, *Optimal Design of Wind-PV-Diesel-Battery System using Genetic Algorithm*, IEEJ Trans. Power Energy, vol. 129, no. 3, pp. 413–420, 2009.

[16]　R. Belfkira, L. Zhang, and G. Barakat, *Optimal sizing study of hybrid wind / PV / diesel power generation unit*, Solar Energy, vol. 85, no. 1, pp. 100–110, 2011.

[17]　Y. Sawle, S. C. Gupta, and A. K. Bohre, *Socio-Techno-Economic Design of Hybrid Renewable Energy System Using Optimization Techniques*, Renewable Energy, vol. 119, no. November, pp. 459–472, 2017.

[18]　Ngoc An Luu. *Control and management strategies for a microgrid. Electric power*. Université de Grenoble, 2014.

[19]　J.H. Holland, *Adaptationin Natural and Articial Systems, University of Michigan Press*, Ann Arbor, 1975.

[20]　A.Gabour, A. Metatla, R. Kelaiaia, F. Bourennani et A. Karboua, *Recent Bibliography on the Optimization of Multi-source Energy Systems*, Archives of Computational Methods in Engineering, vol. 26, no. 4, pp. 809–830, 2019.

[21]　Y. A. Katsigiannis and P. S. G. E. S. Karapidakis, *Multiobjective genetic algorithm solution to the optimum economic and environmental performance problem of small autonomous hybrid power systems with renewables*, IET Renewable Power Generation, vol. 4, no. 5, pp. 404–419,2010.

[22]　L. Zhang, G. Barakat, and A. Yassine, *Deterministic optimization and cost analysis of hybrid PV/wind/battery/diesel power system*, INTERNATIONAL JOURNAL OF RENEWABLE ENERGY RESEARCH, vol. 2, no. 4, pp. 686–696, 2012.

[23]　https://www.globalpetrolprices.com/Algeria/diesel_prices./

[24]　https://www.mathworks.com.

THREE-LEVEL INDIRECT MATRIX CONVERTER WITH TWO SERIES Z-SOURCE NETWORKS

Francis Boafo **EFFAH**[1], Philip **OKYERE**[1], Mubarak Sani **ELLIS**[1] Patrick **WHEELER**[2], Alan **WATSON**[2], Jon **CLARE**[2], Joseph **OJO**[3]

[1] *Kwame Nkrumah University of Science and Technology, Kumasi, Ghana,* [2] *University of Nottingham, UK,* [3] *Tennessee Technological University Cookeville, USA.*

fbeffah.coe@knust.edu.gh

Abstract*: In previous articles, the concept of series Z-source network has been extended to conventional indirect matrix converter to raise the voltage gain to unity and beyond. In this paper, this idea is modified and applied to a three-level indirect matrix converter. Two series Z-source networks are placed on the virtual dc-link between a rectifier and a neutral point clamped inverter on the positive and negative dc rails. Partial shoot-through states are used for voltage boosting. The series Z-source capacitor voltages and starting current stresses are reduced. A virtual space vector PWM method has been developed to ensure voltage boost ability of the converter. Simulation results from SABER are used to demonstrate the superiority of the proposed converter over the existing topology.*

1. INTRODUCTION

AC-AC power conversion is needed in several industrial applications including motor drives, wind energy conversion systems, ship propulsion and aerospace energy systems [1, 2]. The matrix converter (MC) is one of the most popular topologies among the available ac-ac converters because it provides high power density, sinusoidal input and output quantities, controllable input displacement factor, lengthy lifetime, and resilience under unfavourable conditions [3]. The MC topologies can be classified as direct and indirect. The direct MC (DMC) implements single stage ac-ac conversion, but the indirect MC (IMC) performs ac-dc-ac conversion with no intermediate dc-link capacitor. Both of them have the same behaviour, but the latter has simpler commutation than the former [4, 5], and the number of controllable switches was reduced in sparse and ultrasparse IMCs [6]. The three-level IMC (3LIMC) is a

relatively new topology from the IMC family that incorporates a three-level voltage source inverter (VSI) with the matrix converter concept [7]. The topology produces multilevel output voltages with better harmonic content compared to the two-level topology while still maintaining all the advantages outlined for the traditional IMC.

Despite all the attractive features of the MC, its penetration in industry is low compared to existing topologies [8]. This is due to the fact that MCs have two main shortcomings: 1) the voltage gain cannot exceed 0.866; and 2) the output voltage is affected by changes in the input voltage [9, 10]. The output voltage sensitivity drawback can be overcome in a limited range through improved modulation methods [11]. Many over-modulation techniques have been suggested to improve the voltage gain, however they are inadequate and often implemented at the expense of degrading the input current and output voltage quality [12]. A transformer connected between the supply and load could increase the voltage gain but this will impact on the compactness of the MC [13]. Alternatively, when an AC-boost chopper is combined with IMC the voltage gain can increase, but requires more active switches [14].

The Z-source (ZS) network offers a clever boost ability for IMC. In [8], an IMC incorporating a ZS network at the fictitious dc-link to increase the voltage gain was presented. A three-level version of the converter proposed in [8] was presented in [15, 16]. This topology is called three-level cascaded Z-source IMC (3LCZSIMC) in this paper and shown in *fig. 1*.
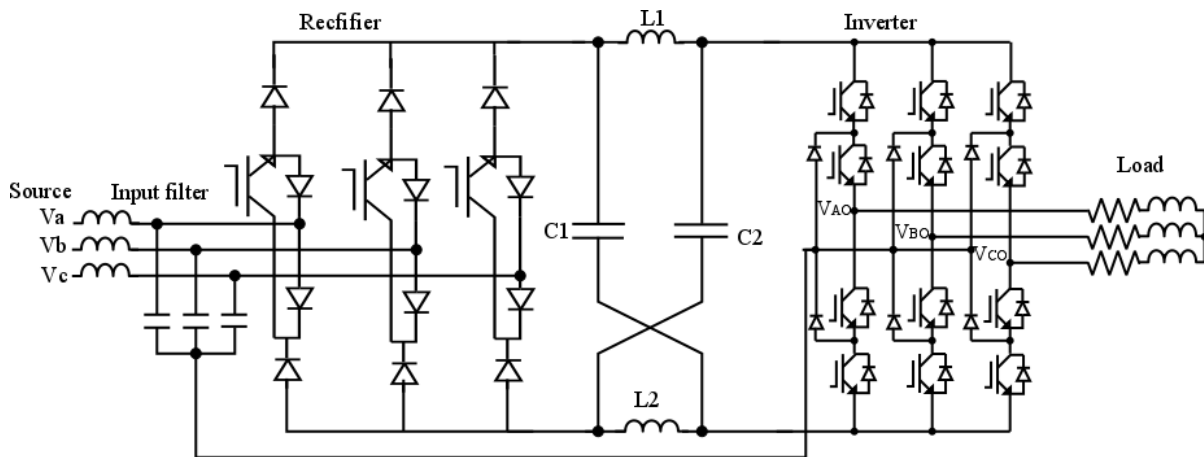
Fig. 1. Three-level cascaded Z-source indirect matrix converter

This converter brings on board the added benefits of multilevel converters such as better harmonic performance of the output waveforms and the use of low-voltage devices for applications that require medium voltage. Nevertheless, there are two weaknesses for this converter. The first issue is that the Z-source capacitor voltages are larger than the supply voltage which means larger capacitors will have to be used thereby increasing the overall cost and volume. The other drawback is that the Z-source converter cannot suppress the inrush

current and resonance between the Z-source capacitors and inductors. This causes voltage and current surges and may destroy the devices [17].

A replacement of the cascaded ZS (CZS) network proposed earlier in [8] with a series ZS (SZS) network was proposed in [18]. This circuit topology brings onboard other advantages over the cascaded topology. These include lower voltage stress on the capacitors and a reduction of the inrush current during start up. A comparison of this new topology with existing topologies for wind power application was given in [19]. In order to enhance the output harmonic performance of the converter proposed in [18], a three-level series ZS IMC (3LSZSIMC) is proposed in this work. Two series Z-source networks are inserted at the positive and negative dc rails of the three-level IMC. A virtual space vector pulse width modulation method is employed to achieve voltage-boost ability for this converter.

The rest of the paper is organized as follows. Following the introduction, the topology of the 3LSZS IMC including its operating principles and governing equations is presented in section 2; section 3 presents the modulation scheme for the converter in detail; in section 4 the criteria for selection of the series Z-source components is established; section 5 presents numerical simulations to verify the theoretical concepts; also performance comparisons with the 3LCZSIMC is given; section 6 draws the final conclusion.

2. STRUCTURE AND PRINCIPLE OF OPERATION

2.1. Structure

Figure 2 shows the topology of the proposed three-level series Z-source indirect matrix converter based on ultra-sparse IMC topology.
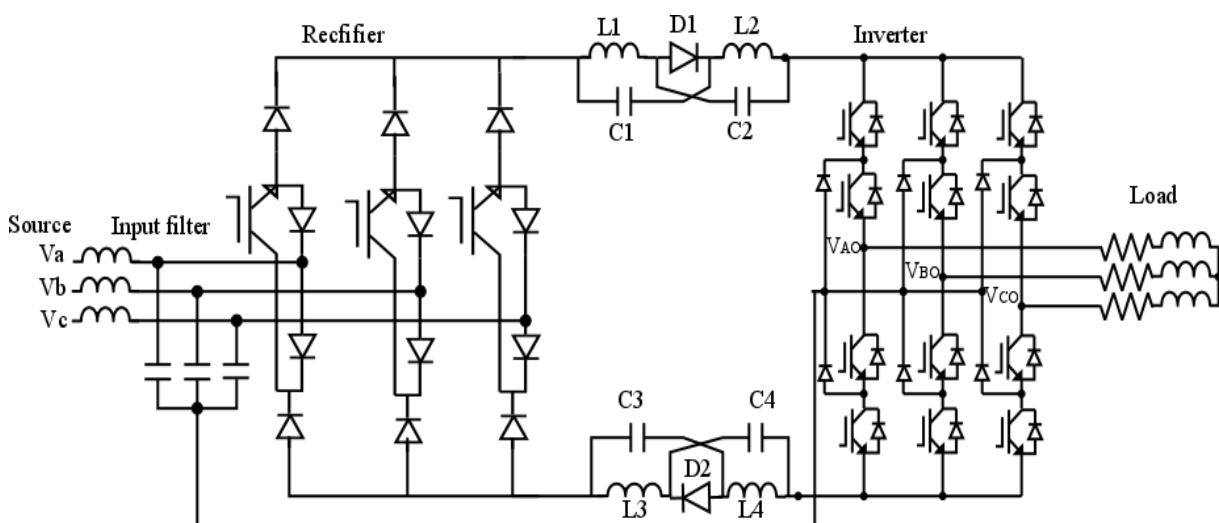
Fig. 2. Three-level series Z-source indirect matrix converter

As already stated, traditional IMCs have a drawback of limited voltage gain. To deal with this limitation, several control procedures and circuit configurations have been proposed. Specifically, the voltage gain can be increased to unity and beyond by employing Z-source network [20]. The basic function of traditional IMCs is commonly achieved in a two-stage power conversion, the first stage being ac-dc and the second dc-ac. The input stage is a current source rectifier (CSR) while the output stage is a conventional NPC inverter. Series Z-source networks are placed at the fictitious dc-link to give it voltage boost capability.

2.2. Operation

This converter is operated by employing shoot-through states as well as active and zero states used in conventional three-level IMCs. The series Z-source networks give this converter its voltage boosting ability. The capacitor voltage stress is reduced and the starting current is limited by the series Z-source networks. All these benefits are achieved while maintaining the same boost ratio of the cascaded Z-source network. Equivalent circuits of 3LSZSIMC under different states are shown in *fig. 3*.
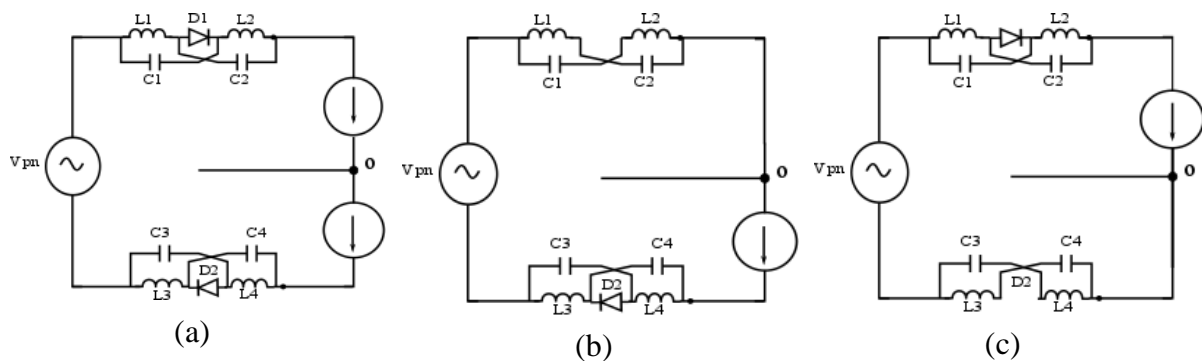
Fig. 3. Equivalent circuits of 3LSZSIMC. (a) NST states, (b) UST states, (c) LST states

For symmetry, inductances of same values and capacitances of same values are used. Thus,

$$V_C = V_{C1} = V_{C2} = V_{C3} = V_{C4} \tag{1}$$

$$V_L = V_{L1} = V_{L2} = V_{L3} = V_{L4} \tag{2}$$

Without loss of generality, the voltage across L1 is used to derive the average capacitor voltages. In the upper-shoot-through (UST) states, the positive terminal of the inverter side is shorted with the neutral point, and the inductor voltages are given by:

$$V_{L1} = V_{po} + V_{C2}, \ V_{L2} = V_{po} + V_{C1} \tag{3}$$

$$V_{L3} = - V_{C3}, \ V_{L4} = -V_{C4} \tag{4}$$

Similarly, during lower-shoot-through (LST) states, the negative terminal of the inverter is shorted with the neutral point, and the inductor voltages are given by:

$$V_{L1} = -V_{C1}, \ V_{L2} = -V_{C2} \tag{5}$$

$$V_{L3} = V_{on} + V_{C4}, \ V_{L4} = V_{on} + V_{C3} \tag{6}$$

In (3) and (6), V_{po} and V_{on} represent the upper and lower halves of the virtual dc link voltage with respect to the inverter neutral point (NP). The summation of the two terms gives the total dc-link voltage (V_{pn}).

Inductor voltages during non-shoot-through (NST) states are:

$$V_{L1} = -V_{C1} \tag{7}$$

$$V_{L2} = -V_{C2} \tag{8}$$

$$V_{L3} = -V_{C3} \tag{9}$$

$$V_{L4} = -V_{C4} \tag{10}$$

Averaging the inductor voltages (using V_{L1} in this case) over a switching period yields:

$$d_{sh-u} * T_{sw} * \left(V_{po} + V_{C1}\right) + d_{sh-l} * T_{sw} * (-V_{C1}) + \\ (-V_{C1}) * [1 - (d_{sh-u} + d_{sh-l})] * T_{sw} = 0 \tag{11}$$

where T_{sw} is the switching period, d_{sh-u} is the duty ratio of UST states while d_{sh-l} is the duty ratio of the LST states. For symmetric operation, d_{sh-u} is made equal to d_{sh-l}. The sum of the two terms is d_{st}. It should also be noted that the average values of V_{po} and V_{on} are equal and their sum equals V_{pn}. Therefore

$$V_C = \frac{d_{st}}{1-d_{st}} \left(\frac{V_{pn}}{4}\right) \tag{12}$$

It is clear from (12) that, for the 3LSZSIMC the Z-source capacitor voltages are zero for zero shoot-through duration. For soft starting, V_c can rise from zero slowly; so if we control d_{st} for it to rise gradually from zero then soft-start is realized. This is not so in a 3LCZSIMC.

In the non-shoot-through state, we can write

$$V_{dc-link} = V_{pn} + 2V_C - 2V_L \tag{13}$$

In (13), $V_{dc-link}$ denotes the output voltage of the series ZS networks which will be the input for the inverter. The boost factor, B, is found using (7), (12) and (13) as follows:

$$V_{dc-link} = \frac{1}{1-d_{st}}V_{pn} = BV_{pn} \tag{14}$$

where

$$B = 1/(1 - d_{st}) \tag{15}$$

The fundamental component of the output line-to-line voltage is given by

$$\hat{V}_{out} = m_i B V_{pn} \tag{16}$$

where m_i represents the modulation index of the inverter.

If we neglect power losses in the rectifier, then the input power equals the output power of the rectifier. Thus,

$$V_{pn}I_{pn} = 3V_{in}I_{in}\cos\theta_i = \frac{3}{2}\hat{V}_{in}\hat{I}_{in}\cos\theta_i \tag{17}$$

Here, I_{pn} is the current in the output of the rectifier; V_{in} is the fundamental component of the supply phase voltage; I_{in} is the fundamental component of the input current; θ_i is input current displacement angle. To get a power factor of unity, θ_i is set to zero. The input stage is a CSR which modulates the source current with modulation index m_r given by:

$$m_r = \frac{\hat{I}_{in}}{I_{pn}} \tag{18}$$

Using (17) and (18), we have

$$V_{pn} = \frac{3}{2}m_r\hat{V}_{in}\cos\theta_i \tag{19}$$

Putting (19) in (16) yields

$$\hat{V}_{out} = \frac{3}{2} m_r m_i B \hat{V}_{in} \cos \theta_i \tag{20}$$

Equation (20) defines the relationship between output and input voltages of 3LSZSIMC. It should be noted that the d_{st} must be lower than m_i; therefore, to get maximum boosting, it is assumed that

$$m_r = 1, \quad d_{st} = 1 - m_i \quad \theta_i = 0. \tag{21}$$

3. MODULATION TECHNIQUE

Modulation of the proposed converter is divided into CSR and voltage source inverter (VSI) modulation, respectively. The CSR has nine possible switching states with six producing non-zero currents in the dc-link. The vector diagram of the CSR is shown in *fig. 4* comprising six sectors. The current reference vector's location within a sector is identified and synthesized by two framing vectors and a null vector.
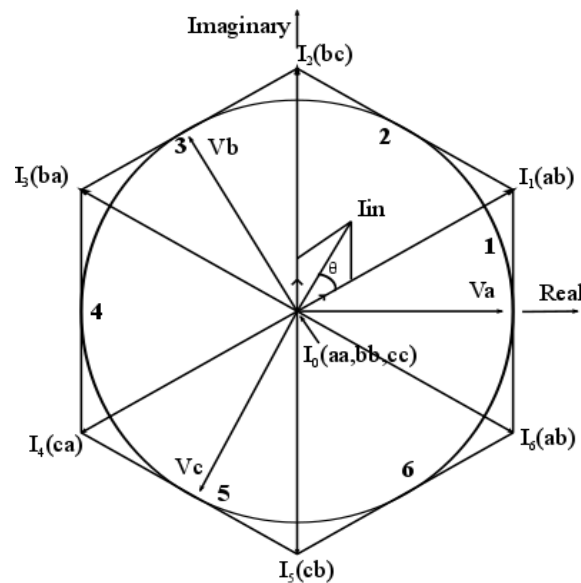
Fig. 4. Space vector diagram of rectification stage

Let angle of current reference vector be θ_r, then duty ratios of active and null vectors are calculated as follows:

$$d_\gamma = m_r \sin\left(\frac{\pi}{3} - \theta_r\right) \tag{22}$$

$$d_\delta = m_r \sin(\theta_r) \tag{23}$$

$$d_{0r} = 1 - (d_\gamma + d_\delta). \tag{24}$$

The output currents circulate through the inversion stage when the output voltage is zero thereby making dc-link current delivered by the CSR zero. We can take advantage of this and make the CSR switching coincide with the instant when the inverter output voltage is zero so as to produce zero current commutation. This reduces the switching losses in the CSR [6, 21] and is achieved by eliminating completely the zero current vector and adjusting the CSR duty ratios as follows:

$$d_\gamma^R = \frac{d_\gamma}{d_\gamma + d_\delta}, \quad d_\delta^R = \frac{d_\delta}{d_\gamma + d_\delta} \tag{25}$$

The back-end inverter is based on three-level NPC inverter controlled using a three-level space vector PWM technique. *Fig. 5* shows the vector diagram of a conventional NPC inverter controlled with conventional three-level space vector PWM. The diagram contains six sectors with twenty-seven switching states. The switching states can be grouped as zero, small, medium and large vectors. The letter 'P', 'O' and 'N' imply two top, middle and bottom switches, respectively, of a phase leg are turned on. In an "O" state, the input capacitors of the NPC inverter formed by the input filter capacitors become charged or discharged depending on the NP current direction. For the capacitors to have equal voltages on them, the NP current should be zero over a switching period. A conventional three-level space vector PWM cannot achieve this since it tries to use currents of small vectors to compensate those of medium vectors. This usually happens when the power factor is low and the modulation index is high.
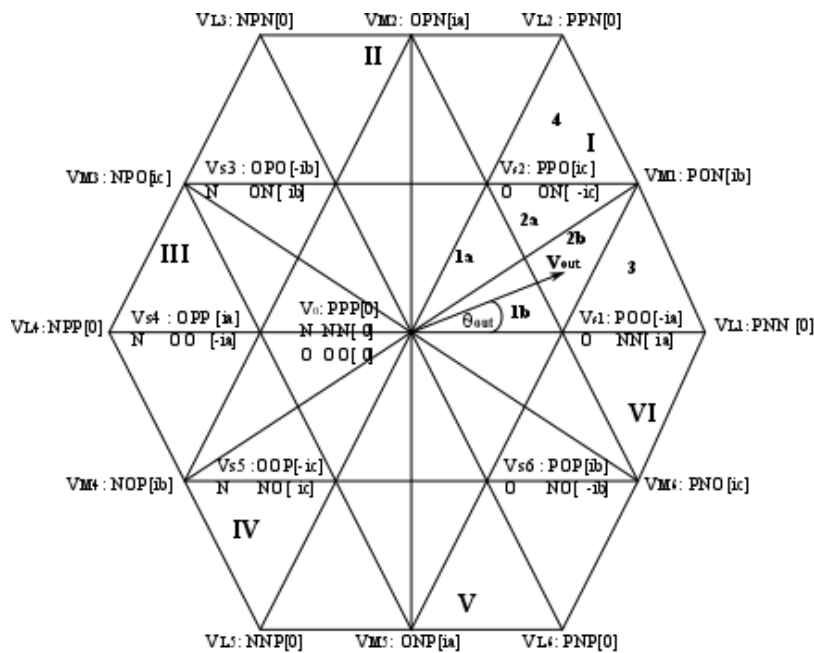
Fig. 5. Space vector diagram of inversion stage

A virtual space vector PWM technique is used to overcome this drawback. In this modulation scheme, virtual vectors are formed from existing vectors so that the average NP current is zero in a switching period. The reference voltage is then created with three nearest virtual vectors. In sector I of *fig. 5*, the virtual vectors produced are shown in *fig. 6*.
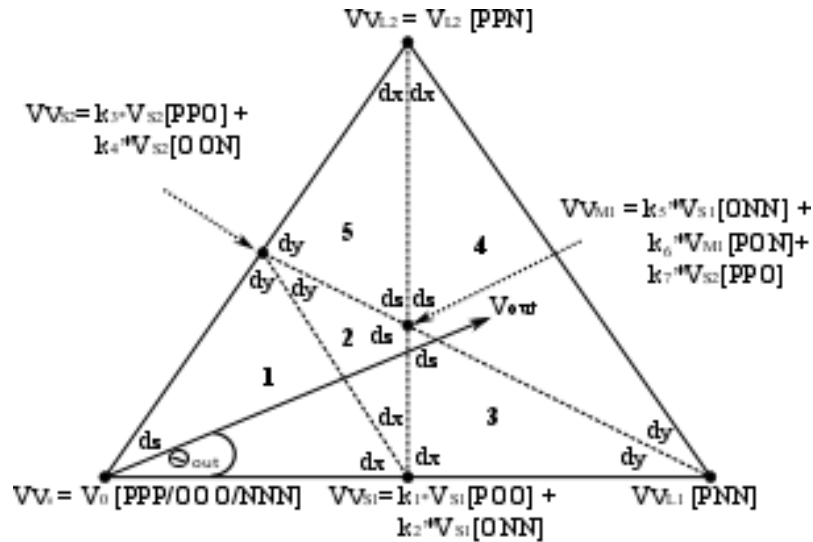
Fig. 6. Virtual space vectors for sector I

The duty ratios of the identified virtual vectors are calculated as follows:

$$d_x.V_{V1} + d_y.V_{V2} + d_z.V_{V3} = \vec{V}_{out} \tag{26}$$

$$d_x + d_y + d_z = 1 \tag{27}$$

The duty ratios of switching states making the virtual vectors are then determined. Consider triangle 3 in *fig. 6* for example. The duty ratio of the selected virtual vectors are given by:

$$d_x = 2 - m_i\left[\sqrt{3}\,\cos(\theta_{out}) + 3\sin(\theta_{out})\right] \tag{28}$$

$$d_y = \sqrt{3}m_i\cos(\theta_{out}) - 1 \tag{29}$$

$$d_z = 3\sqrt{3}m_i\sin(\theta_{out}) \tag{30}$$

In (28) to (30), m_i is the modulation index of the VSI and is defined as:

$$m_i = \frac{\sqrt{3}|\vec{V}_{out}|}{V_{pn,avg}} \tag{31}$$

The CSR and VSI stages are synchronized to ensure balance of input currents and output voltages within a switching period. For instance with the reference vector of the CSR in sector 2 and that of the VSI in triangle 4 of sector I, we have the vectors: I_1 (ac), I_2 (bc) and $V_{VM1}, V_{VL1}, V_{VL2}$. The virtual vectors are made from V_{S1} (ONN), V_{S2} (PPO), V_{M1} (PON), V_{L1} (PNN) and V_{L2} (PPN). The selected vectors are then applied to the input and output stages according to the switching pattern I_1 (ac) $\rightarrow$ I_2 (bc) for the CSR and PPO $\rightarrow$ PPN $\rightarrow$ PON $\rightarrow$ PNN $\rightarrow$ ONN for the VSI.

Partial shoot-through states are applied to phase legs of the VSI to achieve voltage boost operation. The resulting modified switching sequence in the output stage becomes PPO $\rightarrow$ PPL $\rightarrow$ PPN $\rightarrow$ PON $\rightarrow$ PNN $\rightarrow$ UNN $\rightarrow$ ONN with U and L representing UST and LST states, respectively. In an UST state, three top switches in a phase leg are turned on whereas in a LST state three bottom switches in a phase leg are gated on. *Figure 7* shows the switching pattern of the converter where the vectors in the VSI stage are organized in a two-sided sequence so that each side corresponds to an active vector of the CSR stage.
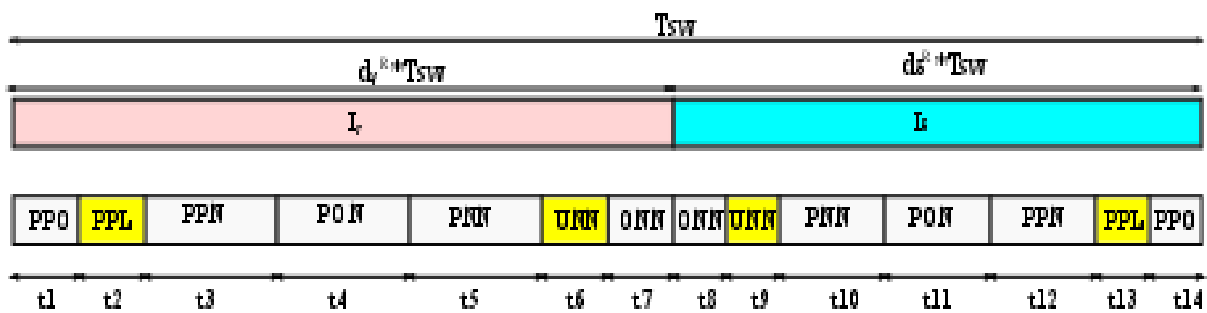
Fig. 7. Switching sequence. Top: CSR stage; Bottom: VSI stage

4. SELECTION OF SERIES Z-SOURCE PASSIVE COMPONENTS

From the analysis in section 2, the average current through the inductors is equal to that of the rectifier dc-link current in steady stste. Thus, the average current through the inductors is given by:

$$I_L = \frac{P_{out}}{V_{pn}} = \frac{P_{out}}{1.5\hat{V}_{in}\cos\theta_i} \tag{32}$$

where P_{out} represents the output power of the converter.

The series Z-source capacitor values are selected based on the desired voltage ripple and capacitor current. During the upper-shoot-through and lower-shoot-through states, as shown in *figures 3(b)* and *3(c)*, the series Z-source inductor current flows through the

capacitors and discharges them; hence, the voltage ripple across the capacitors can be expressed as:

$$\Delta V_c = \frac{I_L}{C} \cdot d_{st} \cdot T_{sw} \cdot \tag{33}$$

With ΔV_c selected to satisfy $\Delta V_c \leq k_v \% V_c$, then

$$C \geq \frac{0.5 \cdot d_{st} T_{sw}}{k_v \% V_c} I_L = \frac{2 \cdot (1 - d_{st}) \cdot T_{sw}}{k_v \% V_{pn}} I_L. \tag{34}$$

Putting (32) into (34) yields:

$$C \geq \frac{(1 - d_{st}) T_{sw}}{1.125 \cdot k_v \% \cdot \hat{V}_{in}^2 \cos^2 \theta_i} P_{out}. \tag{35}$$

Similarly, the series Z-source inductor values are selected based on a specified current ripple. During the NST states, as shown in *fig. 3(a),* the series Z-source inductor current decreases, and the inductor voltage equals the capacitor voltage; therefore, the inductor current ripple can be expressed as:

$$\Delta I_L = \frac{V_C}{L} \cdot (1 - d_{st}) \cdot T_{sw} \tag{36}$$

With ΔI_L selected to satisfy $\Delta I_L \leq k_i \% I_L$, then

$$L \geq \frac{(1 - d_{st}) T_{sw}}{k_i \% I_L} V_C = \frac{d_{st} \cdot T_{sw}}{k_v \% I_L} V_{pn}. \tag{37}$$

Putting (19) and (32) into (37) yields

$$L \geq 0.5625 \frac{d_{st} T_{sw}}{k_i \% P_{out}} \hat{V}_{in}^2 \cos^2 \theta_i. \tag{38}$$

5. RESULTS AND DISCUSSION

The simulations of the proposed 3LSZSIMC topology and the existing 3LCZSIMC topology are performed under the same conditions using Saber software to compare their performance. In the simulations, the converters are fed by a 122-V, 50 Hz three-phase source and supply a three-phase R-L load. For both topologies, the voltage modulation index is set

to 0.85 and the shoot-through ratio set to 0.15. A switching frequency of 10 kHz is used. A summary of the parameters used for the simulation is given in Table I.

Table I. Parameters used for simulation

Description	Value
Input AC voltage	122 V / 50 Hz
Output frequency	100 Hz
Input filter, L and C	0.1 mH and 100 μF
Load, R-L	50 Ω , 10 mH
Series Z-source, L-C	1 mH , 1000 μF
Z-source, L-C	1 mH , 1000 μF
Switching frequency	10 kHz

Figures 8 and *9* show the simulation results for the proposed 3LSZSIMC and the existing 3LCZSIMC respectively.

(a)

(b)

(c)
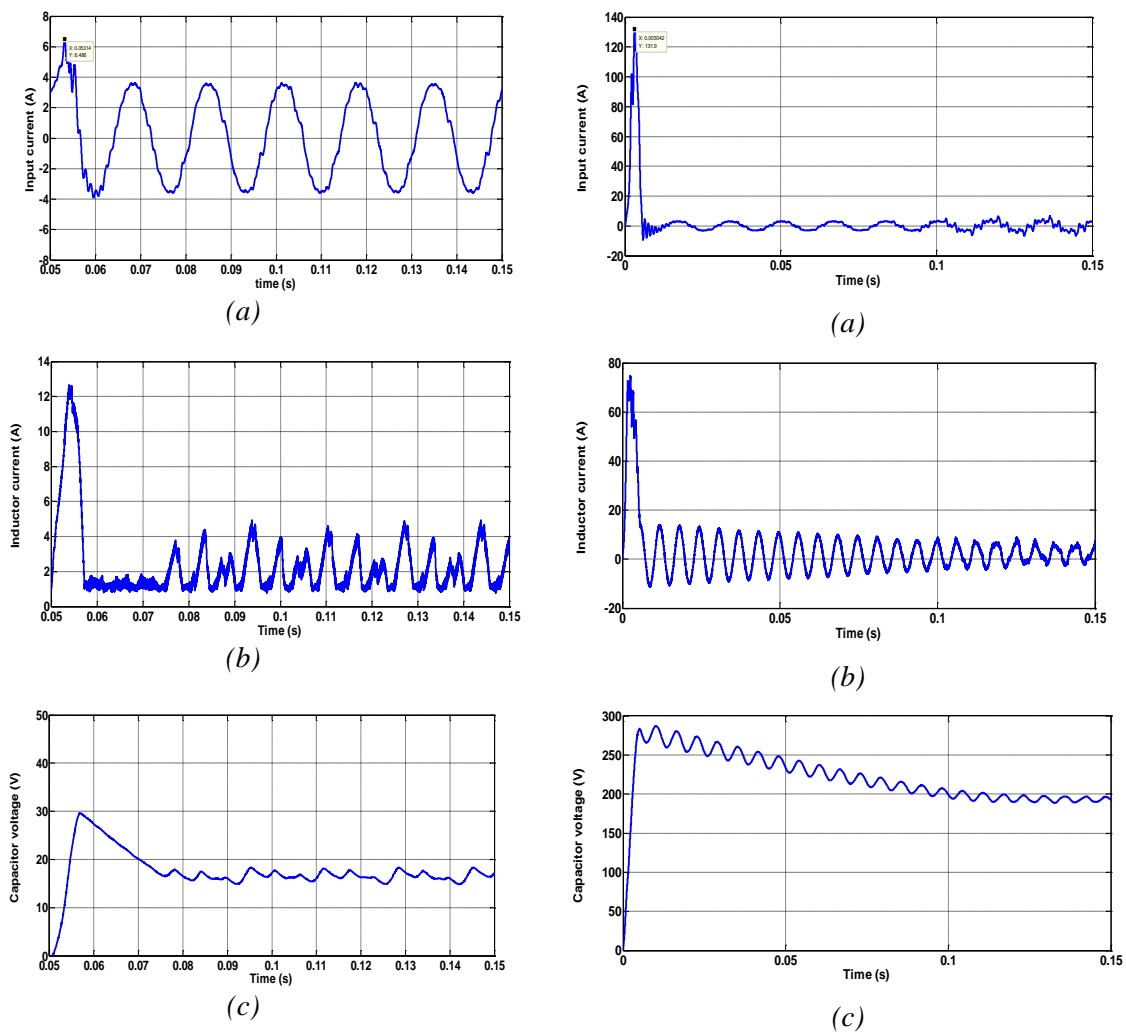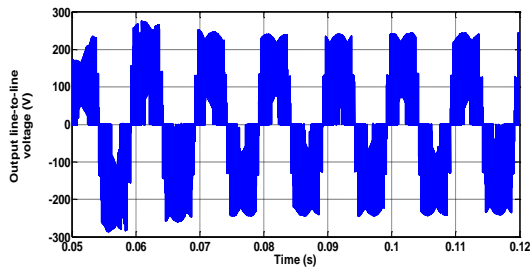
(d)
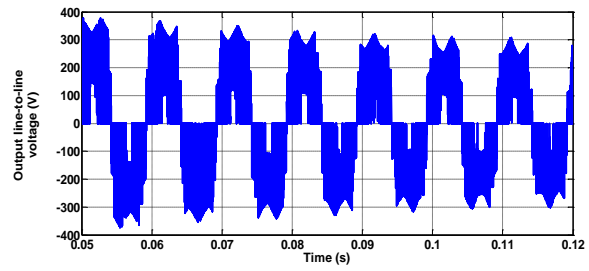
(d)
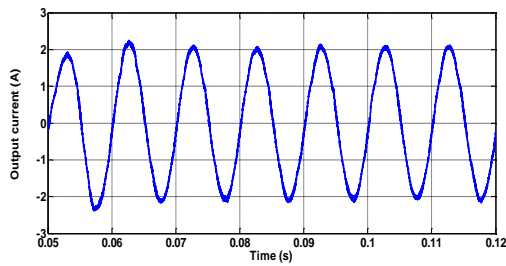
(e)
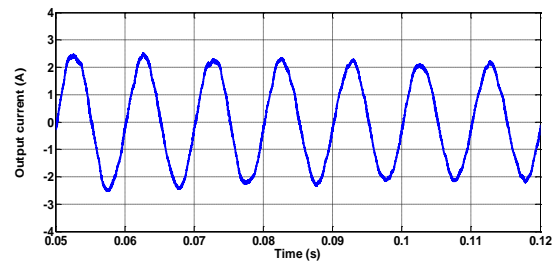
(e)

Fig. 8: 3LSZSIMC. (a) Input phase current. (b) Series Z-source inductor current. (c) Series Z-source capacitor voltage (d) Output line-line voltage. (e) Output phase current.

Fig. 9: 3LCZSIMC. (a) Input phase current. (b) Series Z-source inductor current. (c) Series Z-source capacitor voltage (d) Output line-line voltage. (e) Output phase current.

The simulated results for the two topologies show the soundness of the adopted modulation strategy in terms of output voltage and current waveforms. At start up, the input current drawn by the 3LSZSIMC reaches 6.5 A (see *fig. 8a*) whereas the corresponding value for the 3LCZSIMC is 132 A (see *fig. 9a*). This clearly shows that the inrush current at start up is suppressed in the 3LSZSIMC. The inductor current for the proposed series topology, 3LSZSIMC, reaches 12.7 A as shown in *fig. 8b* whereas the inductor current of the cascaded topology, 3LCZSIMC, reaches 74.7 A (see *fig. 9b*). This means that inductors of reduced sizes can be employed in the proposed topology even though four inductors are required as opposed to two in the cascaded topology.

The voltages across the Z-source capacitors are shown in *fig. 8c* and *fig. 9c*, respectively, for the two topologies. The average Z-source capacitor voltage is 16 V for the 3LSZSIMC and 195 V for the 3LCSZSIMC. The waveforms also show that the Z-source capacitors in 3LSZSIMC and 3LCZSIMC topologies have to withstand at start up peak voltages of about 30 V and 300 V respectively. Therefore, smaller sizes of capacitors can be employed in the proposed converter. Even though four capacitors are required in the proposed topology as opposed to two in the existing one, the smaller sizes of the capacitors mean light weight film capacitors could be used thereby reducing the size and overall volume of the converter.

As shown in *figures 8d* and *9d*, both converters are able to perform voltage boost by employing partial shoot-through states in the inverter state switching sequences. However, a

critical look of the two waveforms shows that the 3LSZSIMC maintains the shape of the traditional 3-level IMC waveforms even when shoot-through states are inserted whiles that of the 3LCZSIMC have some voltage spikes resulting from the extremely high Z-source capacitor voltages of the 3LCZSIMC. The output current waveforms of the two converters, shown in *figures 8e* and *9e*, are all sinusoidal. However, that of the 3LSZSIMC present better output performance in terms of total harmonic distortion (THD).

The above simulation results clearly show that the 3LSZSIMC topology presents better performance in terms of output current THD, and reduced voltage and current stresses on Z-source components and consequently reduced sizes of these components.

6. CONCLUSIONS

The ac-to-ac converter presented in this paper is a three-level indirect matrix converter having two series Z-source networks inserted in the dc link to give it voltage-boost capability. This converter topology would be suitable for applications requiring unidirectional power flow with lower output waveform harmonic content. Where bidirectional power flow is required, it can be achieved by replacing the ultrasparse rectifier with a sparse matrix rectifier. The proposed 3LSZSIMC and existing 3LCZSIMC topologies were simulated and compared in order to determine the suitability of the proposed 3LSZSIMC for applications requiring ac-to-ac power conversion such as wind energy conversion systems (WECSs). The simulation results confirm the voltage-boost ability of the proposed converter. This feature is necessary in WECSs where the generator voltage needs to be boosted so the output voltage could meet the grid requirements. The quality of the output current waveform of the proposed 3LSZSIMC was found to be better than that of the 3LCZSIMC. In addition, the Z-source capacitor voltages and inductor currents of the proposed converter are lower at start up. Therefore, the proposed converter just like the existing 3LCZSIMC is a potential candidate for WECSs.

REFERENCES

[1]   A. Hakemi and M. Monfared, *Very high gain three-phase indirect matrix converter with two Z-source networks in structure*, IET Renewable Power Generation, vol. 11, issue. 5, pp. 633-641, 2017.

[2]   X. Dan and M. F. Rahman, *Sensorless direct torque and flux controlled IPM synchronous machine fed by matrix converter over a wide speed range*, IEEE Trans.Ind. Informat, vol. 9, no.4, pp. 1885-1887, Nvov. 2013.

[3]   S. Liu, B. Ge, X. Jiang, H. Abu-Rub and F. Z. Peng, *Comparative evaluation of three Z-source/Quasi-Z-source indirect matrix converters*, IEEE Trans. Ind. Electron., vol. 62, no. 2,

Feb. 2015.

[4] T. D. Nguyen and H.-H. Lee, *A new SVM method for indirect matrix converter with common-mode voltage reduction*, IEEE Trans. Ind. Informat., vol. 10, no. 1, pp. 61-72, Feb. 2014.

[5] L. Wei and T. A. Lipo, *A novel matrix converter topology with simple commutation*, in Conf. Rec. 36th IEEE IAS Annu. Meeting, Sep. 30-Oct. 4, 2001, vol. 3, pp. 1749-1754.

[6] J. W. Kolar, M. Baumann, F. Schafmeister, H. Ertl, *Novel three-phase AC-DC-AC sparse matrix converter*, 17th Annual Applied Power Electronics Conference and Exposition, vol. 2, pp. 777-791, 2002.

[7] H. Wang, M. Su, Y. Sun, G. Zhang, J. Yang, W. Gui, and J. Feng, *Topology and modulation scheme of a three-level third-harmonic injection indirect matrix converter*, IEEE Trans. Ind. Electron., vol. 64, no. 10, pp. 7612-7622, Oct. 2017.

[8] S. Zhang, K. J. Tseng, T. D. Nguyen, *Novel three-phase AC-AC Z-Source converters using matrix converter theory*, IEEE Energy Conversion Congress and Exposition, pp. 3063-3070, 2009.

[9] X. wang, H. Lin, H. She and B. Feng, *A research on space vetor modulation strategy for matrix converter under abnormal input-voltage conditions*, IEEE Trans. Ind. Electron., vol. 59, no. 2, pp. 93-104, Jan. 2012.

[10] M. Rivera, J. rodriguez, J. R. Espinoza, and H. Abu-Rub, *Instantaneous reactive power minimization and current control for an indirect matrix converter under a distorted AC supply*, IEEE Trans. Ind. Informat., vol. 8, no. 3, pp. 482-490, Aug. 2012.

[11] F. Blaabjerg, D. Casadei, C. Klumpner, and M. Matteini, *Comparison of two current modulation strategies for matrix converters under unbalanced input voltage conditions*, IEEE Trans. Ind. Electron., vol. 49, no. 2, pp. 289-296, Apr. 2002.

[12] G. T. Chiang and J. Itoh, *Comparison of two overmodulation strategies in an indirect matrix converter*, IEEE Trans. Ind. Electron., vol. 60, no. 1, pp. 43-53, Jan. 2013.

[13] O. Ellaban, H. Abu-Rub, S. Bayham, *Z-Source matrix converter: an overview*, IEEE Trans. Power Electron., vol. 31, no. 11, pp. 7436-7450 , Nov. 2016.

[14] J. Kaniewski, Z. Fedyczak, and G. Benysek, *AC voltage sag/swell compensator based on three-phase hybrid transformer with buck-boost matrix-reactance chopper*, IEEE Trans. Ind. Electron., vol. 61, no. 8, pp. 3835-3846, Aug. 2014.

[15] X. Liu, P. C. Loh, F. Z. Peng, P. Wang, F. Gao, *Modulation of three-level Z-source indirect matrix converter*, 2010 IEEE Energy Converesion Congress and Exposition, pp. 3195-3201, Sept. 2010.

[16] F. B. Effah, A. J. watson, P. W. Wheeler, J. C. Clare and L. De-Lillo, *Space-vector-modulated three-level Z-source hybrid direct AC-AC power converter*, 15th European Conference on Power Electronics and Applications (EPE), pp. 1-10, Lille, 2013.

[17] Y. Tang, S. Xie, C. Zhang, *An improved Z-source inverter*, IEEE Trans. Power Electron., vol. 26, no. 26, pp. 3865-3868, Feb. 2011.

[18] E. Karama, M. Farasat, and A. Trzynadlowski, *A comparative study of series and cascaded Z-source matrix converter*, IEEE Trans. Ind. Electron., vol. 61, no. 10, pp. 5164-5173, Oct. 2014.

[19] C. N. El-Khoury, H. Y. Kanaan, I. Mougharbel and K. Al-Haddad, A comparative study of four bidirectional sparse matrix converter topologies for wind power applications, 2015 IEEE

International Conference on Industrial Technology (ICIT), Seville, 2015, pp. 2552-2558.

[20]   Y. Tang, S. Xie, J. Wie, *Grid-tied photovoltaic system with series Z-source inverter*, IET Renewable Power Generation, vol. 7, no. 3, pp. 275-283, 2013.

[21]   S. Zhang, K. J. Tseng, D. M. Vilathgamuwa, T. D. Nguyen, and X.-Y. Wang, *Design of a robust grid interface system for PMSM-based wind turbine generators*, IEEE Trans. Ind. Electron., vol. 58, no. 1, pp. 316-328, Jan. 2011.

[22]   J. Holtz and U. Boelkens, *Direct frequency converter with sinusoidal line currents for speed-variable ac motors*, IEEE Trans. Ind. Electron., vol. 36, pp. 475-479, Nov. 1989.

[23]   S. B. Monge, J. Bordonau, D. Boroyevich, and S. Somavilla, The nearest three virtual space vector pwm – a modulation for the comprehensive neutral-point balancing in three-level npc inverter, IEEE Power Electronics Letters, vol. 2, pp. 11- 15, Mar. 2004.

LIMITS OF EXPOSURE TO ELECTROMAGNETIC FIELDS – A REVIEW OF STANDARDS AND REGULATIONS

Mihaela ŞTEŢ

Technical University of Cluj Napoca

mihaela.stet@cunbm.utcluj.ro

Abstract*: Identification of risks and potential effects of exposure to electromagnetic fields has aroused the interest of researchers in various fields to reduce or even eliminate them. However, the problems they raise, also, determined the need to regulate the exposure limits, thus establishing a series of regulations at the level of different states, of some national and international standards. The paper presents a comparative analysis of several national and international regulations regarding the exposure limits for the general public and for different working environments.*

1. INTRODUCTION

Multiple uses of electricity make it essential for modern everyday life. But, over time, in addition to the undeniable positive effects, various forms of negative impact on humans and the environment have been observed and identified.

Identification of risks and potential effects of exposure to electromagnetic fields has aroused the interest of researchers in various fields to reduce or even eliminate them. However, the problems they raise, also, determined the need to regulate the exposure limits, thus establishing a series of regulations at the level of different states, of some national and international standards.

The paper presents a comparative analysis of several national and international regulations regarding the exposure limits for the general public and for different working environments. The methodology of this study consists in different methods, mainly literature review, data analysis, classification and problem identification.

2. EVOLUTION OF REGULATION ON LIMITING EXPOSURE TO ELECTROMAGNETIC FIELDS

In order to prepare a regulation or a guideline for limiting exposure, different national or international organizations involved in such activities make an extensive review of relevant literature on health and biological effects.

According to Directive 2013/35/EU, effects of electromagnetic fields on human body are direct biophysical effects and indirect effects. The first category includes non-thermal effects, thermal effects and limb currents [1]. Non-thermal effects, associated with different frequency and intensity, are vertigo, nausea (static magnetic fields), effects on sense organs (up to 100 kHz), effects on nerves, muscles (up to 10 MHz). Thermal effects in the form of heating is present also for intermediate frequencies (100 kHz – 10 MHz) and for high frequency fields (10 MHz and above). These effects are identified based on epidemiological, occupational, laboratory, volunteer, cellular and animal studies.

Among the causes of the increase in environmental EMF levels presented by the World Health Organization are high voltage transmission lines, telecommunication and broadcast transmitters, radars, transportation systems and undersea power cables [2].

First countries that introduced regulations on limiting exposure to electromagnetic fields against adverse effect on workers and public were the former Soviet Union USSR and USA. The first standard developed and published in 1958 by the former Soviet Union regulated the limitation of RF exposure of workers [3]. In 1960, the American Standards Association approved the Radiation Hazards Standards project under the co-sponsorship of the Department of the Navy and the Institute of Electrical and Electronics Engineers [4].

In the following period, the number of countries concerned with this issue grew, conducting numerous studies on the effects and risks generated by exposure to electromagnetic fields. Over time, more and more organizations, globally, have addressed the issue of limiting exposure to the undesirable effects of electromagnetic fields (see Table 1).

In 1974, International Radiation Protection Association IRPA formed a working group that analysed the problem of protection against non-ionizing radiation NIR [5] and in 1977, this group became the International Non-Ionizing Radiation Committee INIRC. This organization, in cooperation with Environmental Health Division of WHO developed a series of health criteria documents on NIR.

In 1992, it became International Commission Non-Ionizing Radiation Protection ICNIRP and in 1998 released Guidelines for limiting exposure to time-varying electric, magnetic, and electromagnetic fields (up to 300 GHz).

Starting from this moment a series of regulations, guidelines, recommendations and other documents were issued by national or international bodies, as the number of studies on

the effects of electromagnetic fields has increased, but also due to the growing public interest in the problems generated by the presence of electromagnetic fields (see Table 2).

Table 1. International organisations involved in research or regulation of exposure to electromagnetic fields

Organisation	Short description
IEC International Electrotechnical Commission	worldwide organization for standardization comprising all national electrotechnical committees (IEC National Committees)
ICOH International Commission on Occupational Health	international non-governmental professional society - fosters the scientific progress, knowledge and development of occupational health and safety
CIE International Commission on Illumination	independent, non-profit professional organization, authority on the subject matter of light and lighting
ILO International Labour Organization	U.N. agency, sets labour standards, develops policies and devises programmes promoting decent work for all women and men
ACGIH American Conference of Governmental and Industrial Hygienists	charitable scientific organization that advances occupational and environmental health
ISO International Standards Organization	independent, non-governmental international standard-setting body composed of representatives from national standards organizations
WHO World Health Organization	organization that promotes health, keeps the world safe, and serves the vulnerable.
IEEE Institute of Electrical and Electronic Engineers	technical professional organization designed to serve professionals involved in all aspects of the electrical, electronic, and computing fields and related areas of science and technology
IRPA International Radiation Protection Association	association of radiation protection professionals joining through national and regional radiation protection societies
European COST Cooperation in the Field of Science and Technology	funding organisation for the creation of research networks
CENELEC European Committee on Electrotechnical Standardisation	responsible for standardization in the electrotechnical engineering field
ICNIRP International Commission on Non-Ionizing Radiation Protection	independent group of experts established to evaluate the state of knowledge about the effects of NIR on human health and well being

In the same time, since 1998, WHO has started a project to harmonize EMF standards worldwide, involving 8 international organizations and over 45 countries, starting from the fact that there were large differences between the existing standards at that time, in some cases there were even differences of two orders of size [2].

Regarding the ICNIRP Guidelines, this document distinguished between occupational and general exposure limitations, introducing significantly different values for these types of exposure, justified by the following considerations:
-   general public includes persons of different ages, health conditions,
-   many members of that are unaware of their exposure to EMF and potential risks,
-   no expectations can be raised regarding the adoption by the general public of reasonable measures to minimize or avoid exposure.

Table 2. Regulations, recommendations, guidelines, and other documents related to exposure to electromagnetic fields

Year	Regulation / Document	Regulatory body	Domain / description
1998	Guidelines for limiting exposure to time-varying electric, magnetic, and electromagnetic fields	ICNIRP	Establishes guidelines for limiting EMF exposure that will provide protection against known adverse health effects.
1999	Council Recommendation 1999/519/EC on the limitation of exposure of the general public to electromagnetic fields (0 Hz to 300 GHz)	EC	Recommendations on the limitation of exposure of the general public to EMF (0 Hz to 300 GHz)
2002	IEEE Recommended Practice for Measurements and Computations of Radio Frequency Electromagnetic Fields With Respect to Human Exposure to Such Fields, 100 kHz–300 GHz	IEEE	Revises and develops specifications for preferred methods for measuring and computing external radio frequency electromagnetic fields to which persons may be exposed
2002	ICNIRP Statement - General Approach to Protection against Non-Ionizing Radiation	ICNIRP	Optical radiation including lasers and electromagnetic fields, ultrasound and infrasound exposures
2004	Directive 2004/40/EC on Minimum Health and Safety Requirements Regarding the Exposure of Workers to the Risks Arising from Physical Agents (Electromagnetic Fields)	EC	Lays down minimum requirements for the protection of workers from risks to their health and safety arising or likely to arise from exposure to electromagnetic fields (0 Hz to 300 GHz) during their work
2004	ECC Reccomandation (02)04 (revised 2007) Measuring Non-Ionising Electromagnetic Radiation (9 kHz – 300 GHz)	ECC	Describes a measurement method that should be used to assess electromagnetic radiation against the appropriate reference levels for exposure of human beings to electromagnetic fields (9 kHz – 300 GHz)
2005	IEEE Std C95.1-2005, Standard for Safety Levels with Respect to Human Exposure to Radio Frequency Electromagnetic Fields, 3 kHz to 300 GHz	IEEE	Exposure limits to protect against established adverse effects to human health induced by exposure to RF electric, magnetic and electromagnetic fields over the frequency range of 3 kHz - 300 GHz.
2006	The Electromagnetic Fields Human Exposure Act	WHO	Establishes limits on human exposure to Electromagnetic Fields (EMF) that will provide protection against known adverse health effects from any installation or device emitting such fields.
2006	Human EMF Exposure Limit Regulation	WHO	Protects the public and workers from adverse health effects arising from exposure to electromagnetic fields (EMF) in the living and working environments.
2006	The Electromagnetic Fields Human Exposure Act - Model legislation for electromagnetic fields protection	WHO	Establishes minimum requirements for the protection of the public and workers from risks to their health arising or likely to arise from their exposure to EMF in the frequency range 0 to 300 GHz.
2010	ICNIRP Guidelines for limiting exposure to time-varying electric and magnetic fields (1 HZ – 100 kHZ)	ICNIRP	Establishes guidelines for limiting exposure to electric and magnetic fields (EMF) that will provide protection against all established adverse health effects.
2013	Directive 2013/35/EU on the minimum health and safety requirements regarding the exposure of workers to the risks arising from physical agents (electromagnetic fields)	EU	Minimum requirements for the protection of workers from risks to their health and safety arising, or likely to arise, from exposure to electromagnetic fields during their work
2014	IEEE Std C95.7-2014 Recommended Practice for Radio Frequency Safety Programs, 3 kHz to 300 GHz	IEEE	Guidance for preventing exposures above applicable radio frequency (RF) limits associated with RF sources that operate in the frequency range of 3 kHz to 300 GHz
2019	IEEE Std C95.1™-2019 Standard for Safety Levels with Respect to Human Exposure to Electric, Magnetic, and Electromagnetic Fields, 0 Hz to 300 GHz	IEEE	Exposure criteria and limits to protect against established adverse health effects in humans associated with exposure to electric, magnetic, and electromagnetic fields in the frequency range 0 - 300 GHz

Basic restrictions were based on health effects and the physical quantities used in this regard are specific absorption rate *SAR*, current density *J*, and power density *S* [5] (see Table 3):

- 1 Hz – 10 MHz – restrictions on current density to prevent effects on nervous system,
- 100 k Hz – 10 GHz – *SAR* against whole-body heat stress and excessive localized tissue heating,
- 10 – 300 GHz – power density – excessive heating in tissue at or near the body surface.

Table 3. Basic restrictions - ICNIRP Guidelines

Frequency range	Exposure category	Whole-body average SAR (W/kg)	Localised SAR in the head & trunk (W/kg)	Localised SAR in limbs (W/kg)	Current density for head and trunk (mA/m² rms)	Power density S (W/m²)
Up to 1 Hz	Occupational	-	-	-	40	-
	General public				8	
1 - 4 Hz	Occupational	-	-	-	40/f	-
	General public				8f	
4 - 1000 Hz	Occupational	-	-	-	10	-
	General public				2	
1000 Hz - 100 kHz	Occupational	-	-	-	f/100	-
	General public				f/500	
100 kHz - 10 MHz	Occupational	0,4	10	20	f/100	-
	General public	0,08	2	4	f/500	
10 MHz - 10 GHz	Occupational	0,4	10	20	-	-
	General public	0,08	2	4	-	
10 GHz - 300 GHz	Occupational	-	-	-	-	50
	General public	-	-	-	-	10

Retrieved and processed after ICNIRP Guidelines, 1998

Reference levels are determined by extrapolation from the results of laboratory investigations or mathematical modelling from the basic restrictions, taking into account frequency, human body conductivity, size, shape, and position of the exposed body in the field (Table 4).

Council Recommendation 1999/519/EC introduced for EU general public basic restrictions and reference levels on exposure to radiations emitted by electromagnetic fields, excepting optical radiation and ionising radiation. This document covers the area of static fields, extremely low frequency fields ELF and radiofrequency fields RF, including microwaves, in the frequency range of 0 Hz to 300 GHz [6].

Basic restrictions on the exposure to time-varying fields, based on biological considerations and health effect, are represented by the specific absorption rate *SAR*, magnetic flux density *B*, current density *J* and power density *S* (See Table 5).

Reference levels derived from basic restrictions are electric field strength *E*, magnetic field strength *H*, power density *S* and limb current I_L. At certain frequencies, magnetic flux density *B* and power density *S*, are used as basic restrictions and reference levels. For pulsed fields it is used specific energy absorption *SA* (Table 6).

Table 4. Reference levels to time-varying electric and magnetic fields - ICNIRP Guidelines

Frequency range	Exposure category	E-field strength (V/m)	H-field strength (A/m)	B-field (μT)	Equivalent plane wave power flux density Seq (W/m2)	Maximum contact current (mA)	Induced current in any limbs (mA)
up to 1 Hz	Occupational	-	1.63×10^{5}	2×10^{5}			
	General public	-	3.2×10^{4}	4×10^{4}			
1 - 8 Hz	Occupational	20000	$1.63 \times 10^{5}/f^{2}$	$2 \times 10^{5}/f^{2}$			
	General public	10000	$3.2 \times 10^{4}/f^{2}$	$4 \times 10^{4}/f^{2}$			
8 - 25 Hz	Occupational	20000	$2 \times 10^{4}/f$	$2.5 \times 10^{4}/f$			
	General public	10000	$4000/f$	$5000/f$			
0.025 - 0.82 kHz	Occupational	$500/f$	$20/f$	$25/f$			
0.025 - 0.8 kHz	General public	$250/f$	$4/f$	$5/f$			
0.8 - 3 kHz	General public	$250/f$	5	6.25			
0.82 kHz - 65 kHz	Occupational	610	24.4	30.7			
3 - 150 kHz	General public	87	5	6.25			
0.065 - 1 MHz	Occupational	610	$1.6/f$	$2.0/f$			
0.15 - 1 MHz	General public	87	$0.73/f$	$0.92/f$			
1 MHz - 10 MHz	Occupational	$610/f$	$1.6/f$	$2.0/f$			
	General public	$87/f^{1/2}$	$0.73/f$	$0.92/f$			
10 MHz - 400 MHz	Occupational	61	0.16	0.2	10		
	General public	28	0.073	0.092	2		
400 MHz - 2 GHz	Occupational	$3f^{1/2}$	$0.008f^{1/2}$	$0.01f^{1/2}$	$f/40$		
	General public	$1.375f^{1/2}$	$0.0037f^{1/2}$	$0.0046f^{1/2}$	$f/200$		
2 GHz - 300 GHz	Occupational	137	0.36	0.45	50		
	General public	61	0.16	0.20	10		
0 - 2.5 kHz	Occupational					1	
	General public					0.5	
2.5 kHz - 100 kHz	Occupational					$0.4 f$	
	General public					$0.2 f$	
100 kHz - 110 MHz	Occupational					40	
	General public					20	
10 - 110 MHz	Occupational						100
	General public						45

Table 5. Basic restrictions - Council Recommendation 1999/519/EC

Frequency range	Whole-body average SAR (W/kg)	Localised SAR in the head & trunk (W/kg)	Localised SAR in limbs (W/kg)	Magnetic flux density (mT)	Current density (mA/m² rms)	Power density S (W/m²)
0 Hz	-	-		40		-
>0 - 1 Hz	-	-	-	-	8	-
1 - 4 Hz	-	-	-	-	$8/f$	-
4 - 1000 Hz	-	-	-	-	2	-
1000 Hz - 100 kHz	-	-	-	-	$f/500$	-
100 kHz - 10 MHz	0.08	2	4	-	$f/500$	-
10 MHz - 10 GHz	0.08	2	4	-	-	-
10 GHz - 300 GHz	-	-	-	-	-	10

Source: Council Recommendation 1999/519/EC

Table 6. Reference levels - Council Recommendation 1999/519/EC

Frequency range	E-field strength (V/m rms)	H-field strength (A/m rms)	Equivalent plane wave power flux density Seq (W/m2)	Magnetic flux density B (μT)	Maximum contact current (mA rms)
0 - 1 Hz		$3,2 \times 10^4$		4×10^4	
0 - 2.5 kHz					0.5
1 - 8 Hz	10000	$3,2 \times 10^4/f^2$		$4 \times 10^4/f^2$	
2.5 kHz - 100 kHz					$0,2f$
8 - 25 Hz	10000	$4000/f$		$5000/f$	
0,025 - 0,8 kHz	$250/f$	$4/f$		$5/f$	
0,8 - 3 kHz	$250/f$	5		6.25	
3-150 kHz	87	5		6.25	
100 kHz - 110 MHz					20
0,15 - 1 MHz	87	$0.73/f$		$0.92/f$	
1 MHz - 10 MHz	$87/f^{1/2}$	$0.73/f$		$0.92/f$	
10 MHz - 400 MHz	28	0.073	2	0.092	
400 MHz - 2 GHz	$1.375 f^{1/2}$	$0.0037 f^{1/2}$	$f/200$	$0.0046 f^{1/2}$	
2 GHz - 300 GHz	61	0.16	10	0.20	

Retrieved and processed after Council Recommendation 1999/519/EC

In a study released in 2017, Stam identified three groups of countries in European Union, regarding the EMF policies in member states and their relationship with this recommendation, in what it concerns exposure of the general public [7]:

- Group 1 - recommendation has been transposed in binding national legislation or national policy,
- Group 2 - national limits based on recommendation or ICNIRP are not binding, there is no regulation or there are more lenient limits, and
- Group 3 - stricter basic restrictions or reference levels based on precautionary principle or due to public pressure (see Table 7).

Table 7. EMF Policies in EU Member States – exposure of general public

Type of exposure	Category of EU Members States		
	Group 1 - legal limits based on 1999/519/EC	Group 2 - no legal limits or limits less strict than in 1999/519/EC	Group 3 - stricter limits than in 1999/519/EC
Power frequency fields	Czech Republic, Estonia, France, Germany, Greece, Hungary, Ireland, Luxemburg, Portugal, Romania, Slovakia	Austria, Cyprus, Denmark, Finland, Latvia, Malta, Netherlands, Spain, Sweden, United Kingdom	Belgium, Bulgaria, Croatia, Italy, Lithuania, Poland, Slovenia
Radiofrequency fields	Cyprus, Czech Republic, Estonia, Finland, France, Germany, Hungary, Ireland, Malta, Portugal, Romania, Slovakia, Spain	Austria, Denmark, Latvia, Netherlands, Sweden, United Kingdom	Belgium, Bulgaria, Croatia, Greece, Italy, Lithuania, Luxemburg, Poland, Slovenia

Source: Edited based on *Stam, R., Comparison of international policies on electromagnetic fields (power frequency and radiofrequency fields), 2017*

On the other hands, related to occupational exposure, the EU Member States use national legislation based on directive 2013/35/EU, that established minimum requirements, but allowing, in the same time, the possibility to set stricter limits or rules. In this direction, there are two exceptions, Poland and Czech Republic that use different action levels or exposure limit values.

In Spain, in 2001, it is issued a regulation, Real Decreto 1066/2001 [8], that established conditions for the protection of the public against radioelectric emissions, updated in 2017.

There had been used as basic restrictions the restrictions on exposure to time-varying electric, magnetic, and electromagnetic fields, based directly on known health effects and biological considerations.

In order to specify these constraints, there were used as physical quantities magnetic induction B, current density J, specific energy absorption index SAR and power density S (see Table 8).

Table 8. Basic restrictions for general public – Spain

Frequency range	Whole-body average SAR (W/kg)	Spatial peak SAR in the head & trunk (W/kg)	Spatial peak SAR in limbs (W/kg)	Current density in the head and trunk (mA/m² rms)	Magnetic induction (mT)	Instantaneous power flux density (W/m²)
0 Hz					40	
>0 - 1 Hz				8		
1 - 4 Hz				$8/f$		
4 - 1000 Hz				2		
1000 Hz - 100 kHz				$f/500$		
100 kHz - 10 MHz	0.08	2	4	$f/500$		
10 MHz - 10 GHz	0.08	2	4			
10 GHz - 300 GHz						10

Source: Real Decreto 1066/2001

The reference levels, used to determine the probability that the basic restrictions will be exceeded are (see Table 9):

1. derived quantities from relevant basic restrictions, using measurements or computerized techniques: electric field intensity E, magnetic field intensity H, magnetic induction B, power density S and limb current I_l;
2. quantities that refer to perception and other adverse indirect effects to exposure to radioelectric emissions, respectively contact current Ic and, for pulsatile fields, specific energy absorption SA [8].

Table 9. Reference levels for general public – Spain

Frequency range	E-field strength (V/m rms)	H-field strength (A/m rms)	Equivalent plane wave power flux density Seq (Wm2)	Magnetic induction B (μT)	Maximum contact current (mA rms)
0 - 1 Hz		3.2×10^4		4×10^4	
1 - 8 Hz	10000	$3.2 \times 10^4/f^2$		$4 \times 10^4/f^2$	
8 - 25 Hz	10000	$4000/f$		$5000/f$	
0.025 - 0.8 kHz	$250/f$	$4/f$		$5/f$	
0.8 - 3 kHz	$250/f$	5		6.25	
3-150 kHz	87	5		6.25	
0.15 - 1 MHz	87	$0.73/f$		$0.92/f$	
1 MHz - 10 MHz	$87/f^{1/2}$	$0.73/f$		$0.92/f$	
10 MHz - 400 MHz	28	0.073	2	0.092	
400 MHz - 2 GHz	$1.375 f^{1/2}$	$0.0037 f^{1/2}$	$f/200$	$0.0046 f^{1/2}$	
2 GHz - 300 GHz	61	0.16	10	0.20	
0 - 2.5 kHz					0.5
2.5 kHz - 100 kHz					$0.2 f$
100 kHz - 110 MHz					20

Retrieved and processed after Real Decreto 1066/2001

As it can be seen, the basic restrictions and reference values are similar to those from Council Recommendation 1999/519/EC.

The same situation can be revealed in Romania, where in 2006 Minister of Public Health issued Order no. 1193/2006 for the approval of the Norms regarding the limitation of the exposure of the general population to electromagnetic fields from 0 to 300 GHz [9].

In addition, Romanian Government in 2016 issued a decision HG 520/2016 [10] on minimum safety and health requirements regarding the exposure of workers to risks generated by electromagnetic fields in accordance with Directive 2013/35/EU. In 2018, Institute of Public Health subordinated to Ministry of Health published a practical guide for conformity assessment with national exposure rules of workers in electromagnetic fields [11].

In Australia, in 2002 ARPANSA Australian Radiation Protection and Nuclear Safety Agency issued Radiation Protection Standard for Maximum Exposure Levels to Radiofrequency Fields — 3 kHz to 300 GHz which sets limits for human exposure to radiofrequency (RF) fields in the frequency range 3 kHz to 300 GHz, to prevent adverse health effects [12].

Table 10. Basic restrictions in Australia – occupational and general public

Frequency range	Exposure category	Whole-body average SAR (W/kg)	Spatial peak SAR in the head & torso (W/kg)	Spatial peak SAR in limbs (W/kg)	Spatial peak SA in the head within any 50 μs interval (mJ/kg)	Instantaneous spatial peak SAR in the head and torso (W/kg)	Current density in the head and torso (mA/m² rms)	Time averaged power flux density (W/m²)	Instantaneous power flux density (W/m²)
3 kHz - 10 MHz	Occupational						10 x f		
	General public						2 x f		
100 kHz - 6 GHz	Occupational	0.4	10	20					
	General public	0.08	2	4					
300 MHz - 6 GHz	Occupational				10				
	General public				2				
10 MHz - 6 GHz	Occupational					10000			
	General public					2000			
6 GHz - 300 GHz	Occupational							50	50000
	General public							10	10000

Retrieved and processed after ARPANSA Standard, 2002

In order to develop basic restrictions (see Table 10), there had been taken into consideration different criteria:

- 3 kHz – 10 MHz – restrictions on instantaneous rms current density to prevent electrostimulation of excitable tissues,

- 100 kHz – 6 GHz – whole body average *SAR* against whole-body heat stress, spatial peak SAR in head, trunk and limbs against excessive localised temperature rise in tissue,

- 300 MHz – 6 GHz, for pulse modulated exposure – specific absorption *SA* per pulse for localised exposures to the head to avoid or limit auditory effects,

- 10 MHz – 6 GHz – instantaneous spatial peak *SAR* against associated effects to extremely high-level pulse fields,

- 6 GHz – 300 GHz – instantaneous and time averaged incident power flux density to prevent excessive heating in tissue at or near the body surface and to protect against associated effects to extremely high-level pulse fields [12].

In the Australian standard *E* and *H* reference levels are established for time averaged and instantaneous exposure to rms electric and magnetic fields and are derived from basic restrictions by mathematical modelling and laboratory investigations. In addition, there are set reference levels for instantaneous rms contact current and time averaged rms current induced in any limb over 6-minute period (see Table 11).

Table 11. Reference levels in Australia – occupational and general public

Frequency range	Exposure category	Time averaged exposure to rms electric and magnetic fields (unperturbed fields)			Exposure to instantaneous rms electric and magnetic fields (unperturbed fields)			Time averaged rms	Instantaneous rms contact
		E-field strength (V/m rms)	H-field strength (A/m rms)	Equivalent plane wave power flux density Seq (W/m2)	E-field strength (V/m rms)	H-field strength (A/m rms)	Equivalent plane wave power flux density Seq (W/m2)	Current (mA rms)	Maximum contact current (mA rms)
3 Khz – 65 kHz	Occupational				614	25.0	-		
3 kHz – 100 kHz	Occupational							$0.4 \times f$	
	General public				86.8	4.86	-	$0.2 \times f$	
65 kHz – 100 kHz	Occupational				614	$1.63 / f$	-		
100 kHz - 150 kHz	General public	86.8	4.86	-	$488 \times f^{0.75}$	4.86	-		
100 kHz - 1 MHz	Occupational	614	$1.63 / f$	-	$3452 \times f^{0.75}$	$9.16 / f^{0.25}$	-		
100 kHz - 110 MHz	Occupational							40	
	General public							20	
150 kHz - 1 MHz	General public	86.8	$0.729 / f$	-	$488 \times f^{0.75}$	$3.47 / f^{0.78}$	-		
1 MHz - 10 MHz	Occupational	$614 / f$	$1.63 / f$	$1000 / f^{2}$	$3452 \times f^{0.25}$	$9.16 / f^{0.25}$	$(10^{9} / f)^{0.5}$		
	General public	$86.8 / f^{0.5}$	$0.729 / f$	-	$488 \times f^{0.25}$	$3.47 / f^{0.78}$	-		
10 MHz - 110 MHz	Occupational								100
	General public								45
10 MHz - 400 MHz	Occupational	61.4	0.163	10	1941	5.15	10000		
	General public	27.4	0.0729	2	868	2.30	2000		
400 MHz - 2 GHz	Occupational	$3.07 \times f^{0.5}$	$0.00814 \times f^{0.5}$	$f / 40$	$97 \times f^{0.5}$	$0.258 \times f^{0.5}$	$25 \times f$		
	General public	$1.37 \times f^{0.5}$	$0.00364 \times f^{0.5}$	$f / 200$	$43.4 \times f^{0.5}$	$0.115 \times f^{0.5}$	$5 \times f$		
2 GHz - 300 GHz	Occupational	137	0.364	50	4340	11.5	50000		
	General public	61.4	0.163	10	1941	5.15	10000		

Retrieved and processed after ARPANSA Standard, 2002

In European Union, Directive 2004/40/EC emphasizes the need to assess the risk of workers' exposure by the employer. The directive introduced the term "exposure limit values" defined as "limits on exposure to electromagnetic fields which are based directly on established health effects and biological considerations", a term similar to "basic restrictions" used in other documents in the field [13].

The exposure limit values in this directive established for worker's exposure to electromagnetic fields are also similar to those set as basic restrictions for occupational exposure in other documents: whole body average *SAR*, head and trunk localized *SAR*, limbs localized *SAR*, current density, and power density (see Table 12).

Depending on frequency, they are set in order to prevent the following effects:

- cardiovascular and central nervous system, for time-varying fields up to 1 Hz,
- on central nervous system functions, for 1 – 10 MHz,
- excessive localised heating of tissues and whole-body heat stress, for 100 kHz – 10 GHz,
- excessive localised heating at or near the body surface, for 10 GHz – 300 GHz [13].

Table 12. Exposure limit values according to Directive 2004/40/EC

Frequency range	Whole-body average SAR (W/kg)	Localised SAR in the head & trunk (W/kg)	Localised SAR in limbs (W/kg)	Current density for head and trunk J (mA/m²) (rms)	Power density S (W/m²)
Up to 1 Hz	-	-	-	40	-
1 - 4 Hz	-	-	-	40/f	-
4 - 1000 Hz	-	-	-	10	-
1000 Hz - 100 kHz	-	-	-	f/100	-
100 kHz - 10 MHz	0,4	10	20	f/100	-
10 MHz - 10 GHz	0,4	10	20	-	-
10 GHz - 300 GHz	-	-	-	-	50

Source: Directive 2004/40/EC

For directly measured elements *E*, *H*, *B* and *S*, in directive is used the term "action values". These values are similar to reference values of ICNIRP Guidelines/1998, based on the rationale used by that (See Table 13).

Table 13. Action values according to Directive 2004/40/EC

Frequency range	Electric field strength E (V/m)	Magnetic field strength H (A/m)	Magnetic flux density B (μT)	Equivalent plane wave power flux density Seq (W/m2)	Contact current Id(mA)	Limb induced current I_L (mA)
0 - 1 Hz	-	1.63×10^5	2×10^5	-	1.0	
1 - 8 Hz	20000	$1.63 \times 10^5/f^2$	$2 \times 10^5/f^2$	-	1.0	
8 - 25 Hz	20000	$2 \times 10^4/f$	$2.5 \times 10^4/f$	-	1.0	
0.025 - 0.82 kHz	500/f	20/f	25/f	-	1.0	
0.82 kHz - 2.5 kHz	610	24.4	30.7	-	1.0	
2,5 kHz - 65 kHz	610	24.4	30.7	-	0.4 f	
65 kHz - 100 kHz	610	1600/f	2000/f	-	0.4 f	
0.1 - 1 MHz	610	1.6/f	2.0/f	-	40	
1 MHz - 10 MHz	610/f	1.6/f	2.0/f	-	40	
10 MHz - 110 MHz	61	0.16	0.2	10	40	100
110 MHz - 400 MHz	61	0.16	0.2	10	-	
400 MHz - 2000 Hz	$3f^{1/2}$	$0.008 f^{1/2}$	$0.01 f^{1/2}$	f/40	-	
2 GHz - 300 GHz	137	0.36	0.45	50	-	

Source: Directive 2004/40/EC

The Directive 2004/40/EC was replaced in 2013 by the Directive 2013/35/EU [1]. This directive established exposure limit values ELV (see Table 14), based on biophysical and biological considerations, in relation with thermal and non-thermal effects. However, as the other regulations and documents, it does not address long-term effects of EMF exposure.

These ELVs comprise health effects ELVs, above which employees might be affected by thermal heating or stimulation of nerve or muscle tissue, and sensory effects ELVs, when they might be subject to transient disturbed sensory perceptions and minor changes in brain functions [1].

Table 14. Exposure limit values according to Directive 2013/35/EU

Category of effects	Frequency range	Subcategories of effects	B (T)	E (V/m)	SAR (W/kg)	SA (mJ/kg)	S (W/m²)	Observations
Non-thermal effects	0 - 1 Hz)	Sensory effects - vertigo and other physiological effects	2	-	-	-	-	Normal working conditions
			8	-	-	-	-	Localised limbs exposure
		Health effects	8	-	-	-	-	Controlled working conditions - is applicable on a temporary basis during the shift when justified by the practice or process,
	[1 Hz - 3 kHz)	Health effects - electric stimulation of all peripheral and central nervous system tissues in the body, including the head	-	1.1	-	-	-	spatial peak values in the entire body of the exposed subject
	[3 kHz - 10 MHz]		-	$3.8 \times 10^{-4} f$	-	-	-	
	[1 Hz - 10 Hz)	Sensory effects - on the central nervous system in the head	-	$0.7/f$	-	-	-	spatial peak values in the head of the exposed subject
	[10 Hz - 25 Hz)		-	0.07	-	-	-	
	[25 Hz - 400 Hz)		-	$0.0028f$	-	-	-	
Thermal effects	100 kHz - 6 GHz	Health effects - whole body heat stress	-	-	0.4	-	-	expressed as averaged SAR in the body
		Health effects - localised heat stress in head and trunk	-	-	10	-	-	expressed as localised SAR in the body
		Health effects - localised heat stress in the limbs	-	-	20	-	-	expressed as localised SAR in the limbs
	[0.3 - 6 GHz]	Sensory effects - auditory effects caused by exposures of the head to pulsed microwave radiation	-	-	-	10	-	localised specific energy absorption - averaging mass is 10 g of tissue
	[6 - 300 GHz]	Health effects	-	-	-	-	50	6 - 10 GHz are to be averaged over any six-minute period; >10 GHz shall be averaged over any $68/f^{1.05}$ -minute period

Retrieved and processed after Directive 2013/35/EU

Regarding the term action levels ALs, also used in the previous directive, the ALs are presented separately for non-thermal and thermal effects.

For non-thermal effects, there are used ALs values for electric field strength, magnetic flux density for static and time-varying density, and contact current (see Table 15).

This document introduces, also, for electric fields low and high ALs related to specific protection or prevention measures, and for magnetic fields, low ALs in relation to sensory effects ELVs and high ALs to health effects ELVs. ALs for electric field represent maximum calculated or measures values at the workers' body position and these are established [1].

Table 15. Action values related to non-thermal effects according to Directive 2013/35/EU

Type of ALs	Frequency range	Low ALs E (V/m) RMS	High ALs E (V/m) RMS	Low ALs B (µT) RMS	High ALs B (µT) RMS	ALs for exposure of limbs (µT) RMS	ALs (Ic) (mA) RMS	ALs (B0) (mT)	Observations
Exposure to electric fields	[1 - 25 Hz)	2.0×10^4	2.0×10^4	-	-	-	-	-	
	[25 - 50 Hz)	$5.0 \times 10^5/f$	2.0×10^4	-	-	-	-	-	
	[50 Hz - 1.64 kHz)	$5.0 \times 10^5/f$	$1.0 \times 10^6/f$	-	-	-	-	-	
	[1.64 - 3 kHz)	$5.0 \times 10^5/f$	6.1×10^2	-	-	-	-	-	
	[3 kHz - 10 MHz]	1.7×10^2	6.1×10^2	-	-	-	-	-	
Exposure to magnetic fields	[1 - 8 Hz)	-	-	$2.0 \times 10^5/f^2$	$3.0 \times 10^5/f$	$9.0 \times 10^5/f$	-	-	Exposure of limbs to a localised magnetic field
	[8 - 25 Hz)	-	-	$2.5 \times 10^4/f$	$3.0 \times 10^5/f$	$9.0 \times 10^5/f$	-	-	
	[25 - 300 Hz)	-	-	1.0×10^3	$3.0 \times 10^5/f$	$9.0 \times 10^5/f$	-	-	
	[300 Hz - 3 kHz)	-	-	$3.0 \times 10^5/f$	$3.0 \times 10^5/f$	$9.0 \times 10^5/f$	-	-	
	[3 kHz - 10 MHz]	-	-	1.0×10^2	1.0×10^2	3.0×10^2	-	-	
Contact current	up to 2.5 kHz	-	-	-	-	-	1.0	-	Steady state contact current
	[2.5 - 100 kHz)	-	-	-	-	-	$0.4\,f$	-	
	[100 - 10000 kHz)	-	-	-	-	-	40	-	
Exposure to static magnetic fields	0 Hz	-	-	-	-	-	-	0.5	Interference with active implanted devices
		-	-	-	-	-	-	3	Attraction and projectile risk in the fringe field of high field strength sources (> 100 mT)

Retrieved and processed after Directive 2013/35/EU

For thermal effects, there had been specified as action values electric field strength and magnetic flux density of time varying electric, respectively magnetic fields, power density of electromagnetic waves and contact current (see Table 16). Of these, only the limb induced current has exactly the same value as in the previous directive.

Table 16. Action values related to thermal effects according to Directive 2013/35/EU

Type of ALs	Frequency range	ALs E (V/m) RMS	ALs B (µT) RMS	ALs S (W/m²)	ALs (Ic) (mA) RMS	ALs I_L (mA)	Observations
Exposure to electric and magnetic fields	[100 kHz - 1 MHz)	6.1×10^2	$2.0 \times 10^6/f$	-	-	-	
	[1 - 10 MHz)	$6.1 \times 10^8/f$	$2.0 \times 10^6/f$	-	-	-	
	[10 - 400 MHz)	61	0.2	-	-	-	
	[400 MHz - 2 GHz)	$3 \times 10^{-3}/f^{1/2}$	$1 \times 10^{-5}/f^{1/2}$	-	-	-	
	[2 - 6 GHz)	1.4×10^2	4.5×10^{-1}	-	-	-	
	[6 - 300 GHz]	1.4×10^2	4.5×10^{-1}	50	-	-	
Contact and induced limb currents	[100 kHz - 10 MHz)	-	-	-	40	-	Steady state contact current
	[10 - 110 MHz]	-	-	-	40	100	Induced limb current in any limb

Retrieved and processed after Directive 2013/35/EU

The latest standard issued by the IEEE in 2019 IEEE Std C95.1™-2019, which establishes safety levels regarding human exposure to electromagnetic fields, brings some changes, including terminology, compared to the previous standard in 2005.

The term "basic restrictions" is replaced by "dosimetric reference limit" DRL and "maximum permissible exposure" MPE by "exposure reference level" ERL. The IEEE Standard addresses three frequency bands: 0 – 100 kHz, 100 kHz – 6 GHz, and 6 GHz – 300 GHz in approaching biological effects of exposure [14]. It is not just a standard that applies to persons permitted in restricted environments and to the general public in unrestricted environments, but also an extensive, documented scientific work, extremely useful for researchers in the field.

3. CONCLUSIONS

Although the harmonization process began more than 20 years ago, there are still notable differences between the different states of the world, the differences being sometimes significant even at the level of a continent or a region.

However, in the European Union, Recommendation 1999/519/EC and Directive 2013/35/EU open the way for a harmonization of Member States' regulations, even if there are still some different approaches of EMF policies. Moreover, these regulations, recommendations and guidelines do not limit Member States in introducing more restrictive measures.

It can be observed, also, attempts of harmonization in the elaboration of different standards and regulations at the level of national and international bodies in the field, by taking into account the points of view, the reference elements and the studies on which other worldwide regulations are based.

REFERENCES

[1]　Directive 2013/35/EU of the European Parliament and of the Council of 26 June 2013 on the minimum health and safety requirements regarding the exposure of workers to the risks arising from physical agents (electromagnetic fields) (20th individual Directive within the meaning of Article 16(1) of Directive 89/391/EEC) and repealing Directive 2004/40/EC

[2]　WHO, *Electromagnetic Fields and Public Health: The International EMF Project* (Fact Sheet 181), http://www.who.int/docstore/peh-emf/publications/factsyress/efact/efs181.html

[3]　Repacholi, M. Grigoriev, Y. Bushmann, J. and Pioli, C.*, Scientific basis for the soviet and Russian radiofrequency standards for the general public,* Bioeletromagnetics, vol. 33, no. 8, pp. 623_633, 2012

[4]   IEEE, *Recommended Practice for Measurements and Computations of Radio Frequency Electromagnetic Fields With Respect to Human Exposure to Such Fields, 100 kHz-300 GHz,* IEEE Standard C95.3-2002, 2002

[5]   ICNIRP, *Guidelines for limiting exposure to time-varying electric, magnetic, and electromagnetic fields (up to 300 GHz)*, Health Physics, vol. 74, no. 4, pp. 494_522, Apr. 1998

[6]   Council of the European Union, *Council Recommendation of 12 July 1999 on the Limitation of Exposure of the General Public to Electromagnetic Fields (0 Hz to 300 GHz)*, *(1999/519/EC)*, Official Journal of the European Communities, L 199, 30 July 1999

[7]   Stam, R., *Comparison of international policies on electromagnetic fields (power frequency and radiofrequency fields)*, National Institute for Public Health and the Environment, RIVM, Netherlands, 2017

[8]   BOE-A-2001-18256*, Real Decreto 1066/2001, de 28 de septiembre, por el que se aprueba el Reglamento que establece condiciones de protección del dominio público radioeléctrico, restricciones a las emisiones radioeléctricas y medidas de protección sanitaria frente a emisiones radioeléctricas,* Spain, Accessed: 2019. [Online]. Available: https://www.boe.es/eli/es/rd/2001/09/28/1066/con

[9]   Ministerul Sanatatii Publice, *ORDIN nr. 1193 din 29 septembrie 2006 pentru aprobarea Normelor privind limitarea expunerii populaţiei generale la câmpuri electromagnetice de la 0 Hz la 300 GHz*

[10]   Guvernul Romaniei, *HOTĂRÂRE Nr. 520/2016 din 20 iulie 2016 privind cerinţele minime de securitate şi sănătate referitoare la expunerea lucrătorilor la riscuri generate de câmpuri electromagnetice,* Bucuresti, 2016

[11]   Goiceanu, C., Calotă, V., Dănulescu, R., Neamţu, A., Dănulescu, E., *Ghid practic pentru evaluarea conformitatii cu normele nationale de expunere a lucratorilor la campuri elecromagnetice (adoptate prin HG 520/2016)*, Institutul de Sanatate Publica, Ministerul Sanatatii, Bucuresti, 2018

[12]   Australian Radiation Protection and Nuclear Safety Agency (ARPANSA), *Radiation Protection Standard, Maximum Exposure Levels to Radiofrequency Fields — 3 kHz to 300 GHz,* Radiation Protection Series Publication No. 3, 2002

[13]   Directive 2004/40/EC of the European Parliament and the Council of 29 April 2004 on the minimum health and safety requirements regarding the exposure of workers to the risks arising from physical agents (electromagnetic fields) (18th individual Directive within the meaning of Article 16(1) of Directive 89/391/EEC)

[14]   IEEE Std C95.1-2019, *IEEE Standard for Safety Levels with Respect to Human Exposure to Electric, Magnetic, and Electromagnetic Fields, 0 Hz to 300 GHz,* 2019

INSTRUCTIONS FOR AUTHORS

Name **SURNAME**[1], Name **SURNAME**[2], ...

[1] *Affiliation of 1st author,* [2] *Affiliation of 2nd author, ...*
Email of 1st author, Email of 2nd author, ...(it is compulsory only for the first author)

Keywords: List 3-4 keywords *(aligned to the left, 10 pt. bold, separated by commas; please choose keywords from* IEEE Approved Indexing Keyword List*)*

Abstract*: Abstract of max. 200 words, justify, 10 pt. italic.*

1. INTRODUCTION

The paper must be written in English. It shall contain at least the following chapters: introduction, research course (mathematical algorithm); method used; results and conclusions, references.

1.1. Fonts

Use DIN A4 Format (297 x 210 mm) MSWord format. Margins: top, bottom, left and right 2.5 mm each. The text should be written on one side of the page only. Use Times New Roman fonts, line spacing 1.3. The font formats are: paper title: 14 pt, bold, italic, capital letters, author's name(s): 12 pt, regular for name and 12 pt., bold, for surname; Affiliation: 11 pt., italic; key words: 10 pt., bold; Abstract: 10 pt., italic, word Abstract in 10 pt., bold; chapter titles (do not use automatic numbering): 12 pt., bold, capital letters; subtitles: 12 pt., bold, lower case letters; subsubtitles: 12 pt., italic, lower case letters; body text: 12 pt., regular; tables and figures caption: 11 pt.; italic; references: author 11 pt.; regular, title 11 pt. italic, year, pages, ... in regular.

1.1.1. Number of pages

The number of pages is not restricted.

2. FIGURES AND TABLES

Figures have to be made in high quality, which is suitable for reproduction and printing. Don't include photos or color prints if there are not clearly intelligible in gray scale option. Place figures and tables at the top or bottom of a page wherever possible, as close as possible to the first reference to them in the paper. Use either *fig. 1* or *figure 1* when necessarily.
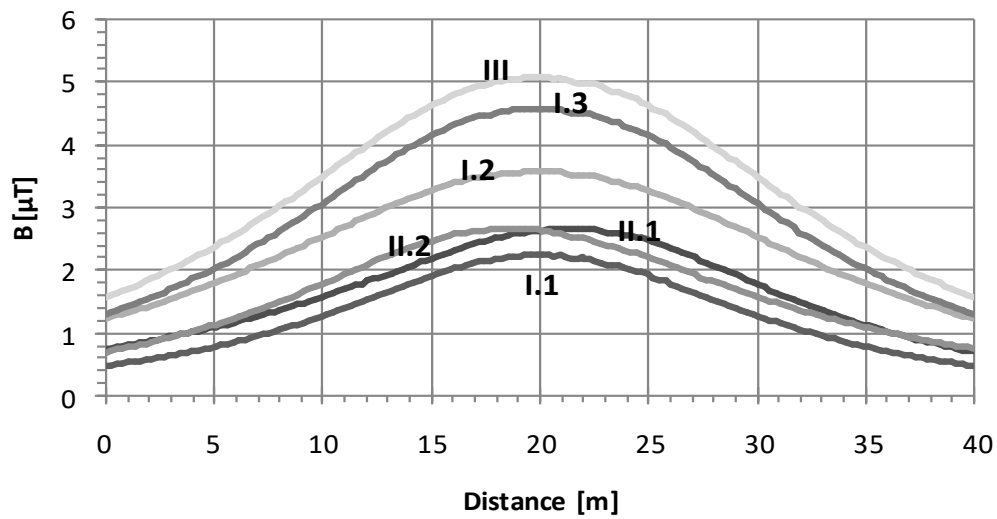
Fig. 1. Magnetic flux density at 1 m above the ground

Table 1. Transposing principle

	Circuit											
	1	*2*	*1*	*2*	*1*	*2*	*1*	*2*	*1*	*2*	*1*	*2*
1/3	*R*	*T*	***R***	***R***	*R*	*S*	*R*	*T*	*R*	*S*	***R***	***R***
line	***S***	***S***	*S*	*T*	*S*	*R*	*S*	*R*	*S*	*T*	***S***	***S***
length	*T*	*R*	*T*	*S*	***T***	***T***	*T*	*S*	*T*	*R*	***T***	***T***
1/3	*T*	*S*	***T***	***T***	*T*	*R*	*T*	*S*	*T*	*R*	***T***	***T***
line	***R***	***R***	*R*	*S*	*R*	*T*	*R*	*T*	*R*	*S*	***R***	***R***
length	*S*	*T*	*S*	*R*	***S***	***S***	*S*	*R*	*S*	*T*	***S***	***S***
1/3	*S*	*R*	***S***	***S***	*S*	*T*	*S*	*R*	*S*	*T*	***S***	***S***
line	***T***	***T***	*T*	*S*	*T*	*S*	*T*	*S*	*T*	*R*	***T***	***T***
length	*R*	*S*	*R*	*T*	***R***	***R***	*R*	*T*	*R*	*S*	***R***	***R***
Name	*I.1*		*I.2*		*I.3*		*II.1*		*II.2*		*III*	

3. EQUATIONS

Equations are centred on page and are numbered in round parentheses, flush to right margin.

$$a = b + c \tag{1}$$

Between equations, not interfered by text, there is only one empty line:

$$a = b + c \tag{2}$$

$$a = b + c \tag{3}$$

In text respect the following rules: all variables are italic, constants are regular; the references are cited in the text between right parentheses [1], the list of references has to be arranged in order of citation.

REFERENCES

[1]   International Commission on Non-ionizing Radiation Protection, *Guidelines for limiting exposure to time-varying electric, magnetic and electromagnetic fields (Up to 300 GHz)*, Health Physics, vol. 74, no. 1, pp. 494-522, 1998.

[2]   A. Marincu, M. Greconici, *The electromagnetic field around a high voltage 110 KV electrical overhead lines and the influence on the biological systems*, Proceedings of the 5th International Power Systems Conference, pp. 357-362, Timisoara, 2003.

[3]   Gh. Hortopan, *Compatibilitate electromagnetică*, Ed. Tehnică, 2005.